1.06 MICROMETER WIDEBAND LASER MODULATOR — FABRICATION AND LIFE TESTING

J.R. Teague

MCDONNELL DOUGLAS ASTRONAUTICS COMPANY—EAST

P.O. BOX 516

ST. LOUIS, MISSOURI 63166

SEPTEMBER 1975

FINAL REPORT

Prepared for:

Goddard Space Flight Center

Greenbelt, Maryland 20771

PREFACE

This report was prepared by the McDonnell Douglas Astronautics Company - East, McDonnell Douglas Corporation, St. Louis, Missouri, under contract NAS5-20605 1.06 Micrometer Wideband Laser Modulator - Fabrication and Life Testing. This report covers the period from 25 July 1974 through 25 July 1975 and is the final report of this contract.

The work described herein was carried out by the Advanced Space Avionics Department at the McDonnell Douglas Astronautics Company - East, Box 516, St. Louis, Missouri 63166.

The Project Engineer was Dr. J. R. Teague. Other contributors to the program were W. E. Heafner, Dr. V. H. Nettle, Dr. L. B. Allen, G. H. Burkhart, E. J. Conderman, H. Koenig, S. F. Pursley, F. J. Richterkessing. The program received technical direction from R. A. Stacy (Branch Manager) in the MDAC organization. J. A. Callahan coordinated artwork and reports.

CONTENTS

CONTENTS (CONTINUED)

APPENDIX

LIST OF FIGURES

LIST OF FIGURES (CONTINUED)

LIST OF FIGURES (CONTINUED)

LIST OF FIGURES (CONTINUED)

LIST OF TABLES

ABSTRACT

This program included the design, fabrication, test, and delivery of an optical modulator which will operate with a mode-locked Nd:YAG laser at 1.06 micrometers. The system transfers data at a nominal rate of 400 Mbps. This wideband laser modulator can transmit either Pulse Gated Binary Modulation (PGBM) or Pulse Polarization Binary Modulation (PPBM) formats. The modulator contained a modulator assembly, modulator electronics assembly and a laboratory modulator power supply. The modulator system was a complete package and only required an input optical beam, a low level signal source for operation and a 120 Vac 60 Hz input. The modulator contained a solid state driver which accepted digital signals with Motorola Emitter Coupled Logic (MECL) logic levels, temperature controller to maintain a stable thermal environment for the modulator crystals, and electronic compensators (both automatic and manual) and manual thermal differential compensator to maximize the extinction ratio. The modulator used two 20 mm long lithium tantalate crystals optically in series in a single pass configuration. The crystals were tapered in the C-axis to reduce switching voltage without imparing modulator transmission. The small cross sectional ends were back to back in the center of the modulator where the beam waist was located; this configuration preserved the safety factor while reducing the half-wave switching voltage. The laser beam entered the modulator and passed through both crystals; approximately 1% of the transmitted beam was split from the main beam and analyzed for the AEC signal; the remaining part of the beam exits the modulator.

The delivered modulator when initially aligned and integrated with laser and electronics performed very well. The optical transmission was 69.5%. The static extinction ratio was 69:1. The worst case dynamic extinction ratios were 22:1 and 17.5:1 for P_1 and P_2 respectively. Both polarizations had an average extinction ratio in excess of 30:1. This modulation required only 32 watts of electrical power for normal operation.

During this program a 1000 hour life test was conducted with the delivered modulator. A 1.06 μm mode-locked Nd:YAG laser test source was used with a output of 90 mW average power; however due to mirror losses only 65 mW was focused into the modulator. A 63 bit pseudorandom code signal was used as a

driver input. Optical transmission, static extinction ratio and dynamic extinction ratio of the wideband laser modulator were measured and recorded on a weekly basis during the life test. At the conclusion of the life test the modulator optical transmission was 71.5%, the static extinction ratio was 65:1 and the dynamic extinction ratio worst case was 30:1 and 31:1 for P_1 and P_2 respectively. Therefore the life test was highly successful and no apparent degradation was noted in modulator performance. There was no component failure during this life test including the 1.06 μm mode-locked Nd:YAG laser.

1. INTRODUCTION AND PROGRAM SUMMARY

1.1 INTRODUCTION.

The objective of this program was to design, fabricate, test, and deliver a 1.06 μm wideband laser modulator for use in a 400 Mbps Pulse Gated Binary Modulation (PGBM) or Pulse Polarization Binary Modulation (PPBM) laser communications system.

The modulator design consisted of a modulator assembly and an electronics assembly interconnected by a 1.33 meter semirigid coaxial cable bundle. This design approach permitted the modulator assembly to be located in the optical path between the laser source and the transmitting optics while the electronics assembly was located with the other laser communication system electronics. The interconnecting cable length was not critical. A separate power supply was also designed and fabricated for laboratory operation of the modulator.

The modulator assembly was designed and fabricated using two 20 millimeter long, high quality lithium tantalate crystals of small rectangular tapered cross-section. The crystals were arranged in a cross-axis, single-pass configuration and physically mounted in a temperature stabilized enclosure with input and output optical ports. Electrically, the crystals were incorporated in a 50 ohm broadband matching network and driven by the 400 Mbps solid state driver.

The completely solid state electronic assembly designed and fabricated during this program consisted of a 400 Mbps modulator driver, automatic electronic compensator, manual electronic compensator, manual thermal differential compensator, and temperature controller for the crystal oven.

After fabrication and test of the assemblies, a 1000-hour life test was conducted with the complete 1.06 μm wideband laser modulator. A 400 Mbps 1.06 μm mode-locked Nd:YAG laser test source was used as the input optical beam. A 63 bit pseudorandom code signal was used as the driver input. Optical transmission, static extinction ratio, and dynamic extinction ratio of the modulator were measured and recorded on a weekly basis during the

life test. The modulator met all of the performance goals and no apparent degradation was noted in modulator performance at the completion of the life test.

The modulator and laboratory power supply were delivered to the NASA Goddard Space Flight Center at the completion of the 1000-hour life test.

1.2 PROGRAM SUMMARY. In the initial part of the program, the modulator design was finalized for use in either a PGBM or PPBM laser communications system with a data rate range of 10^4 to 4×10^8 bits per second. In PGBM, pulses emitted by a mode-locked laser are either transmitted by the modulator to represent a logic "1" or blanked by the modulator to represent a logic "0". In PGBM, one half of the optical power is not transmitted. In PPBM, both logic levels are transmitted with the logic "1" being one polarization and logic "0" being polarized orthogonally to the logic "1". Therefore, PPBM is a more efficient communications approach than PGBM since all of the optical power is transmitted. However, two detectors and additional electronics are needed in the receiver for PPBM. In the modulator final design, the change in modulation format was simply accomplished by removing or inserting an optical element without disturbing the optical alignment of the modulator.

Four 20 mm long lithium tantalate crystal slabs were procured from Crystal Technology, Inc. The crystal slabs were evaluated by conducting tests which included microscopic examinations, near field retardation patterns, Schlieren examination, far field extinction patterns, optical absorption, and transmission measurements. As a result of these tests, a crystal slab taken from the approximate center of the boule was selected to fabricate the small cross-section modulator crystals.

Three 20 mm long modulator crystal cross-section sizes were fabricated for evaluation: (1) 0.25 mm x 0.20 mm, (2) 0.27 mm x 0.20 mm, and (3) 0.27 mm x 0.27 mm at one end tapered to 0.27 mm x 0.23 mm at the other end. From data obtained from measurements of these crystals it was decided to fabricate tapered crystals (tapered in the c-axis) which reduced the switching

voltage to 28 Vdc and still maintain a safety factor of 1.6 for the focused laser beam.

Modulator size crystals were then fabricated and examined for surface quality and surface periphery squareness. From these examinations, crystals were selected to be strain-relieved and anti-reflection (AR) coated. Transmission measurements were done to determine which crystals would be electroded, soldered to copper electrodes and pill mounted. Transmission measurement were made again to determine which pill mounted crystals were to be assembled in a modulator oven core. Four crystal pairs were fabricated and two oven cores were assembled from which one oven core crystal pair was delivered in the final modulator.

The two 400 Mbps crystal oven cores were fabricated and their performance was evaluated under typical operating conditions. For each of the modulator units, operating parameters and figure-of-merit such as optical transmission, static and dynamic extinction ratio, and required electrical power were recorded. The first completed modulator evaluated had optical transmission of 56.9%. The static extinction ratio for this modulator was 88:1. The 400 Mbps 63 bit PGBM format dynamic extinction ratio was 18.3:1 worst case with an average extinction ratio of 30:1 or greater. The optical transmission was lower than desired; therefore, a second pair of modulator crystals was fabricated.

The second crystal oven core was integrated with the laser and electronics and was evaluated in the test bed. Initially the modulator had optical transmission of 69.5%. The static extinction ratio was 69:1 initially. The worst case dynamic extinction ratios were initially 22:1 and 17.5:1 for P_1 and P_2, respectively. Both polarizations had an average extinction ratio in excess of 30:1. The range of timing adjustment between the optical pulses and the driver input signal measured $\pm$300 ps. Therefore, the initial data, using the second crystal oven core, was exceptionally good and had considerable timing flexibility. The second fabrication oven core required 32.4 watts of electrical power for normal operation.

TABLE 1

PERFORMANCE LOG OF THE 1.06μm WIDEBAND MODULATOR LIFE TEST

HRS	TRANSMISSION (AVERAGE)	STATIC EXTINCTION RATIO	DYNAMIC EXTINCTION RATIO (WORST CASE)	
			P_1	P_2
0	69%	69:1	22:1	17.5:1
156	68.5%	65:1	22:1	20:1
348	69%	65:1	25:1	23:1
468	71%	53:1	23:1	25:1
540	69.5%	62:1	25.5:1	22:1
684	71%	55:1	28:1	28:1
779	72%	60:1	30:1	27:1
947	71%	67:1	27:1	30:1
1099	71.5%	60:1	30:1	31:1

A 1000 hour modulator life test was conducted using a 1.06 μm mode-locked Nd:YAG laser test source with an average power output of 90 mW; however, due to mirror losses only 65 mW was focused into the modulator. A 63 bit pseudorandom code signal was used as a driver input. Optical transmission, static extinction ratio, and dynamic extinction ratio of the wideband laser modulator was measured and recorded on a weekly basis during the life test. Table 1 lists the weekly performance data of the 1.06 μm wideband laser modulator life test. As listed in Table 1, the life test was highly successful and no apparent degradation was noted in modulator performance. Initially the modulator optical transmission was 69.5% and at the end of the 1099 hours of continuous operation the transmission was 71.5%. It would appear that the transmission did increase gradually, however the instrumentation error was probably ±1%. The improved transmission could be due to strain and crystal relaxing in the pill mounts and oven after many hours of continuous use. The static extinction ratio was initially 69:1 and at the end of the 1099 hour life test the static extinction ratio was 65:1. Worst case dynamic extinction ratios for the PPBM format were initially 22:1 and 17.5:1 for P_1 and P_2, respectively, and at the close of the 1099 hour life test P_1 and P_2 had worst case dynamic extinction ratios of 30:1 and 31:1, respectively.

A performance summary of the modulator unit is given in Table II. This table summarizes the critical modulator parameters measured before and after the life test while also listing the goals of this program.

TABLE II

Wideband Laser Modulator -- Performance Summary

Characteristics	Initial Performance	End Performance	Goal
Transmission	69.5%	71%	70%
Static Extinction Ratio	69:1	65:1	50:1
Dynamic Extinction Ratio	22:1 P_1	30:1 P_1	20:1
	17.5:1 P_2	31:1 P_2	20:1
Power Dissipation	32.4 watts	32.4 watts	45 watts

As can be seen this data is exceptionally good and each of the goals of this program was exceeded.

Definition of the above terms are given below:

1) Transmission $= \frac{P_{out\ ave}}{P_{in\ ave}} \times 100$

2) Static Extinction Ratio $= \frac{P_{out\ ave}\ (all\ 1's)}{P_{out\ ave}\ (all\ 0's)}$

3) Dynamic Extinction Ratio $= \frac{\text{Minimum 1 level in optical pulse train}}{\text{Maximum 0 level in optical pulse train}}$

4) Power Dissipation - electrical power necessary to operate the modulator in its normal mode of operation.

Table III lists the modulator characteristics for this program as compared to the achieved performance characteristics of the 400 Mbps double-pass laser modulator delivered under program NAS5-11474. In addition to the improved performance of the single-pass concept over that of the double-pass, new techniques have been developed which improve the performance of the single-pass unit. The first improvement was that of separately matching the crystals; this results in faster crystal response. The second technique was that of strain relieving the $LiTaO_3$ crystal which was developed under an in-house program approximately three years ago. Using this strain relief process, the entire aperture of the crystal can be utilized without loss in extinction ratio. This uniform extinction ratio is due to achieving a uniform retardation pattern which implies the absence of index of refraction anomalies. The last improvement was the focusing of the optical signal onto the photodiode for AEC circuitry signal enhancement. This approach resulted in a gain of six in the signal input to the gate of the AEC circuitry which imrpoved the compensator holding performance due to increased signal/noise ratio in the AEC detector.

The mechanical design of the modulator assembly was to retain simplicity, ease of alignment while keeping electrical power consumption low. The modulator assembly was as compact as crystal dimensions and heater efficency would allow. The unit consumed less heater power due to fiber glass insulation surrounding the oven core. A removable beamsplitter was inserted in the optics tail for a simple change between operation with PGBM and PPBM modulation formats. The modulation and electronic packages were

TABLE III

400 Mbps 1.06 Laser Modulator Characteristics

Characteristic	Double Pass Mod (NAS5-11475)	Single Pass Mod (NAS5-20605)
Transmission	50%	70%
Depth of Modulation	> 97%	100%
Extinction Ratio		
Static	> 30:1	65:1
Dynamic	> 13:1	30:1
Power Dissipation	30 Watts	32.4 Watts
Crystal Length	10 mm	20 mm
Crystal Cross Section	.3 x .3 mm	.27 mm tapered to .23
Crystal Capacitance	4.7 pf/crystal	10.1 pf/crystal
Switching Voltage	30V	28V

separated by a 1.33 meter cable. The separation of the laser modulator into two major assemblies permitted the electro-optic modulator assembly to be precisely aligned in the optical path of the laser beam and the transmitter optics, while the electronics assembly may be remotely located with the remainder of the transmitter electronics.

2. TECHNICAL DISCUSSION

The 400 Mbps modulator was designed to accept 400 Mpps optical input from a mode-locked fundamental frequency Nd:YAG laser and a 400 Mbps low level electrical input signal composed of a 400 Mbps pseudorandom data channel for the modulator driver input and a 400 MHz clock signal to drive the Manchester code for the automatic electronic compensator (AEC) circuitry. The modulator consisted of a modulator assembly, a modulator electronics assembly, and a modulator electronics laboratory power supply. A block diagram of the modulator (less the power supply) is shown in Figure 1. The modulator was a single-pass 1.06 μm wideband laser modulator mounted onto an "L" bracket which was attached to a Huber camera mount for fine alignment of the modulator to the laboratory input laser beam. The laser beam passes straight into the modulator assembly through the two crystals, the beamsplitter pellicle and then out (as shown by the dashed line); also shown in modulator assembly are the heater, thermistor, matching networks, and the compensator's polarizer, lens and avalanche photodiode; the input and output lens are not shown.

The heater receives power and control from the temperature controller with the thermistor used as the sense element for a closed loop control system to control the crystals oven to the proper operating temperature. The thermal differential compensator is a manual adjustment to produce a small unbalanced heating in each half of the oven heater. Unbalanced heating provides compensation by using the thermal characteristics of the crystals.

The binary modulator input signal (400 Mbps pseudorandom data) is amplified by the modulator driver (Module E) and provides two complementary output to drive the crystals through the matching network, the broadband load (Module D) provides the final load termination for the driver.

The electronic compensation is applied to the crystals by a differential output bias voltage amplifier through the broadband load and matching network. Slow frequency dither oscillator signal is also summed with one side of the bias voltage and applied to the crystals. The beamsplitter monitors a portion of the output beam; the laser pulses are detected with the photodiode, amplified by a R.F. pulse amplifier, and passed through an electronic

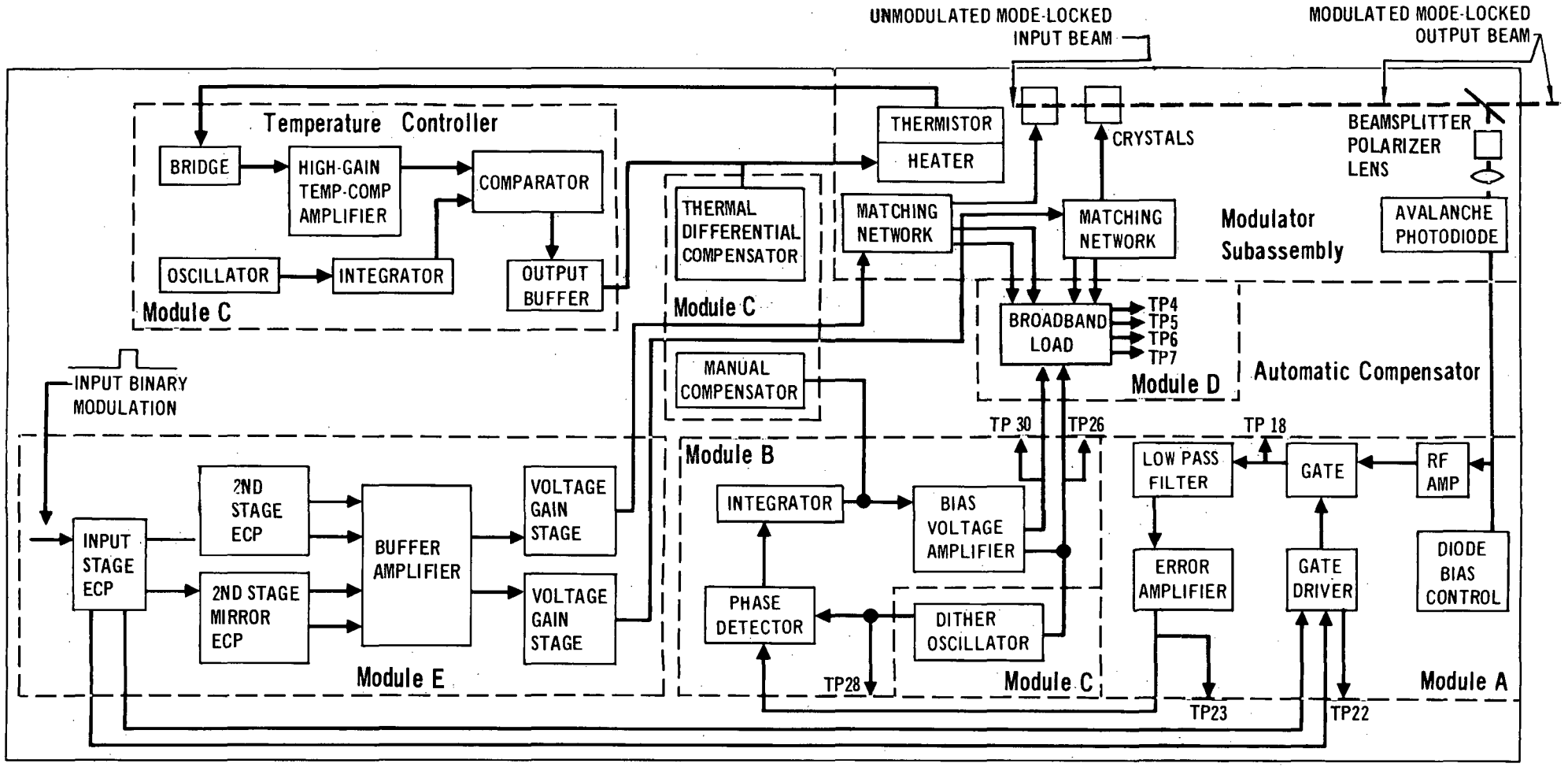

FIGURE 1 MODULATOR FUNCTIONAL BLOCK DIAGRAM

gate circuit where ambiguous states are resolved. The gate drive signal is a data synchronized signal from the modulator driver. The dither signal is recovered from the laser pulses at the low pass filter amplified as an error signal, passed through a phase detector (comparing recovered phase with initial oscillator phase), amplified again with an integrating amplifier and applied as an input to the bias amplifier with a phase that will change the compensator bias in a direction to reduce the recovered dither signal and thus provide a better operating point. Manual compensation is accomplished by turning off power to the error and integrator amplifiers and applying power to a manual controlled potentiometer used as the input to the bias amplifier. The compensator temperature controller, driver, and broadband load modules are located in the modulator electronics package.

The paragraphs which follow contain a more detailed discussion and description of the modulator crystals, the modulator assembly, associated electronics assembly, laboratory power supply, and mechanical design.

2.1 CRYSTAL MATERIAL EVALUATION. The 20 mm crystal slabs were received and evaluated during this contract. A number of measurements were performed on the crystals for thorough evaluations of expected performance. The specific tests conducted on the crystal slabs included microscopic examinations (using both a laser and stereoscopic microscope), near field retardation patterns, Schlieren examination, far field extinction patterns, optical absorption, and transmission measurements. The bulk of the effort was directed toward measuring those properties which have the greatest impact on high speed modulation design. The tests and test results are discussed in the order listed above.

Figure 2a shows a schematic of the experimental arrangement used for the laser microscopic examination. To detect striations, the crystal was viewed in transmitted polarized laser light. The light source was apertured to pass paraxial rays and was polarized either parallel or normal to the z-axis of the crystal. The striations were readily visible under such viewing conditions. The spacing and regularity of growth striations were readily determined in this manner. Inclusions, cracks, line defects, and other refractive index anomalies were readily detectable in a similar

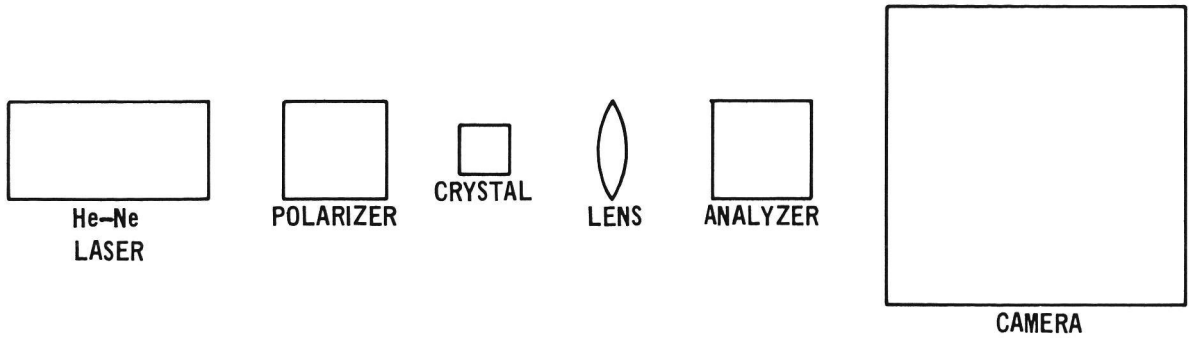

CRYSTAL CAN BE EXAMINED BY POLARIZED LIGHT EITHER PARALLEL OR NORMAL TO THE C-AXIS OF THE CRYSTAL. THE EXTINCTION RATIO CAN BE DETERMINED BY CROSSING THE POLARIZER AND ANALYZER FOR BOTH THE ORDINARY AND EXTRAORDINARY LIGHT.

FIGURE 2a SCHEMATIC FOR MICROSCOPIC EXAMINATION

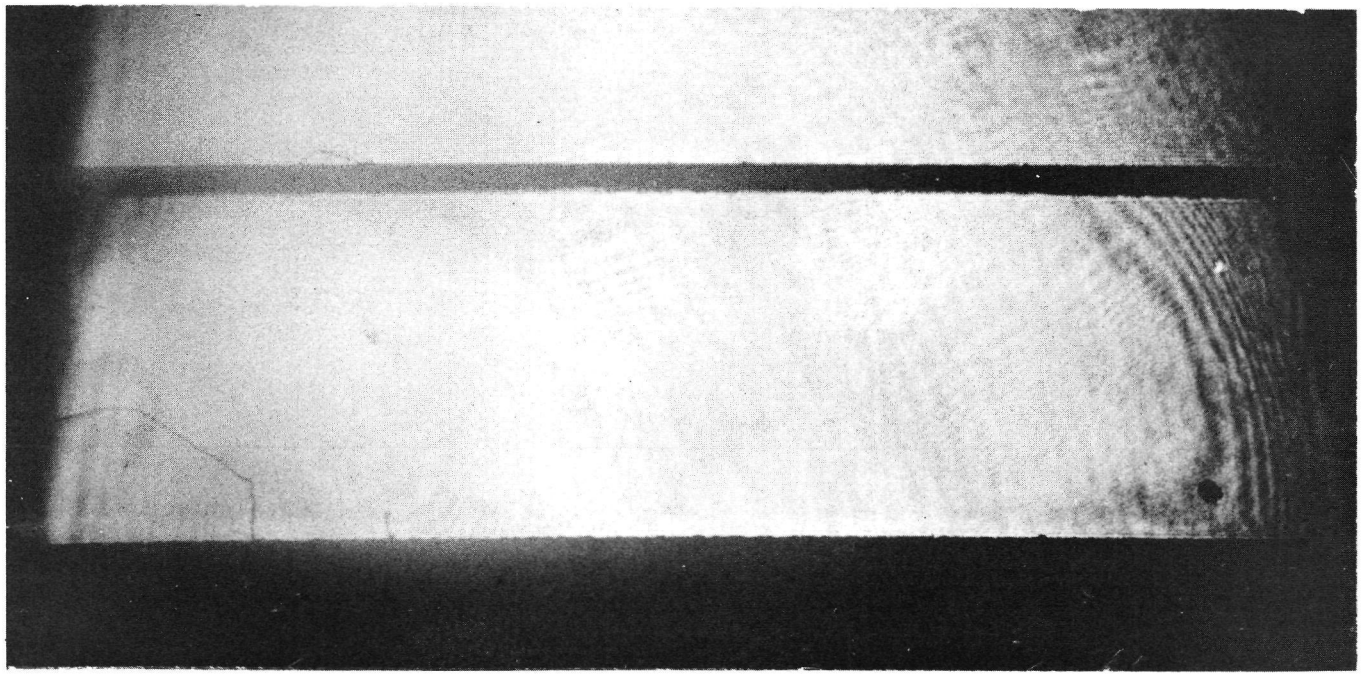

FIGURE 2b MICROSCOPIC EXAMINATION PHOTOGRAPH OF A 20 mm CRYSTAL SLAB

manner. Any scattering sites scattered light and any refractive index anomalies produced detectable wave front distortion. By changing the polarization it was possible to identify the affected index as ordinary or extraordinary. Surface quality was also determined during this examination.

Figure 2b is a photograph resulting from the laser microscopic examination of a crystal slab. From this photograph it was seen that the material was free of local refractive index anomalies, and other crystalline defects of a potentially serious nature. The fringes around the periphery were wavefront distortion due to change in crystal width of the slab. This change in the width of the slab was in the b-axis direction and occurred as the light propagated down the optical axis, i.e., the slab was not orthorhombic.

Other microscopic evaluations consisted of examining the laser polished surfaces under a stereoscopic microscope to estimate the frequency of pits, scratches, streaks, and other surface polishing defects. This microscopic examination permitted accurate evaluation of the surface polish and also optical coating quality. This evaluation of uncoated crystal surfaces was necessary for transmission studies, etc. A photograph of a crystal surface is shown in Figure 3.

Near-field examinations were done on each crystal slab to assess modulator material quality. The apparatus used for this test is shown in Figure 4a. The polarizer was oriented at 45° to the c-axis of the crystal while the fast axis of the compensator was oriented parallel to the c-axis. When the analyzer was oriented parallel to the c-axis of the specimen, the image represented the near-field distribution of the extraordinary light transmitted by the crystal. When the analyzer was oriented perpendicular to the c-axis of the specimen, the near-field distribution of the ordinary transmitted light was observed. When the analyzer was at either +45° or -45° to the c-axis of the crystal, the near-field retardation pattern was observed. Examination of both large aperture and small aperture specimens was performed using the equipment described. The image was magnified several times and was several centimeters in width at the camera back.

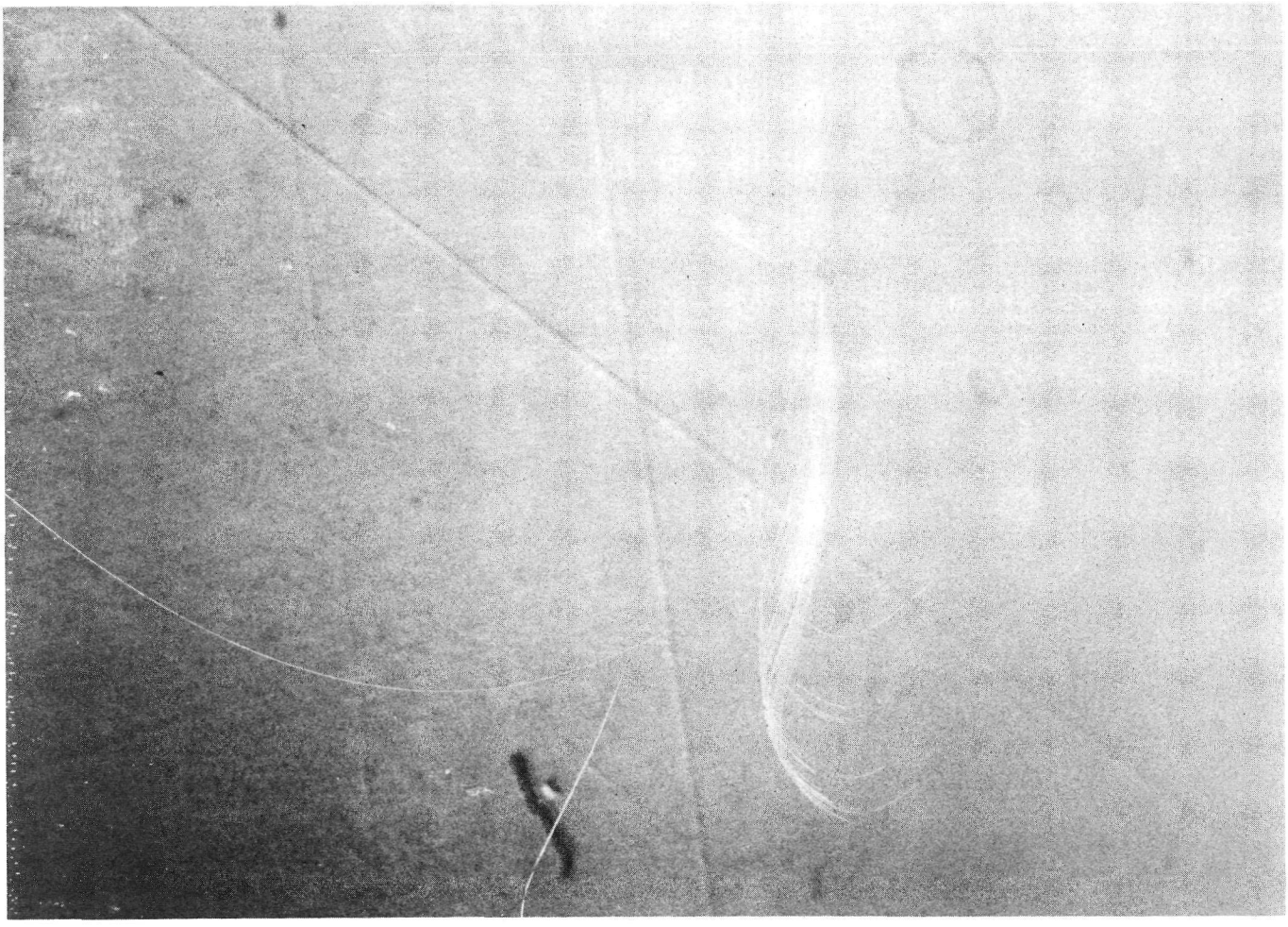

FIGURE 3 MICROSCOPIC EXAMINATION OF A CRYSTAL SURFACE USING A STEREOSCOPIC MICROSCOPE

The most useful camera for crystal evaluation work was a Graflex unit with a focal plane shutter. Figure 4b shows a retardation pattern for one of the crystalline slabs. From this photograph the birefringence of the crystal slab was found to be rather uniform. Since the b-axis width was 18 mm and the c-axis width was 4 mm, several modulator crystals can be fabricated from the region where the birefringence was uniform. The fringes in the periphery were wavefront distortions from surface non-parallelism since the b-axis width was not constant along the optical axis (the slab is tapered) as mentioned before.

Each slab was examined by the Schlieren technique. A block diagram of a Schlieren examination is shown in Figure 5a. In the Schlieren examination a large diameter Gaussian beam from an HeNe laser was passed through a crystal and the rear face of the crystal was imaged onto a card or camera back by a suitable lens. An optical knife edge was then inserted at the focal point of the lens from different directions. As the focused spot was apertured off, the only light arriving at the screen was due to large angle forward scattering from various scattering sites or defects. This technique revealed surface scattering, striations, inclusions, line defects, and surface wedging. Moreover, the polarization dependence of the scattering sites was readily determined and quantitive estimates of scattering losses can be made. Figure 5b shows a Schlieren examination photograph for one of the lithium tantalate slabs. As seen in the photograph there was no internal scattering sites in the material. The bright line which was seen was a cleaning fiber on the surface of the crystal. This shows how easily scattering sites, line defects and other crystal imperfections were observed.

The extinction ratio achievable with the bulk crystal was measured for the slab material. A block diagram for focused extinction ratio tests is shown in Figure 6a. The extinction ratio of a modulator, which is the ratio of the maximum transmitted power to the minimum transmitted power when the modulator is switched, is one of its most significant optical parameters. The extinction ratio was therefore measured in several ways, always using TEM_{∞} laser power. The specific methods for measuring passive extinction ratio were:

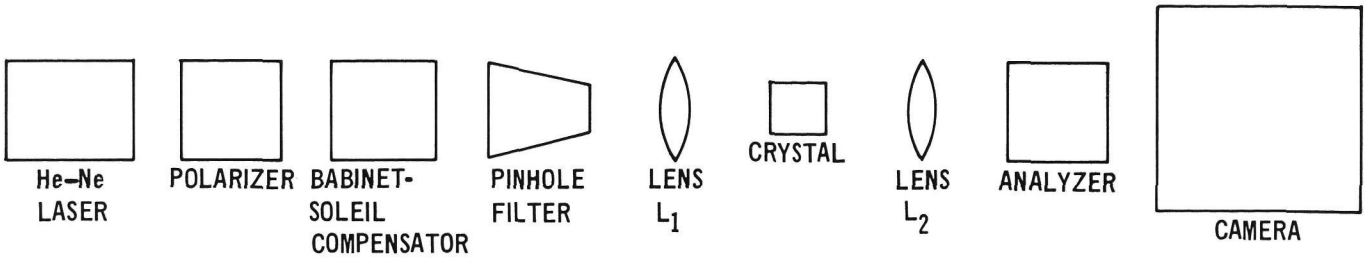

THE INSTRUMENTATION IS SIMILAR TO THAT USED IN THE BEAM DEGRADATION TESTS.

THE SECOND LENS, L_2, IS USED TO FORM AN IMAGE OF THE EXIT CRYSTAL FACE ON A CAMERA BACK.

THE POLARIZER IS ORIENTED AT $+45^0$ TO THE C-AXIS OF THE CRYSTAL AND THE COMPENSATOR IS ORIENTED PARALLEL TO THE C-AXIS.

IF THE ANALYZER IS ORIENTED PARALLEL TO THE C-AXIS OF THE CRYSTAL, THE IMAGE REPRESENTS THE NEAR FIELD DISTRIBUTION OF THE EXTRAORDINARY LIGHT TRANSMITTED BY THE CRYSTAL.

IF THE ANALYZER IS ORIENTED PERPENDICULAR TO THE C-AXIS OF THE CRYSTAL, THE NEAR FIELD DISTRIBUTION OF THE ORDINARY TRANSMITTED LIGHT IS OBSERVED.

WHEN THE ANALYZER IS AT EITHER -45^0 OR $+45^0$C TO THE C-AXIS DIRECTION, THE NEAR FIELD RETARDATION PATTERN IS OBSERVED.

FIGURE 4a SCHEMATIC FOR NEAR FIELD EXAMINATION

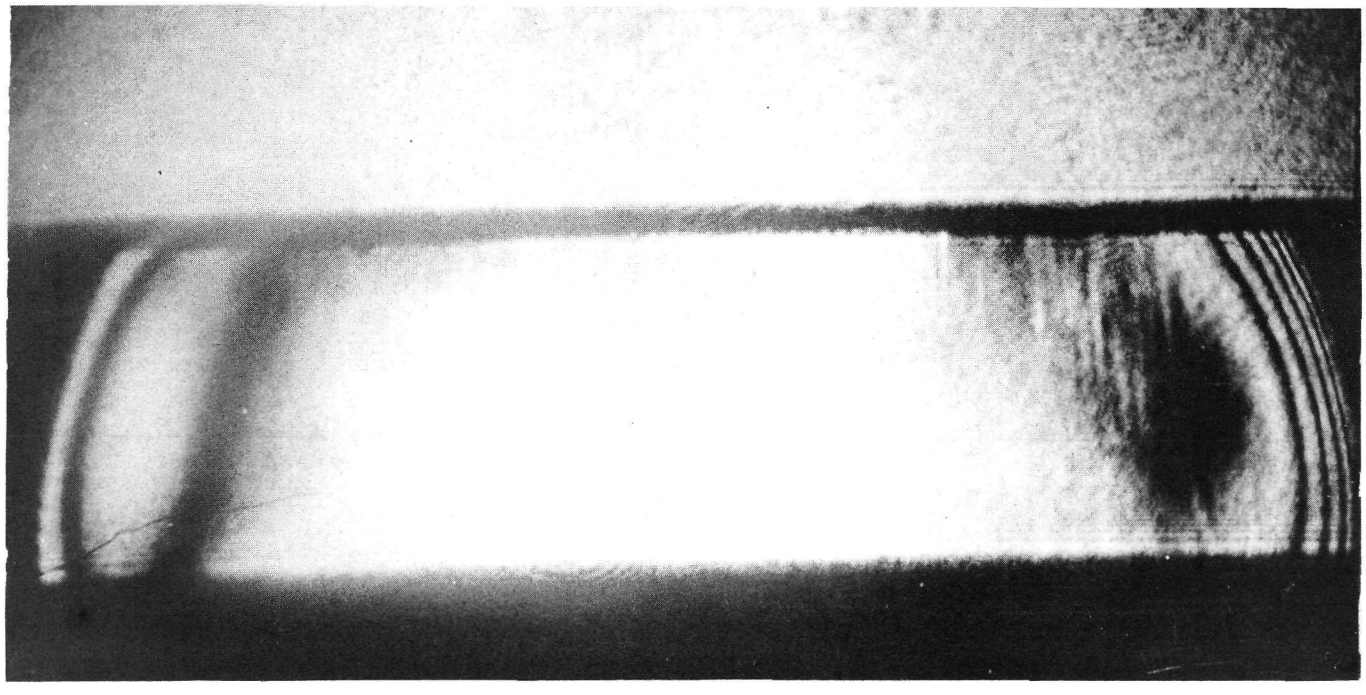

FIGURE 4b NEAR FIELD RETARDATION PATTERN FOR A 20mm CRYSTAL SLAB

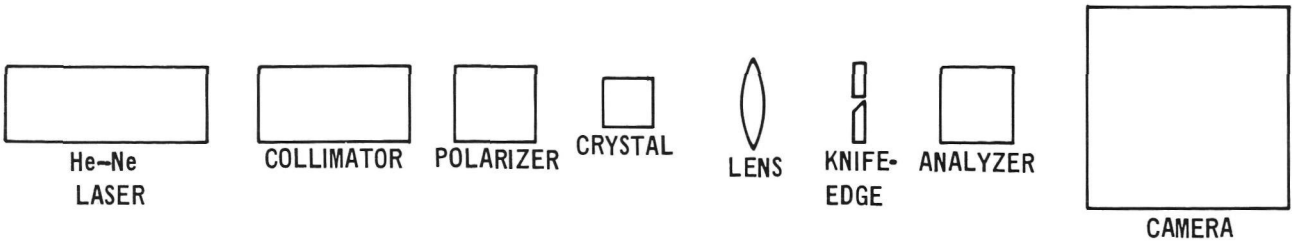

THE POLARIZER AND ANALYZER HAVE PARALLEL ORIENTATION AND THE EXAMINATION ARE DONE WITH THE POLARIZER AND ANALYZER BOTH PERPENDICULAR AND PARALLEL TO THE C-AXIS OF THE CRYSTAL. THIS MEANS THAT THE CRYSTAL IS EXAMINED IN EXTRAORDINARY LIGHT (E11C-AXIS) AND ORDINARY LIGHT (ELC-AXIS)

FIGURE 5a SCHEMATIC OF SCHLIEREN EXAMINATION

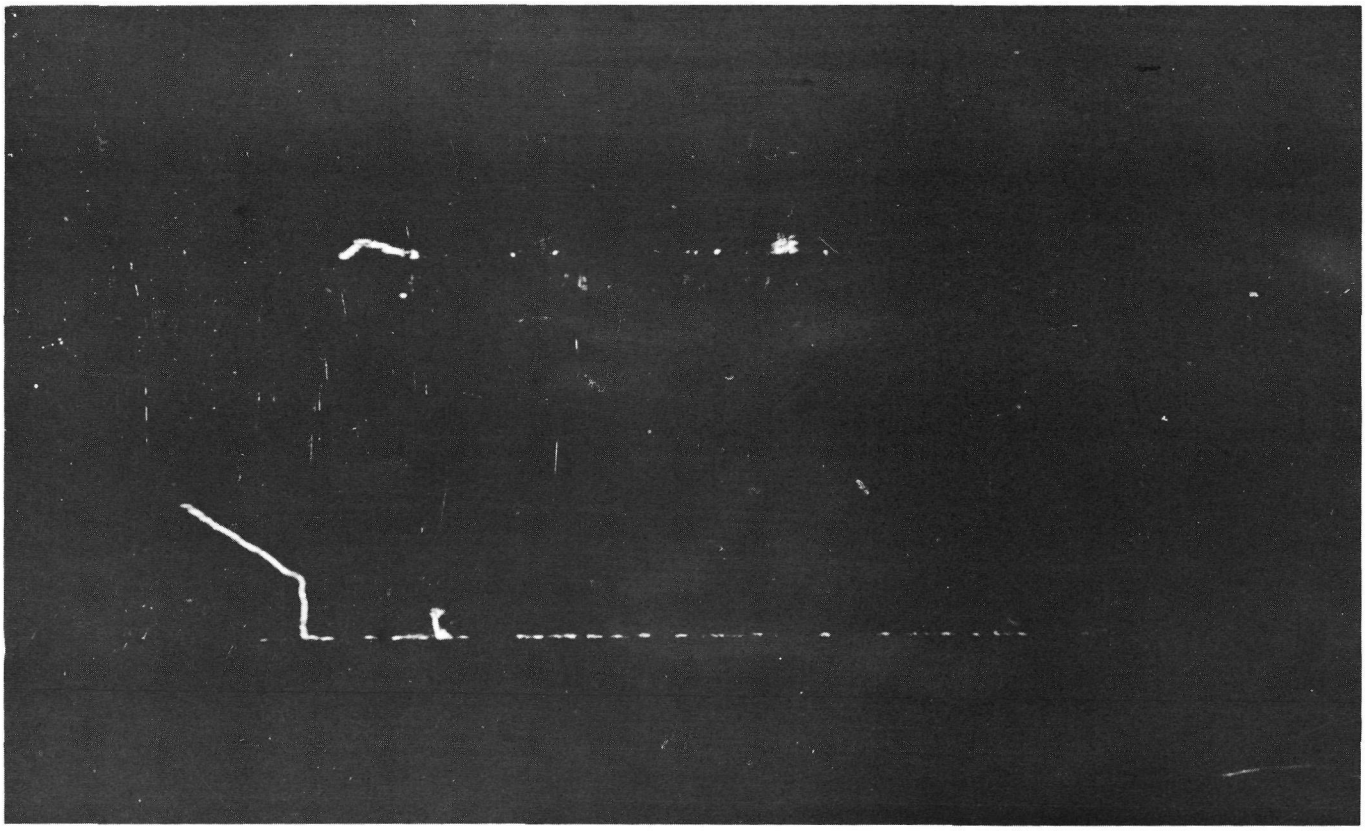

FIGURE 5b SCHLIEREN EXAMINATION PHOTOGRAPH
OF A 20 mm CRYSTAL SLAB

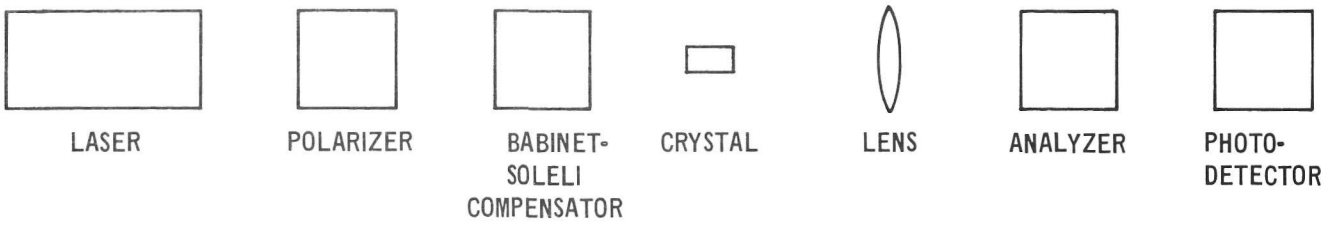

THE BEAM EMERGING FROM THE CRYSTAL IS COLLECTED BY THE LENS AND IMAGED ON A LARGE APERTURE PHOTODETECTOR. THE POLARIZER AND ANALYZER ARE ORIENTED $+45^0$ AND -45^0 TO THE C-AXIS OF THE CRYSTAL RESPECTIVELY. THE COMPENSATOR IS ORIENTED PARALLEL TO THE C-AXIS OF THE CRYSTAL SPECIMEN.

FIGURE 6a SCHEMATIC FOR FOCUSED EXTINCTION RATIO TESTS

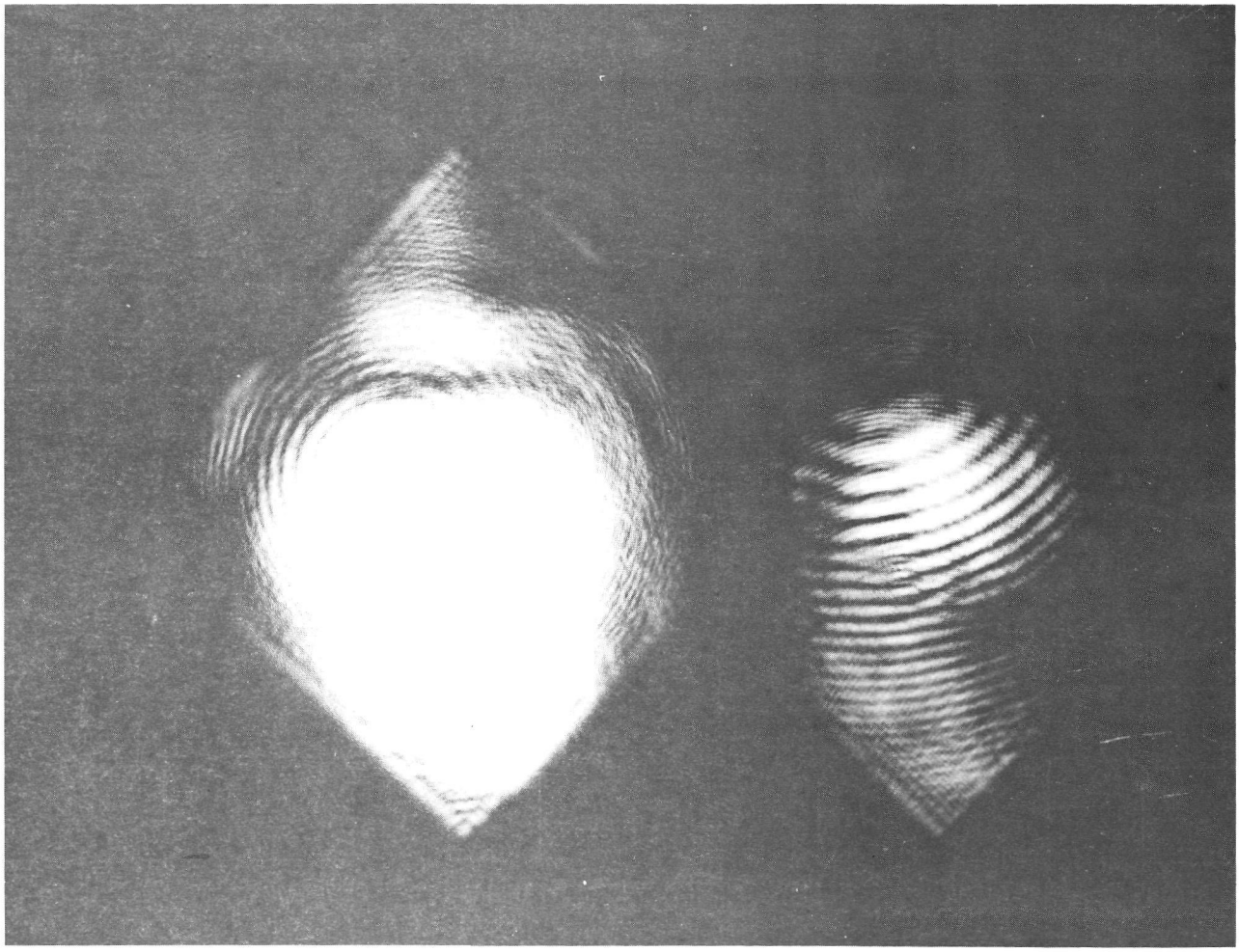

FIGURE 6b FOCUSED EXTINCTION IN A 20mm CRYSTAL SLAB
(20dB EXTINCTION RATIO)

(1) Focused Near-Field Measurement - The image of the laser spot on the exit face of the crystal was imaged on a large aperture photodetector. The ratio of the maximum transmitted power to the minimum power was measured as the compensator is adjusted.

(2) Total Transmitted Extinction Ratio Measurement - The beam emerging from the modulator crystal was collected by a suitable lens and imaged on a large aperture photodetector. The ratio of the maximum transmitted power to the minimum transmitted power was then measured as the compensator was adjusted.

(3) Far-Field Gaussian Extinction Ratio Measurement - The transmitted beam was passed through a pinhole spatial filter. The filtered Gaussian beam was collected by a lens and focused on a photodetector. The ratio of the maximum transmitted power to the minimum transmitted power was then measured as the compensator was adjusted. The insertion loss of the filter was also measured.

The most important extinction ratio measurement from the viewpoint of system performance was the far-field Gaussian extinction ratio. Normally this value was higher than the total transmitted extinction ratio, since most of the total transmitted power leakage was not in the far field Gaussian beam.

We measured the total transmitted extinction ratio for our samples and it varied from 80:1 for each of the two slabs that come from the boule edge to 120:1 for each of the two central slabs from the boule. Figure 6b is a photograph showing the passive extinction ratio of one of the two central slabs from the boule.

The optical evaluation results of the four slabs showed that the two from the central portion of the boule have the best optical quality. Therefore the modulator crystals were fabricated from the two central boule slabs.

Optical transmission measurements were made using a 1.06 μm laser, a Bausch and Lomb monochromator set for 1.06 μm light output, and a Beckman DK-2 spectrophotometer. The laser light was detected with a photodetector and was first measured with the crystal out of the beam path and then

measured with the crystal inserted into the beam path. The transmission through the $LiTaO_3$ crystal measured 73.5% at normal incidence and greater than 97.5% at Brewster's angle. The loss at Brewster's angle was indicative of scattering loss; therefore, the crystal surface polishing could have been better. However, this was the value which we generally measured for $LiTaO_3$ at Brewster's angle with Crystal Technology Inc. (CTI) laser polished surfaces. At normal incidence, since the polished surfaces were uncoated, Fresnel losses were present which limited the expected transmission to a maximum value of 75.6% (73.5% measured). Therefore, there was an additional measured loss of 2.1%. From the microscopic examination it was noted that the polished surfaces had some scratches and pits which perhaps caused the 2% additional loss. Again, it should be emphasized that these were the values which were generally measured for most CTI $LiTaO_3$ material.

Figure 7 is an optical transmission plot for an $LiTaO_3$ slab from the center of the boule. This wavelength versus transmission plot was taken using a Beckman DK-2 spectrophotometer. In the 1.06 μm region, the crystal had very little absorption. The reason for the differences in the transmission levels between the reference and the sample spectra were Fresnel losses which is reflection of light from the uncoated crystal polished faces. The optical evaluations showed that the optical quality of the $LiTaO_3$, from which the 1.06 μm wideband laser modulator was fabricated, was good.

2.2 FABRICATED MODULATOR CRYSTAL EVALUATION. Several $LiTaO_3$ modulator size crystals were evaluated to determine what minimum size should be used in the modulator for optimum transmission and extinction ratio. The modulator crystal sizes used were 0.25 mm x 0.20 mm cross section, 0.27 mm x 0.20 mm cross section, and crystals with 0.27 mm x 0.27 mm cross section tapered to 0.27 mm x 0.23 mm cross section. The best transmission achieved was 71.5% for the tapered crystal using a 1.06 μm Nd:YAG laser source. The static extinction ratio for this crystal was only 40:1. However, at the time of these measurements the crystal was neither strain relieved nor AR coated.

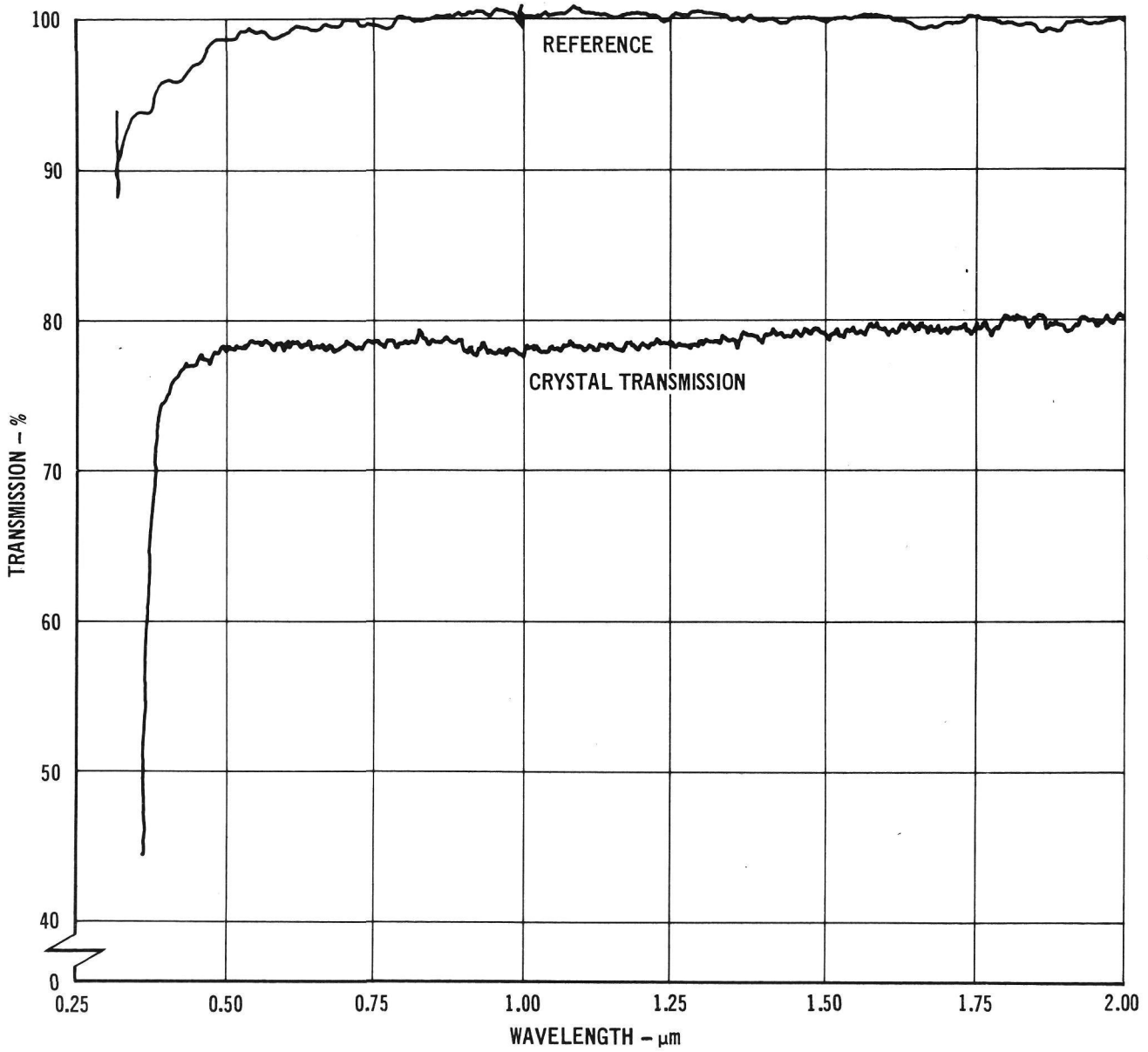

FIGURE 7 TRANSMISSION VERSUS WAVELENGTH FOR $LiTaO_3$ CRYSTAL SLAB

From this data it was decided that the modulator would be fabricated from crystals with a cross section of 0.27 mm x 0.27 mm tapered to 0.27 mm x 0.23 mm. The crystals were tapered in the c-axis which enabled the switching voltage to be minimized while maintaining optimum performance. The switching voltage for the modulator using the above size crystals should be 28 Vdc. Having determined the crystal modulator size to be used, fabrication of the modulator crystals began.

Several modulator size crystals were examined for surface quality and surface periphery squareness using a stereoscopic microscope. A photograph of a crystal surface is shown in Figure 8a and crystal edge roughness is seen in Figure 8b. From these photographs decisions were made to strain relieve certain crystals for modulator fabrication. Crystal discrimination judgements were based on surface quality such as pits, stratches, streaks and other surface polishing defects. This microscopic examination of modulator size crystals permitted accurate evaluation to determine their usefulness as a possible modulator element. If many defects were found, or if only a few were located in the center of the crystal face, the transmission would be degraded and hence, the crystal was not usable. If the crystal surface periphery was rough this resulted in low transmission due to scattering (low safety factor). This examination was critical for this modulator development as the safety factor was low ($\sim$ 1.6) which restricts the movement of the crystal relative to the input beam to miss any surface defects.

After the crystals had been cut to modulator size and microscopic examinations completed (including surface photographs), crystals were chosen on the basis of their surface figure merit for strain relieving. The procedure for modulator crystal fabrication then included the following steps. After strain relieving, the crystals were examined in a laser beam for transmission. The crystals with the highest transmission were AR coated. Transmission measurements were made also after AR coating. The crystal was then electroded, soldered to an electrode and mounted in a boron nitride pill. After pill mounting, the crystals were outgassed in a vacuum at 160°C. The crystals were then checked for transmission and the best were step pill mounted and flat pill mounted. Crystals were aligned in a laser beam and oven mounted. After oven

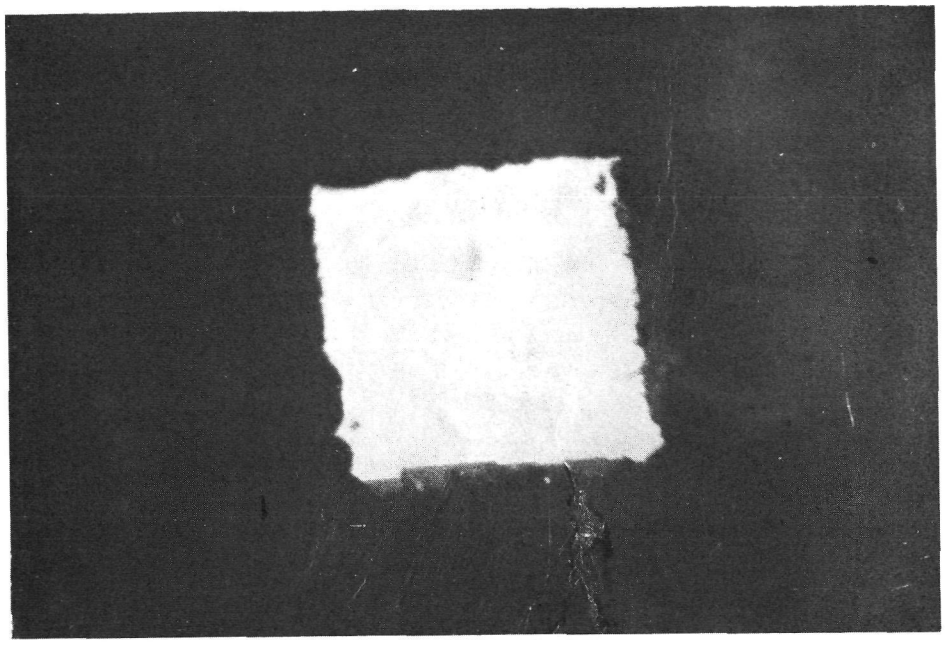

(A) ACCEPTABLE CRYSTAL:
SURFACE FIGURE SMOOTH
AND CRYSTAL EDGE SHARP

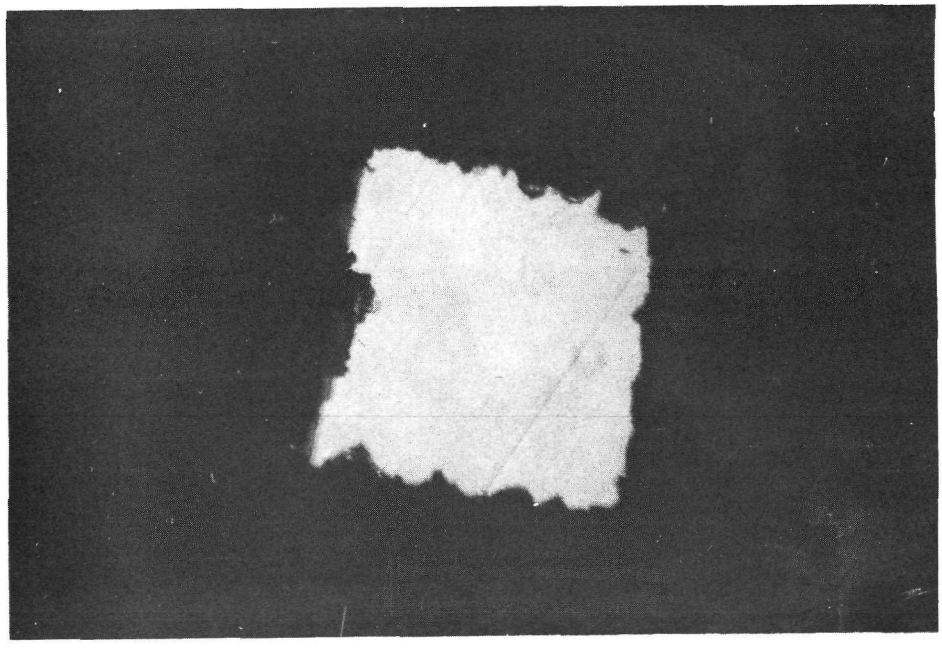

(B) UNACCEPTABLE CRYSTAL:
EDGE TOO ROUGH AND
SCRATCHES ON SURFACE

FIGURE 8 MICROSCOPIC EXAMINATION OF MODULATOR SIZE CRYSTALS

mounting the crystal pills, the oven core was outgassed. Then the oven core was assembled into the modulator oven housing and impedance matched. This concluded the fabrication of the modulator crystals and oven housing.

Care had to be taken in every step to optimize transmission, static extinction ratio, and dynamic extinction ratio. The crystals were kept in a laminar flow bench when not in use to prevent particles of dust from contacting AR coated faces.

2.3 CRYSTAL ANTIREFLECTION (AR) COATING EVALUATION. The modulator crystals were fabricated as described above from larger crystals of lithium tantalate, and the crystal faces were antireflection (AR) coated with a single layer of silicon dioxide to reduce surface reflections. Vapor deposited silicon dioxide (SiO_2) AR coating for lithium tantalate ($LiTaO_3$) was studied to determine the optical properties and aging. A thin film of SiO_2 was deposited onto a piece of $LiTaO_3$ using a commercial electron ("e") beam evaporator enclosed in a vacuum chamber and a film deposition rate of $10\text{Å}\cdot s^{-1}$. The $LiTaO_3$ substrate was held at a temperature of 200°C during the deposition period. Ellipsometric measurements were made immediately after depositing the film to determine the refractive index and thickness. The sample was then mounted in an oven and heated to a temperature of 150°C and held at that temperature for 111 hours. The sample was then removed and the film properties measured to determine the degree of aging. The results of these measurements are shown in Table IV. These measurements indicate that the film is somewhat oxygen-deficient since the initial refractive index is larger than that of bulk fused silica (n = 1.46) and the fact that aging reduced the value of the refractive index. Although the vapor deposited SiO_2 film did age, the degree of aging was much smaller than exhibited by ThF_4 thermally aged for a similar period of time.

TABLE IV

Summary of Ellipsometric Measurements*

Property	Initial Measurements	Measurement After 111 Hrs.	Change %
Thickness (Å)	1675	1703	+1.6
Refractive Index	1.486	1.474	-0.8

*These measurements were made using an He-Ne laser (λ = 6328Å).

Silicon dioxide antireflective coatings were used for the 1.06 μm modulator crystal for the following reasons:

1) It provided a very low reflectivity (best match to $LiTaO_3$ at 150°C for the 1.06 μm wavelength).
2) The coating was more chemically stable than ThF_4 at 150°C.

The SiO_2 coating was reliably deposited on $LiTaO_3$ of correct thickness for minimum reflectivity. The measured reflectivity of less than 0.1% using the SiO_2 AR coating deposited on $LiTaO_3$ using a 1.06 μm laser beam indicated that this was a good index match. Finally, as mentioned beforehand, the film stability appeared to be better than ThF_4 which was the only other known single layer quarter wave material match for $LiTaO_3$ currently feasible.

2.4 MODULATOR ASSEMBLY. The modulator assembly consisted of the modulator oven with the crystals, heater, thermistor, and matching network; the optics tail with the pellicle, polarizing beamsplitter, lens, and automatic compensator photodiode; and the front and rear lens holders. A cutaway drawing of the modulator subassembly is shown in Figure 9. As shown in the figure the modulator assembly utilized two high quality lithium tantalate crystals as the modulating material. The lithium tantalate used in these modulators was grown by Crystal Technology, Inc.

2.4.1 Oven Assembly. Each of the modulator crystals were 20 mm in length and were fabricated to have cross-sectional dimensions of 0.27 mm x 0.27 mm tapered to 0.27 mm x 0.23 mm with the tapered direction being the c-axis of the crystal. Tapering the c-axis of the crystal reduced the switching voltage by approximately 8% for these dimensions from that of a 0.27 mm x 0.27 mm cross-sectional crystal.

The modulator crystals were oriented in a crossed axes configuration as shown in Figure 10, and the linearly polarized, pulsed, input laser beam entered the modulator through the input lens as shown in Figure 9 and passed through the crystals whose longitudinal axes were parallel to the light beam. These crystals were aligned so that the input optical beam entered the crystals polarized at 45° with respect to the crystal axes. In this configuration, the input light beam was divided equally into the two polarizations within the crystal, i.e.,

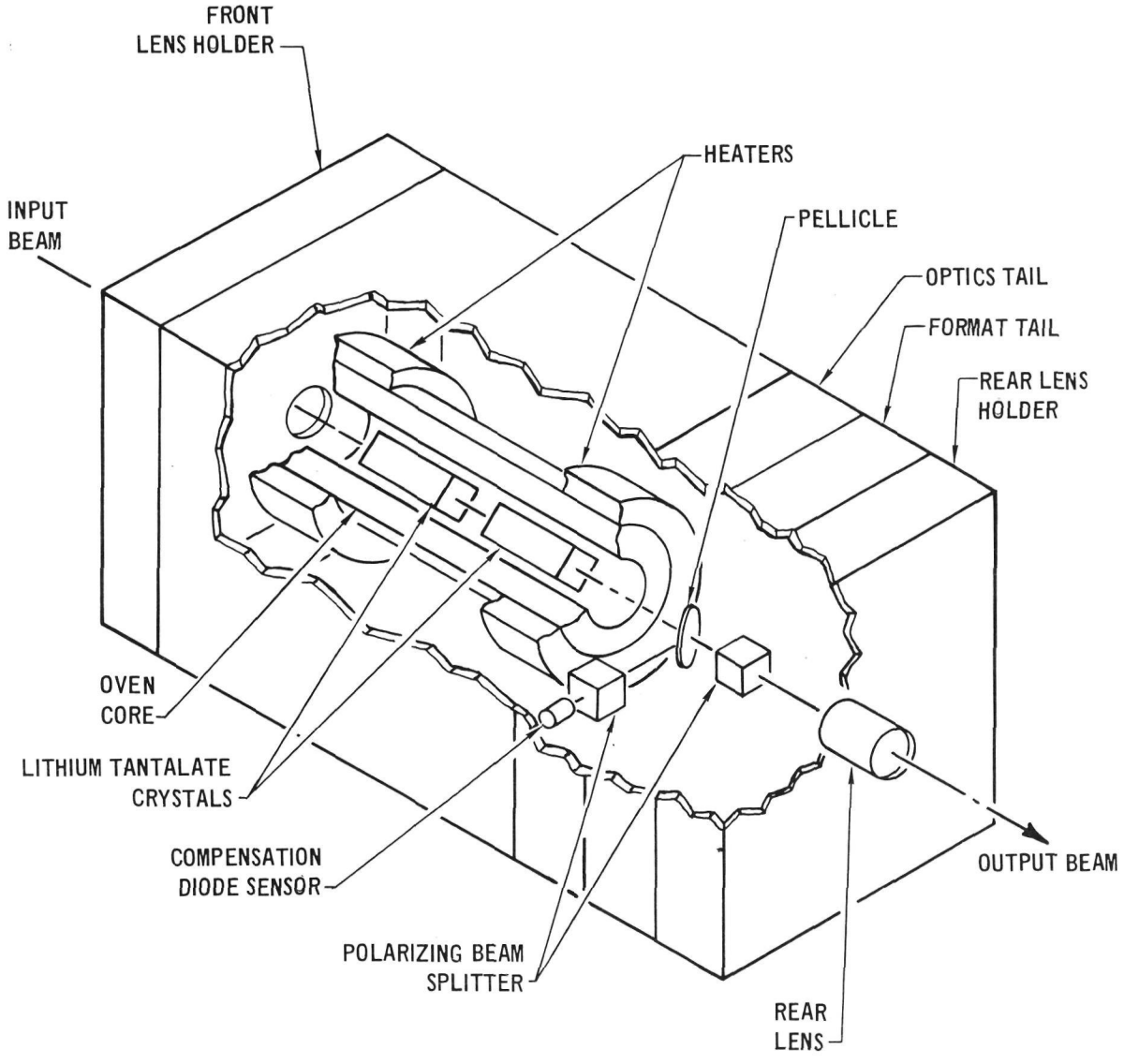

FIGURE 9 MODULATOR ASSEMBLY CUTAWAY VIEW

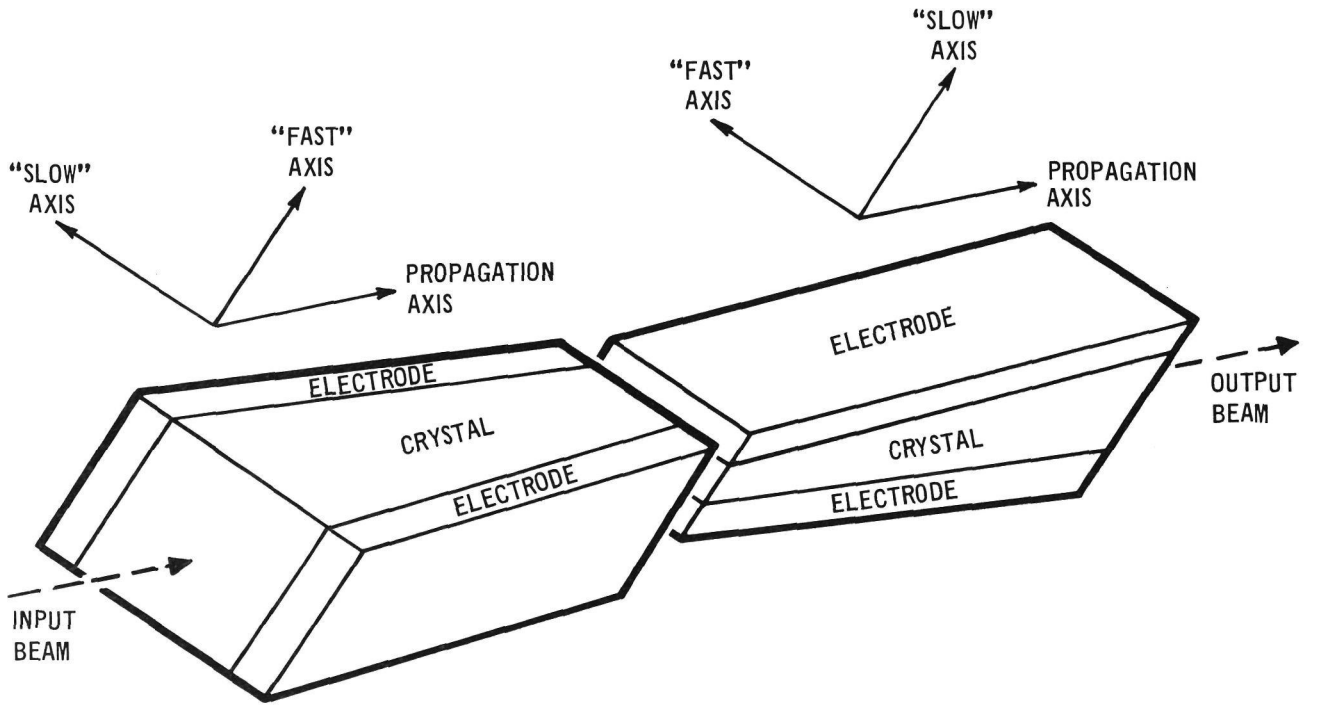

FIGURE 10 CROSSED-AXES TAPERED CRYSTAL MOUNTING ARRANGEMENT

ordinary wave and extraordinary wave. The two crystals were oriented so that their axes were crossed. The light which traveled as O-wave light in the first crystal traveled as E-wave in the second crystal. Similarly, light which traveled as E-wave light in the first crystal traveled as O-wave light in the second crystal. When the two crystals are identical in length as they were when cut from a single piece of material the total optical length traversed by each polarization was identical, provided that each crystal was at the same temperature. This provided cancellation of most of the natural birefringence of the crystals so that the control range required by the automatic electronic compensator and the accuracy of control required by the temperature controller were reduced by approximately two orders of magnitude.

The modulator crystals modulated the incident light beam by rotating the incident polarization in response to the voltage supplied by the modulator driver via the matching network. The modulation process can be explained using the illustration presented in Figure 10. Metal electrodes were applied to opposite sides of each crystal, so that an electric field can be applied. Light polarized parallel to the direction of the applied field, i.e., along the z-direction, traveled at a slower rate than light polarized perpendicular to the applied field (extraordinary and ordinary light, respectively). The net retardation of the slow wave depended upon the exact difference between the ordinary and extraordinary refractive indices. The net retardation can be changed slightly by an applied field through the linear electrooptic effect (Pockel's effect). The input beam was polarized at 45° to the applied field so that equal ordinary and extraordinary components were produced. If the net retardation between the two components was an even multiple of π radians upon completing a single pass through the crystals, the emerging light was polarized the same as the input. However, if the net retardation was an odd multiple of π radians, the emerging light was polarized at 90° to the incident light. By adjusting the crystal birefringence, the crystal could be made to induce no change for no modulating voltage, and a 90° rotation for the full switching voltage. The polarizing beam-

splitter prism in the optics tail acted as an analyzer to convert the polarization modulation to amplitude modulation at the output for a PGBM format. However, if a polarizing beamsplitter prism was used exterior to the modulator package, both polarizations could be transmitted and data acquired at the receiver in the PPBM format.

The process of adjusting the crystal birefringence to the desired operating point is termed "optical compensation." The term "optical bias" is sometimes used to describe this phenomena because it is analogous to the bias setting of a transistor or vacuum tube in order to establish a quiescent operating point. In lithium tantalate (and a number of other similar electrooptic materials) the crystal birefringence was a function of both the voltage applied to the crystal and crystal temperature. Optical compensation produced by an applied voltage had been termed "electronic compensation," and optical compensation produced by a temperature change or differential had been termed "thermal differential compensation." Both types of optical compensation were used in the modulator fabricated for this program. These compensation modes are discussed in Section 2.10.

The crystals were soldered to copper electrodes. The solder was pure tin, and the soldering operation was performed in a vacuum. One crystal was mounted in a flat configuration in which the electrode came in from the side. It mounted between two flat boron nitride pills. The other crystal was placed between two similar electrodes, one above and one below the crystal. The electrodes used in both mounting configurations had the same design. The boron nitride pills used for mounting this crystal had a step of height equal to the crystal and electrode thickness. The pills were attached to the electrodes with an RTV cement. The pills were then optically aligned in the oven core and cemented in place in the same manner. Figure 11 shows an exploded view of the crystal oven which illustrates the crystal mounting components.

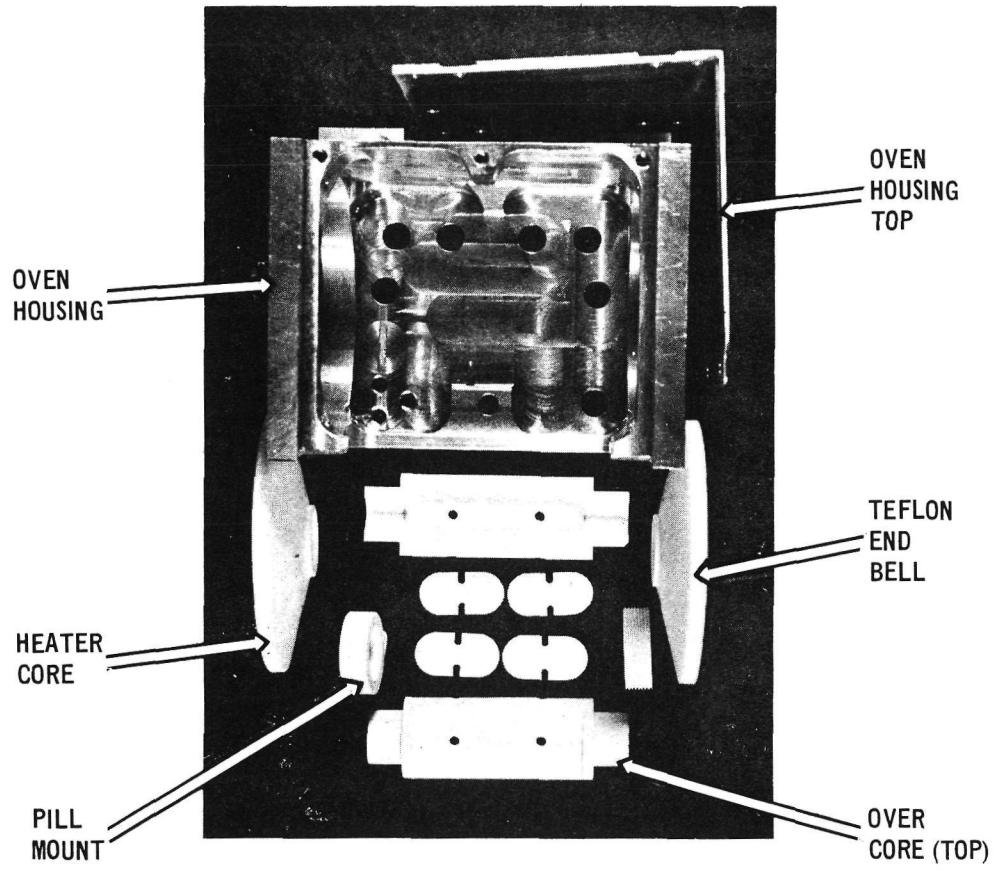

FIGURE 11 OVEN ASSEMBLY COMPONENTS FOR 1.06 μm MODULATOR

The two 20 mm long $LiTaO_3$ crystals were individually driven and independently matched to 50 ohm loads in order to maintain a rise time and fall time for 400 Mbps drive pulses equivalent to the parallel matched 10 mm crystals used in the double-pass 1.06 micrometer modulator (NASA contract NAS5-11474). Each modulator crystal was incorporated in an electrical matching network which consisted of 2 parallel paths. One was a series RLC containing the modulator crystal, and the other was a parallel LC in series with R. Proper selection of L's and C's resulted in a frequency independent 50Ω match which was the desired configuration. The 50Ω load is returned to the power supply for proper driver transistor biasing through the broadband load. A schematic of the matching network is shown in Figure 12.

The heater and thermistor in the modulator assembly operated in conjunction with the temperature controller to maintain the oven core at constant temperature. The oven housing, oven core, pill mounts, teflon oven end bells, heater cores, and copper electrodes were similar in design as those for a two-10 mm crystal modulator except the lengths were enlarged for fabrication of a two-20 mm crystal modulator. With the exception of the aluminum housing and teflon end bells, all of the oven components were made of boron nitride because of its good thermal conductivity and high electrical insulation properties. The pill mounts were oval to provide mounting strength for the entire 20 mm crystal length without adding extra width to the oven core which would result in excessive thermal mass and increased oven diameter. The oven core was made of boron nitride. The oven core holds the mounted crystals, heaters, and thermistor. It acts as the high temperature isothermal enclosure. The ends of the oven core were shaped to hold the heaters. The nichrome wire heaters were wound in grooves in boron nitride cylinders which fit snugly around the ends of the oven core. The length of the groove in each cylinder was chosen so that 22 ohms of nichrome wire was used. This impedance was chosen to match the temperature controller output stage. The heaters were located away from the oven center so that there was as little electrical interaction as possible between the heaters and matching network. The oven core was held in place by the teflon end bells. These end bells were shaped

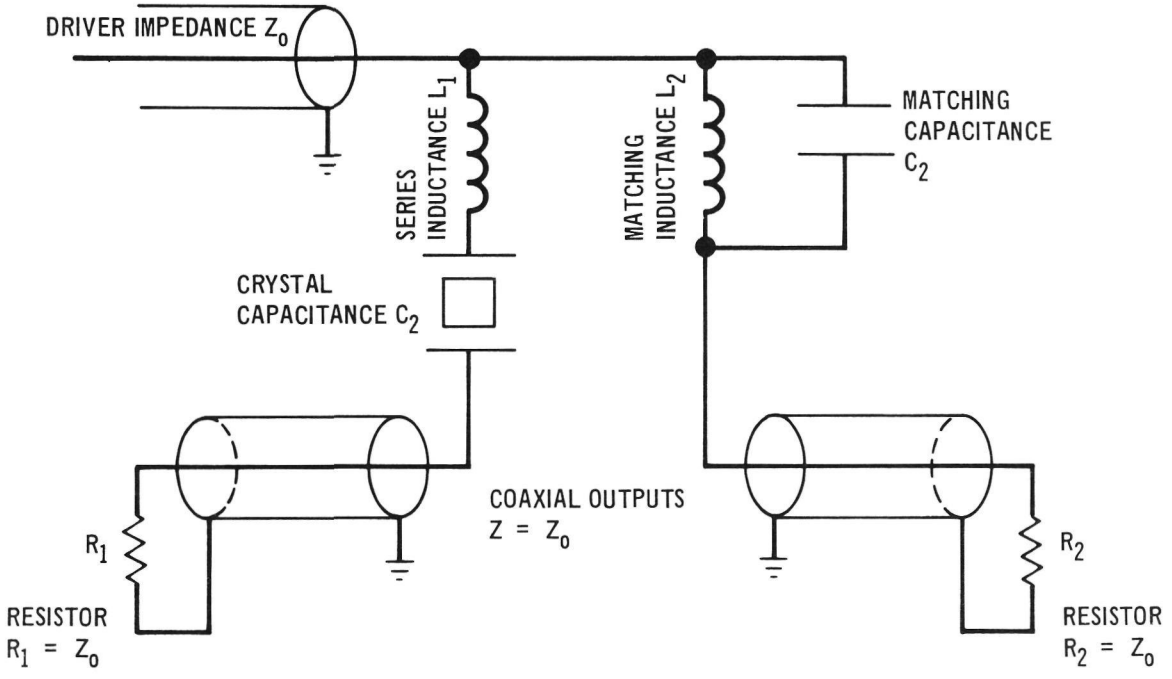

FIGURE 12 MATCHING NETWORK*

*PATENT APPLIED FOR

for maximum support of the oven core and also provided a minimal heat leak from the oven core to the oven housing. The end bells were made of teflon to minimize the reactive interaction with the matching network components. Figure 13 shows the mechanical drawing of the oven assembly.

Heater efficiency within the modulator ovens was achieved with a) teflon end bells supporting the crystal assembly, b) minimum total cross-sectional area of connecting wires, c) utilization of the low emissivity uncoated machined finish on inside and outside surfaces of the oven-body walls to achieve minimal radiative heat transfer, and d) utilization of radiative insulation between oven core and modulator oven housing.

2.4.2 OPTICS TAIL. The optics tail of the modulator assembly consists of pellicle, lens, polarization beamsplitter and photodiode necessary for operation of the automatic electronic compensator. There are two translation adjustments in the optics tail both perpendicular to the propagation of the optical beam (one adjustment has ±1.6mm range and the other has a range of ±0.8mm). These movements are required to obtain optimum focusing on the photodiode. Figure 14 shows the mechanical drawing and schematic layout of the optics tail components. The beamsplitter is a nonpolarization sensitive pellicle which diverts 1% of the modulator output beam toward the automatic electronic compensator (AEC) photodiode detector. As shown in Figure 9, the pellicle is placed directly in the output beam of the modulator. The lens is used to focus the output through a polarizer #1 onto the sensitive surface of the photodiode. Polarizer #1 passes only one polarization of the optical beam so that operation of the AEC is independent of the modulation format. Polarizer #2 is used only for the PGBM modulation format and is readily removed from the modulator output beam path for PPBM operation. The polarization rejected in the PGBM modulation format is the polarization that the photodiode detects for AEC operation. The polarization beamsplitter on the input to the photodiode functions as an analyzer and converts the polarization modulator of the crystals to amplitude modulation for a PGBM format.

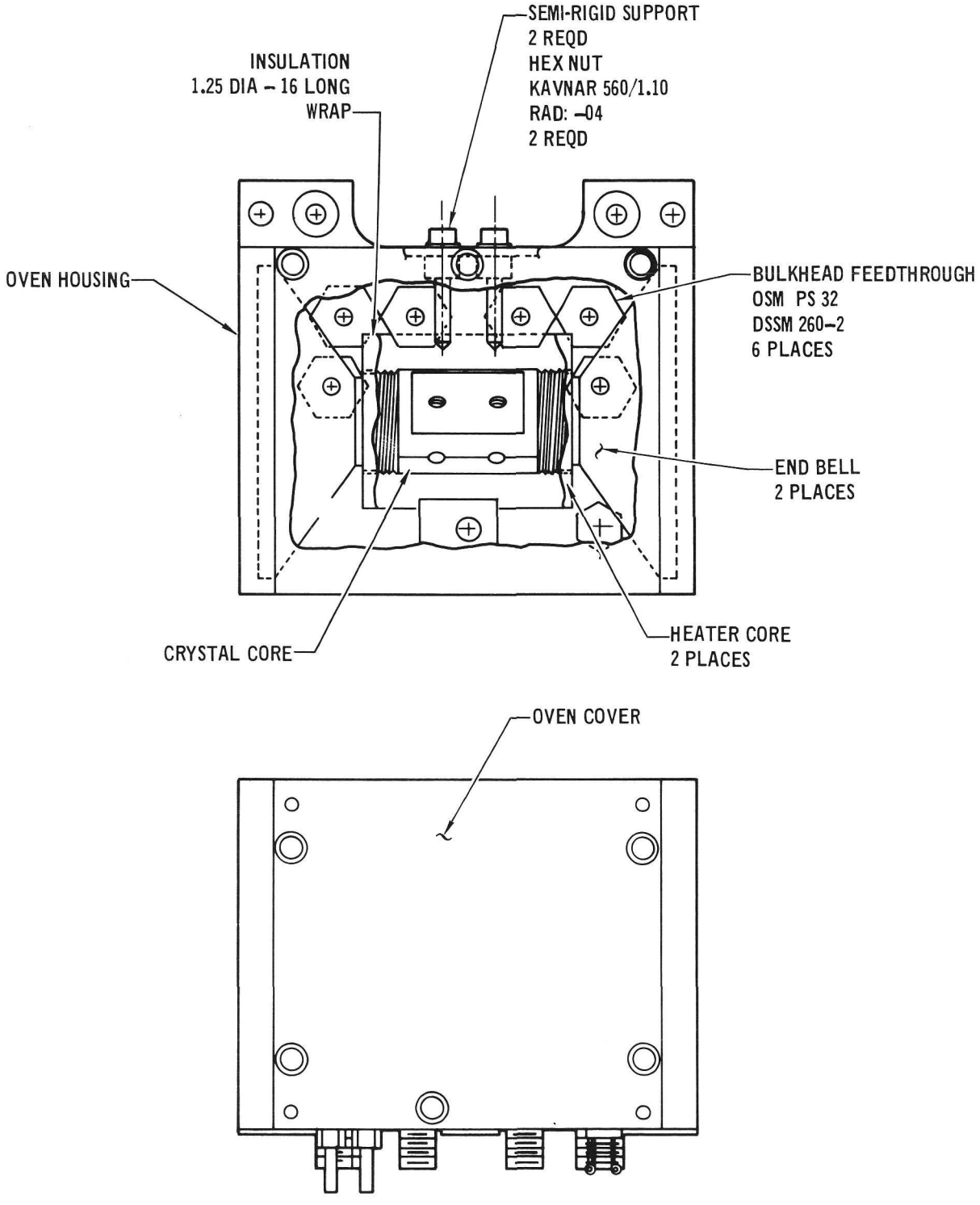

FIGURE 13 OVEN ASSEMBLY

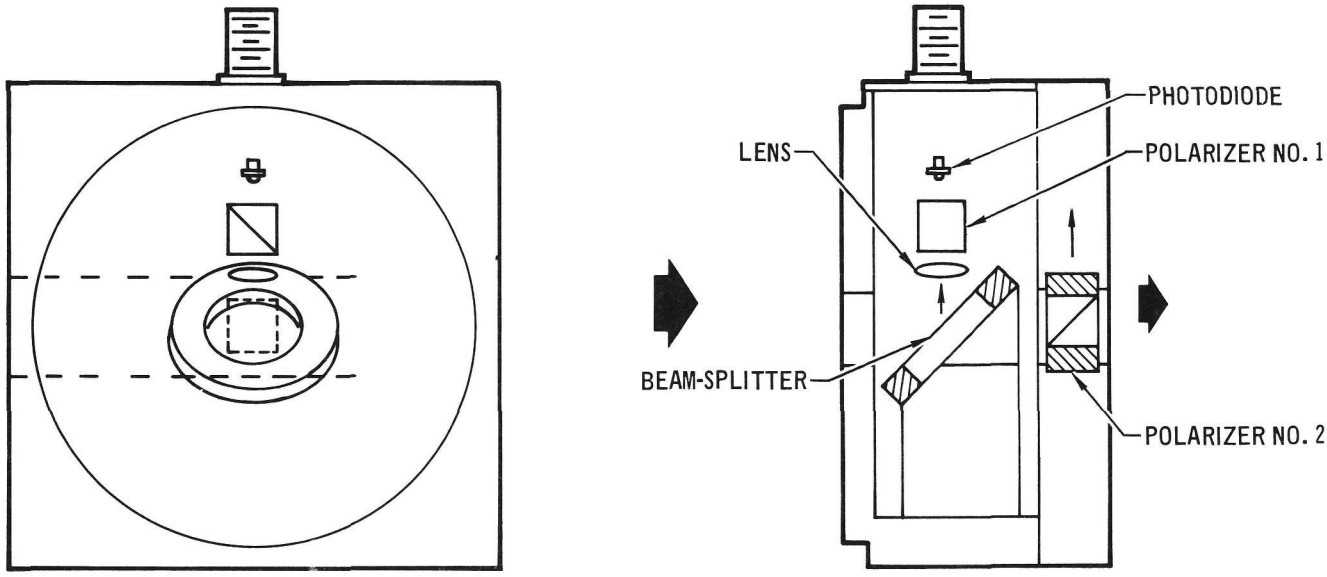

FIGURE 14 SCHEMATIC FOR OPTICS TAIL

These optical pulses which are passed by the polarization beamsplitter and received by the photodiode and are utilized to produce a maximum extinction ratio as will be described in the automatic electronic compensator section of this report.

2.4.3 LENS TRANSLATORS. The front and rear lens holders of the modulator subassembly hold and position the 84mm focal length input and output lenses. The input lenses produced the required confocal focusing of the beam through the modulator crystals, and the output lenses collimated the modulated output beam to the diffraction limit. The lens holders were designed to facilitate lens removal for initial modulator alignment, and they provided for motion of the lens both parallel and transverse to the optical beam. Locking screws were also provided to insure that lens position was maintained once it had been adjusted.

Figure 15 shows a mechanical design of the lens translator. The x and y motion have a range of $\pm$1.6mm. The z motion is variable to obtain confocal focusing in the modulator and collimation of the output modulated beam.

2.5 MODULATOR ELECTRONICS ASSEMBLY. The modulator electronics assembly consisted of a modulator driver, load box, temperature controller, automatic electronic compensator (AEC), manual thermal differential compensators (TDC), and interconnections. The electronics package was mounted on a separate coldplate and was interconnected with the optics package via shielded cables. Although the electronics package was designed to minimize size, weight, and power, it was constructed using brassboard fabrication techniques which were adequate for a laboratory environment.

2.5.1 MODULATOR DRIVER. The modulator driver consisted of a low level hybrid emitter coupled front end, 2 parallel discrete intermediate stages, buffers, and a pair of final output voltage gain stages. The hybrid section consisted of 9 DC coupled emitter coupled pairs. These are shown as the "-1," and the "-1M" stages in Figure 16. This configuration minimized timing errors in the low level stages. Two auxiliary outputs were available from the second emitter coupled pair of the

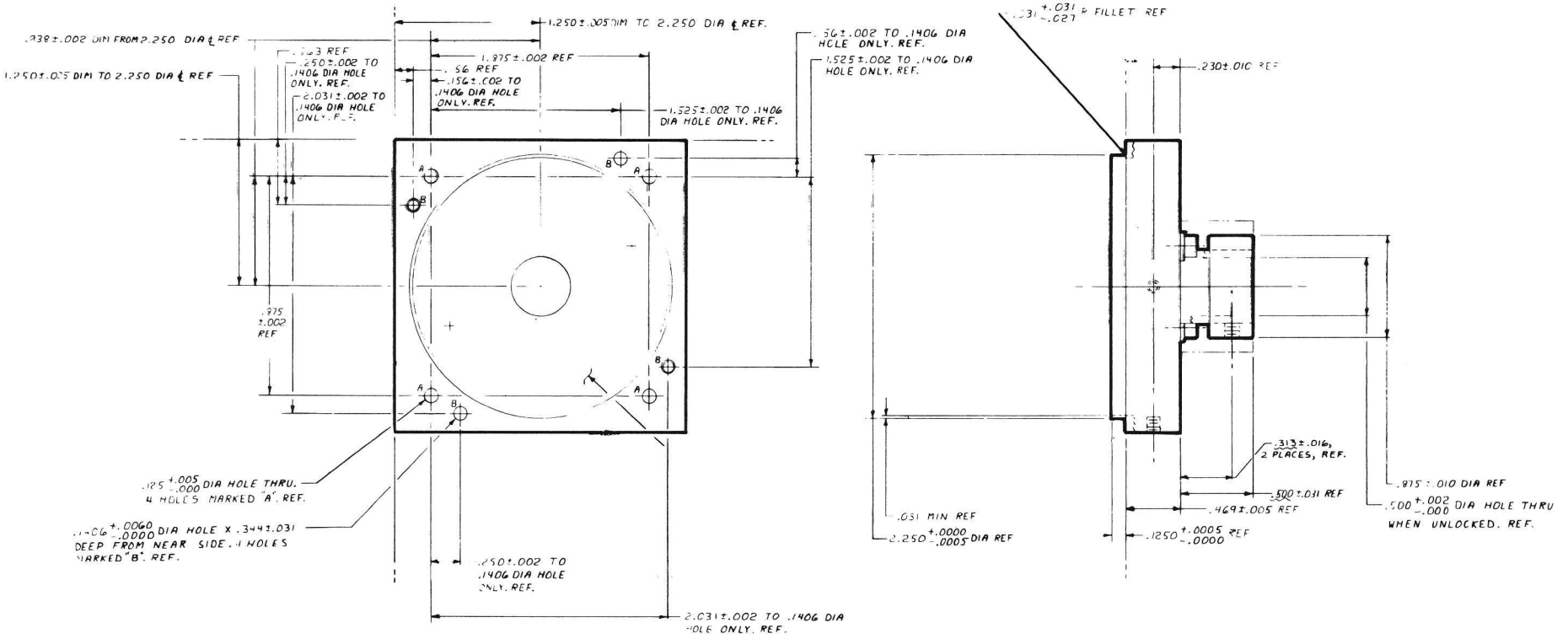

FIGURE 15 LENS TRANSLATOR

chain. The following intermediate stages, shown as "-2" in Figure 16, consisted of two parallel emitter coupled pairs whose collector currents were summed into a grounded base transistor. An emitter follower interfaced between the grounded base transistor's load and the inverting gain stage. Elimination of 1 gain stage at the output relative to previous designs allowed power savings of ~10 watts (2[25V x .2A]).

Figure 16 shows the interconnection of the parts of the modulator driver as described above.

Figures 17, 18, 19, and 20 are schematics of the various sections of the modulator driver.

The driver waveforms are shown in Figure 21 using the GFE 63 bit, 400 MHz NRZ pseudorandom code generator. The waveforms were taken using an instrumentation test-probe installed in the coax cable at the driver outputs. The driver voltage swing was 27 volts for full half-wave switching of the modulator crystals. This voltage was close to the goal of 28 volts for full half-wave switching of the modulator crystals. However, since the required driver voltage swings were lower, the power consumption was reduced. The initial estimate of the driver and load power consumption required was 37.7 watts, however, the actual power consumption was only 24 watts.

The driver waveform had rise and fall times of $\leq$ 1000 ps as shown in Figure 22 for a Q and $\overline{Q}$ "1-0-1" portion of the code. The driver output timing accuracy with respect to the system clock measured $\leq \pm 320$ ps, as seen in the Lissajous Pattern plot (I-pattern) shown in Figure 23. These plots were taken using a sampling scope with two inputs; one the driver output under test and the other the 400 MHz clock with which the driver output timing accuracy was specified. The deviation in the horizontal direction at vertical zero crossings were the timing accuracy of the driver. The timing accuracy of the driver was measured when operating at 400 Mbps using a 63 clock pulse length NRZ pseudorandom code.

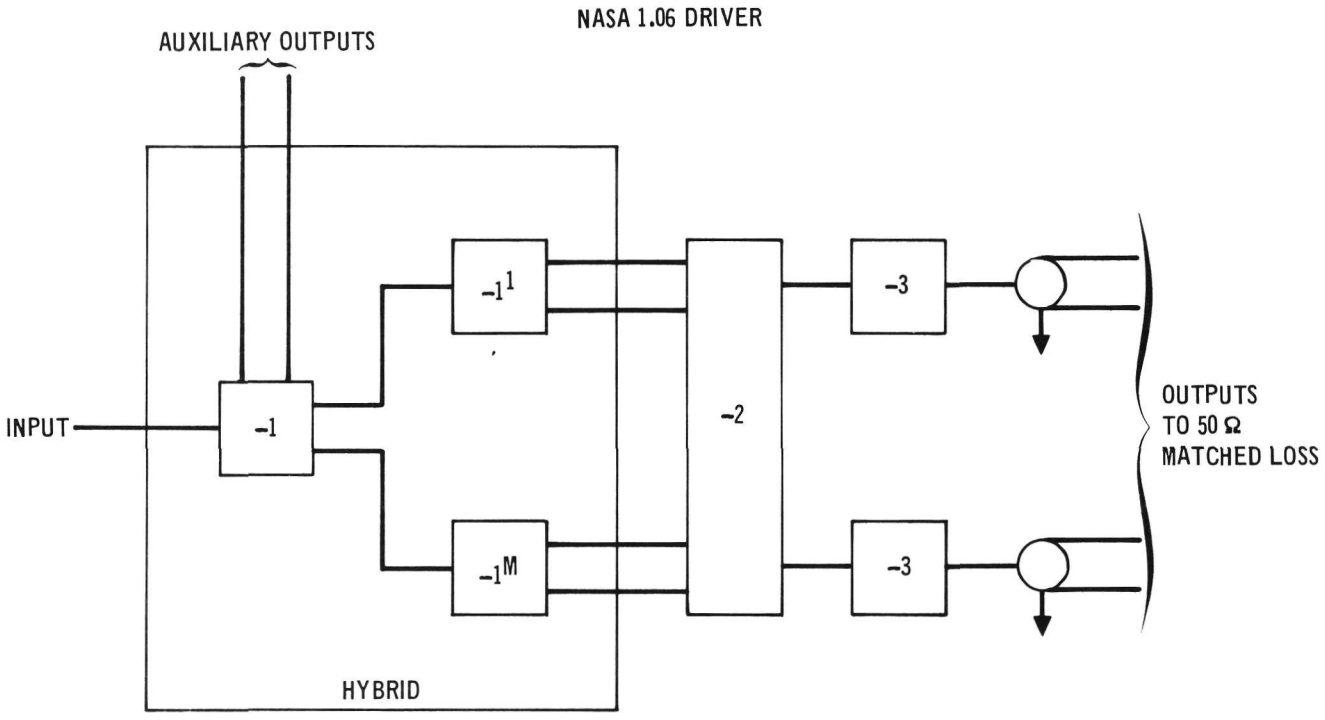

FIGURE 16 MODULATOR DRIVER COMPOSITION

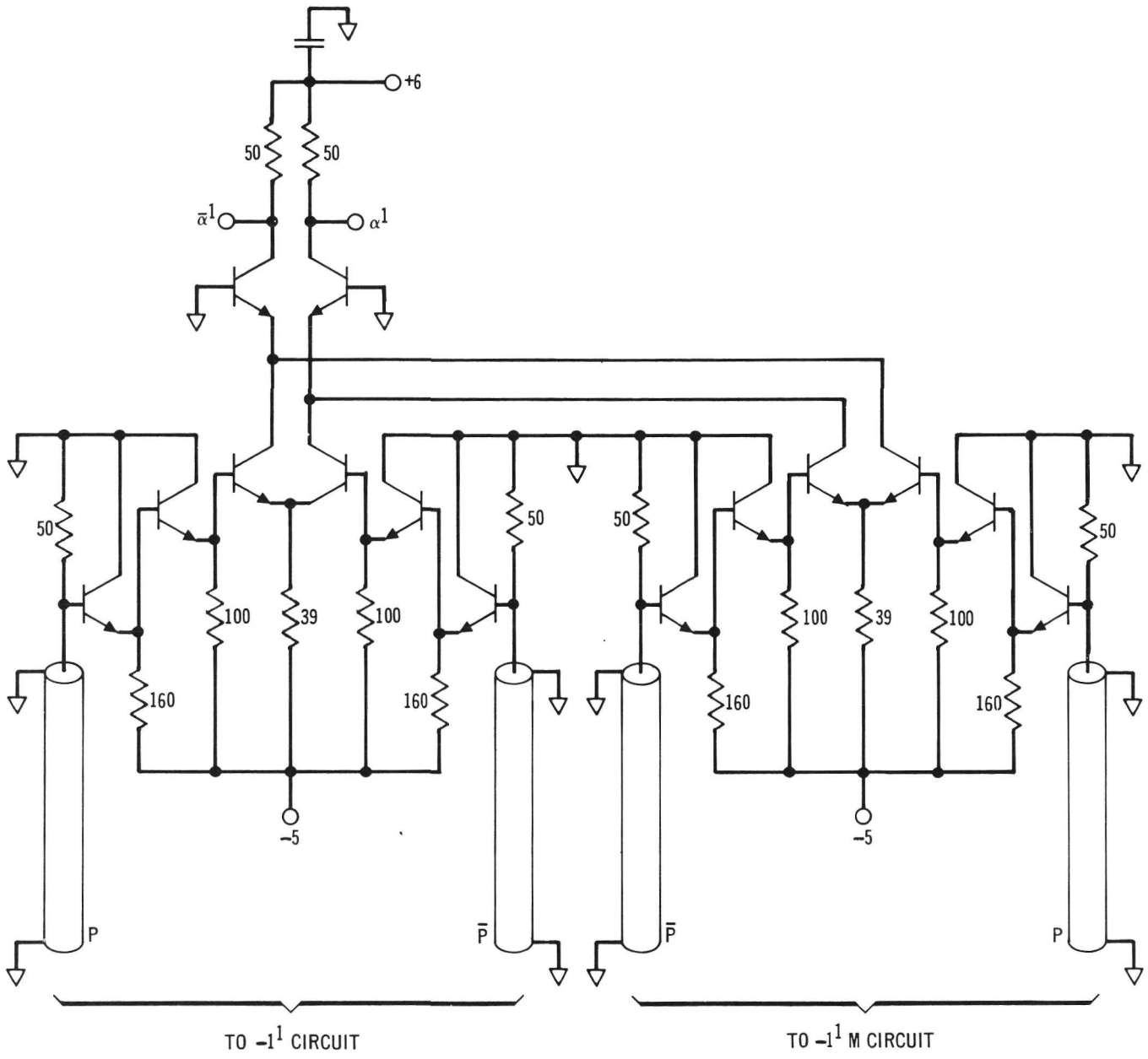

FIGURE 17 MODULATOR DRIVER "–2" CIRCUIT

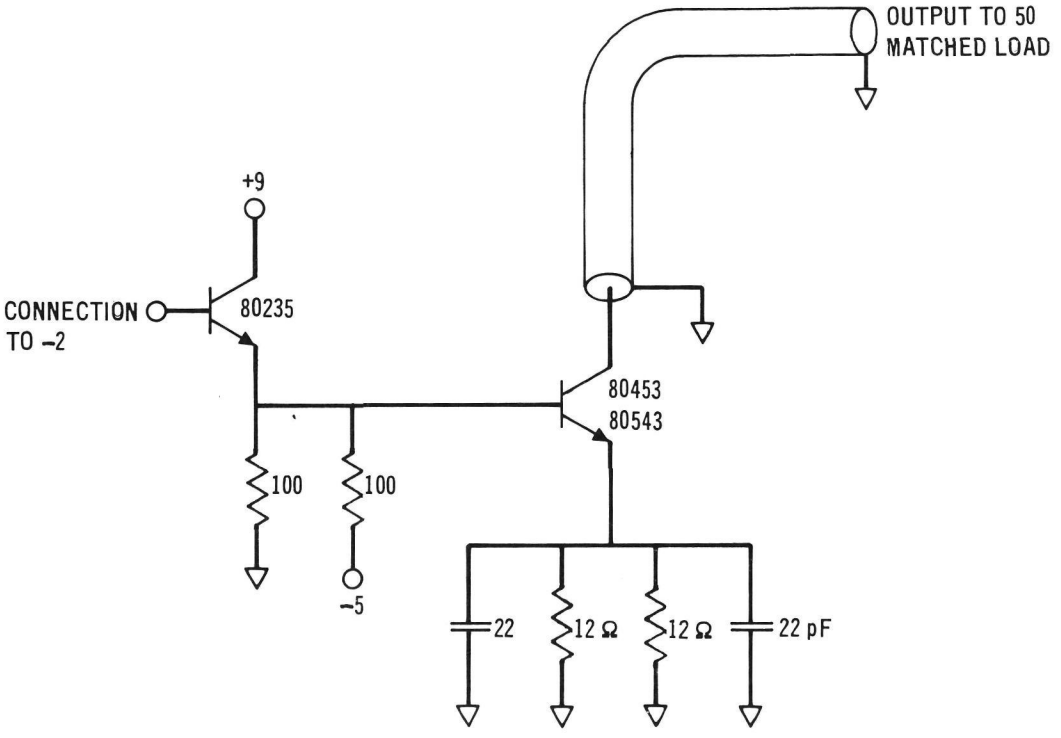

FIGURE 18 MODULATOR DRIVER -3 CIRCUIT

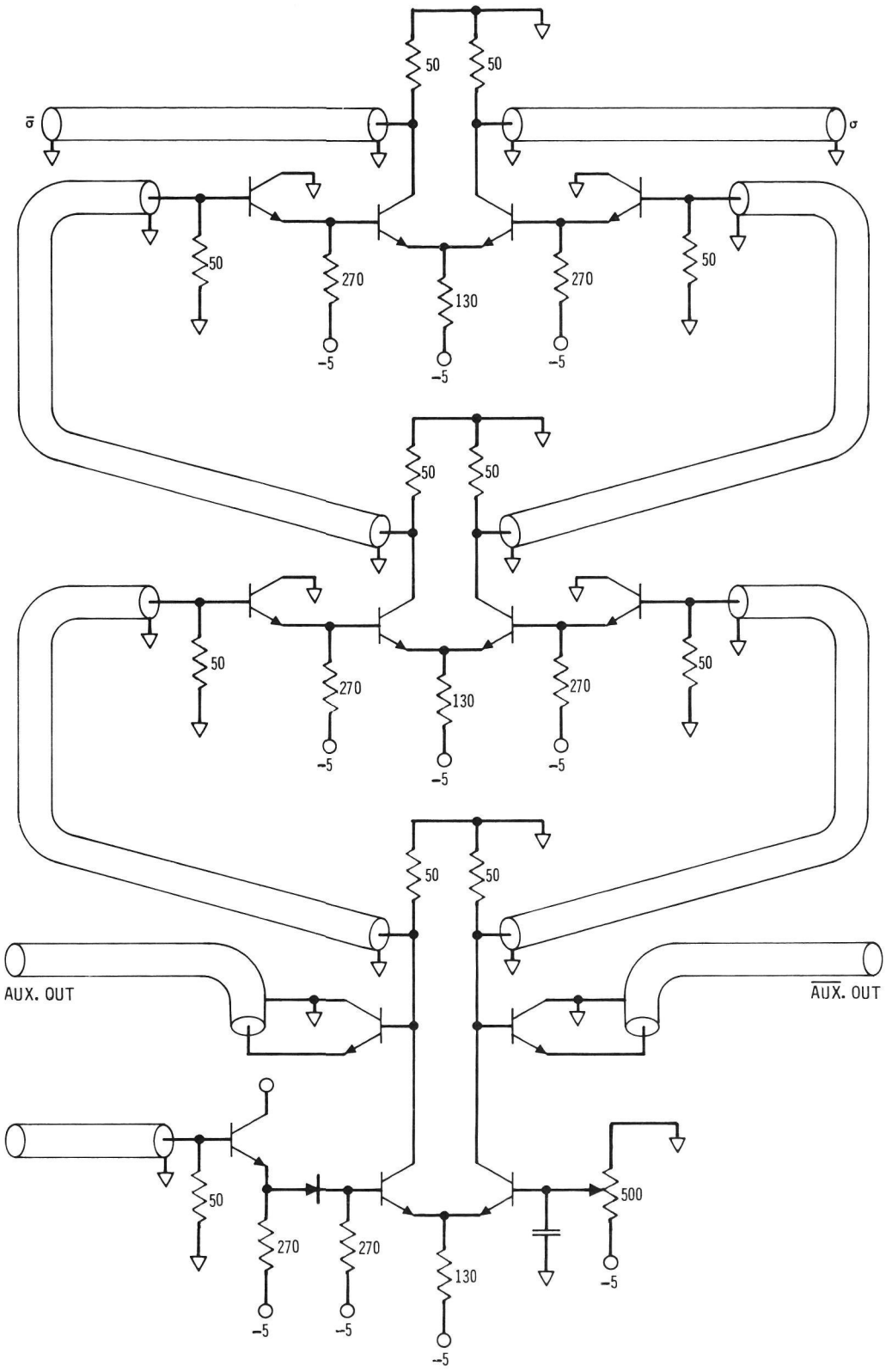

FIGURE 19 MODULATOR DRIVER -1 STAGE

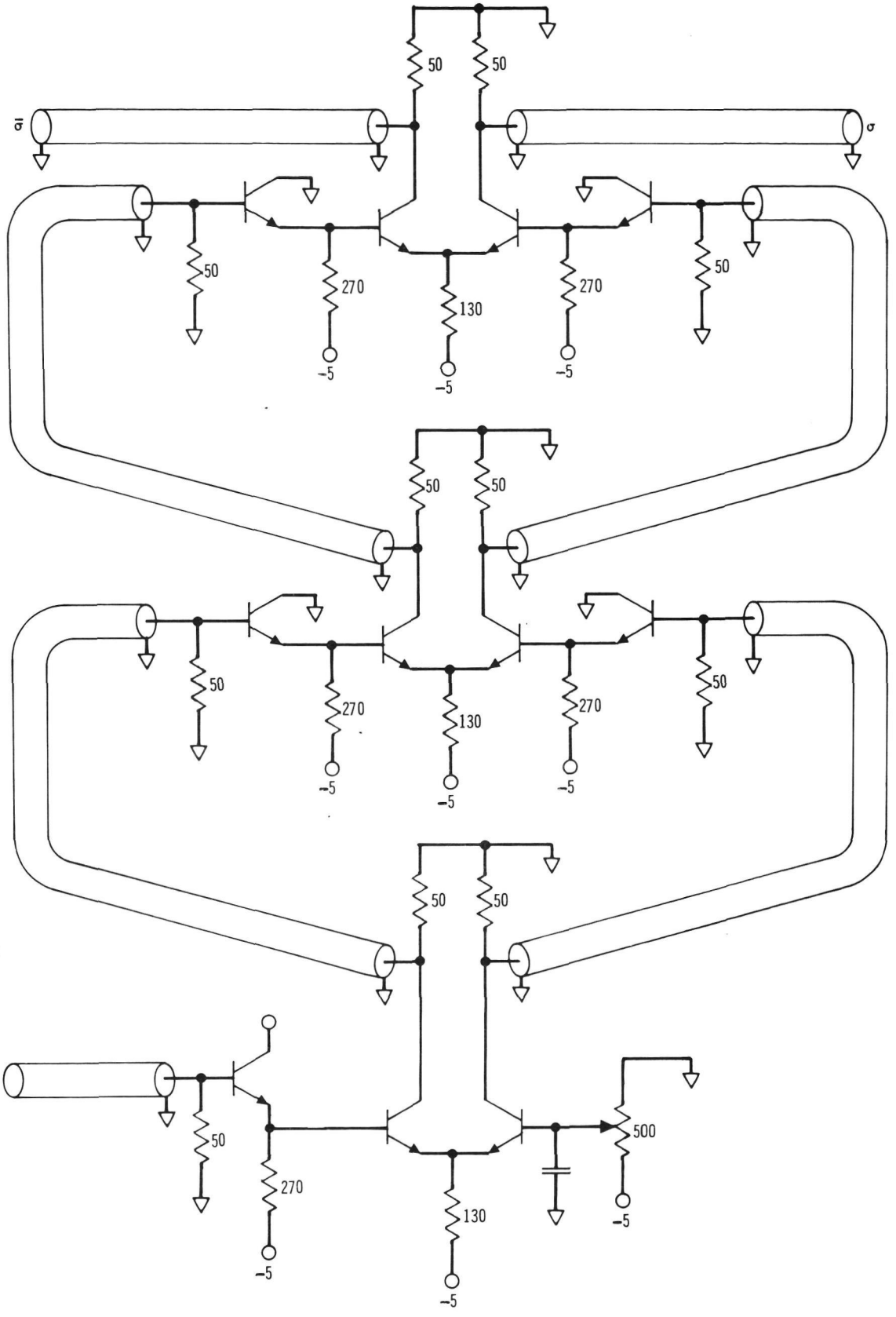

FIGURE 20 MODULATOR DRIVER-1 – IM STAGES

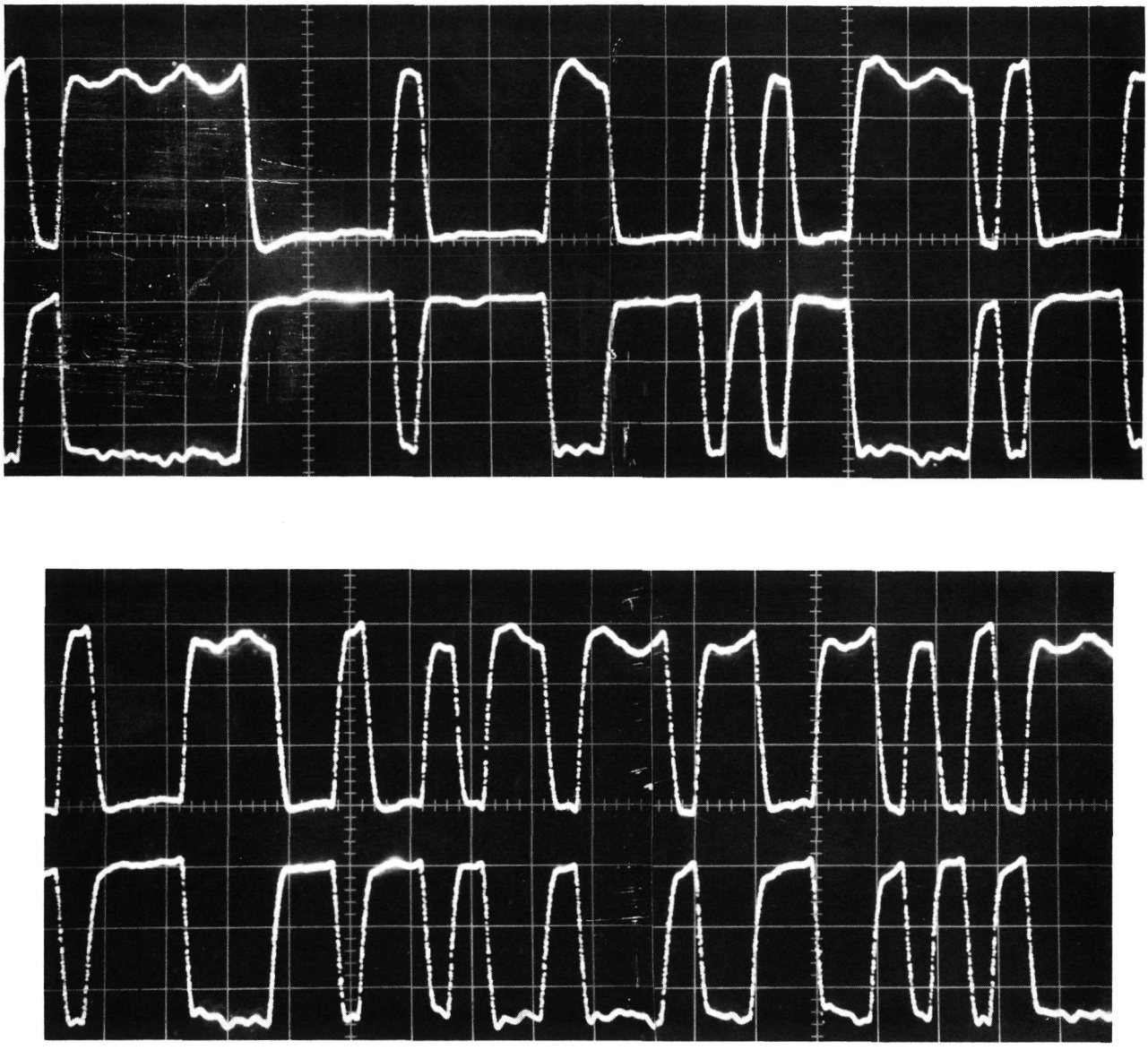

UPPER TRACE: DRIVER OUTPUT NO. 35
LOWER TRACE: DRIVER OUTPUT NO. 36

FIGURE 21 63 BIT 400 Mbps DRIVER OUTPUT WAVEFORMS

HORIZONTAL SCALE: 5 nSEC/DIV
VERTICAL SCALE: 10 VOLT/DIV

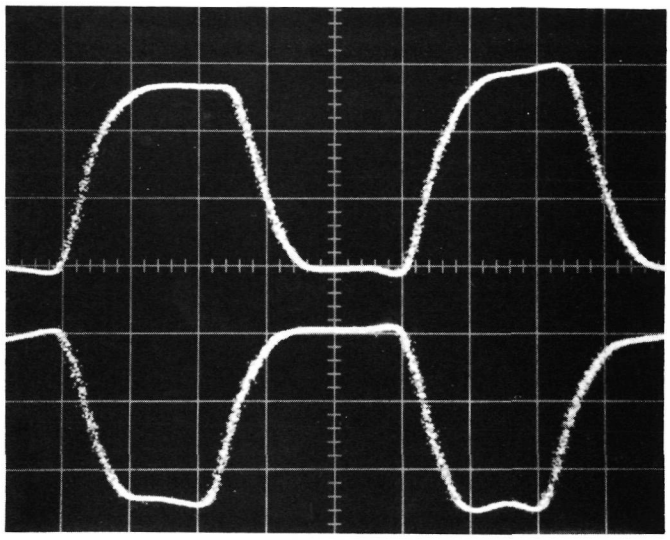

DRIVER NO. 35
OUTPUT

DRIVER NO. 36
OUTPUT

FIGURE 22 TYPICAL MODULATOR DRIVER RISETIMES AND FALLTIMES

HORIZONTAL SCALE: 1 nSEC/DIV
VERTICAL SCALE: 10 VOLTS/DIV

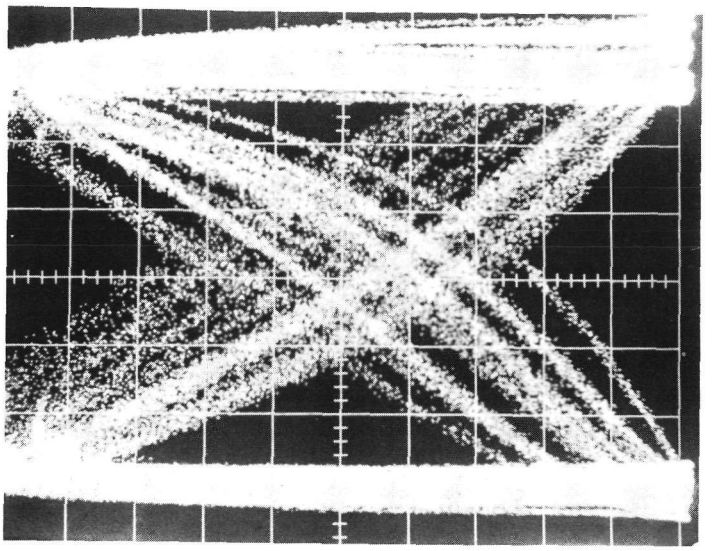

DRIVER NO. 35 OUTPUT

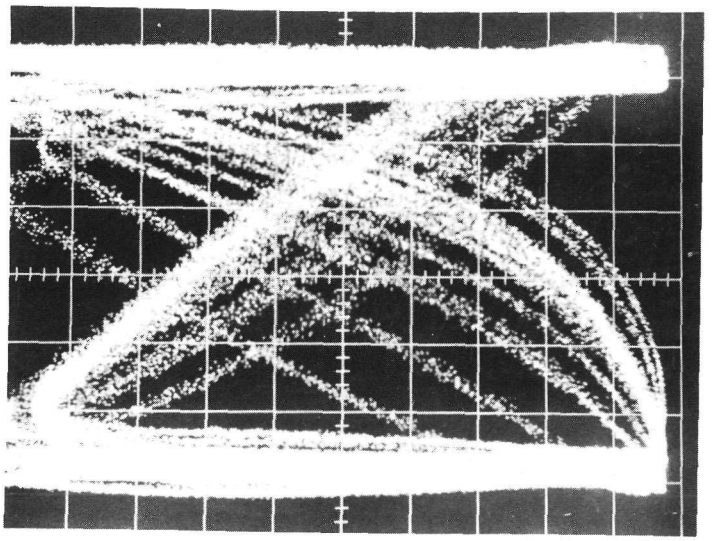

DRIVER NO. 36 OUTPUT

FIGURE 23 LISSAJOUS PATTERN PLOTS (I-PLOTS) OF THE MODULATOR DRIVER OUTPUT TIMING ACCURACY

HORIZONTAL SCALE: 80 PS/DIV

2.5.2 LOAD BOXES. The load module contained four 50 ohm loads. Two were matched for the capacitive ("C") side of the modulator crystal and two were matched for the inductive ("L") side of the modulator crystal matching network. Test points were installed on each of the four load resistors, to monitor driver operation without interference with the driver input to the crystals. Figure 24 shows an assembled load box.

2.5.3 TEMPERATURE CONTROLLER. The function of the temperature controller was to provide slow-response, long-term temperature control of the modulator crystals. Crystal temperature was controlled at 150° ±1°C by heaters that were supplied with electrical power from the temperature controller.

Figure 25 includes the block diagram of the temperature controller. The circuit consisted of the sensor bridge, temperature compensated high gain amplifier, oscillator, integrator, comparator, and output buffer amplifier. The temperature sensing thermistor located in the modulator assembly was connected to one leg of a bridge, and precision resistors were used in the other legs. The thermistor in the bridge had a temperature coefficient of approximately 1% per degree centigrade, and had a nominal impedance of 200 ohms at 150°C. The resistors were selected so that the bridge output was nulled at the desired operating temperature. The heater in this system was switched completely on or off at any given time, with the amount of heating being controlled by the on-to-off ratio of the heater. The oscillator developed a rectangular waveform which was integrated to produce a triangular waveform with zero average value. This triangular waveform was the reference voltage for a high gain comparator. The other input to the comparator was the amplified error signal from the thermistor bridge. The output buffer amplifier controlled the power supplied to the heater in the oven.

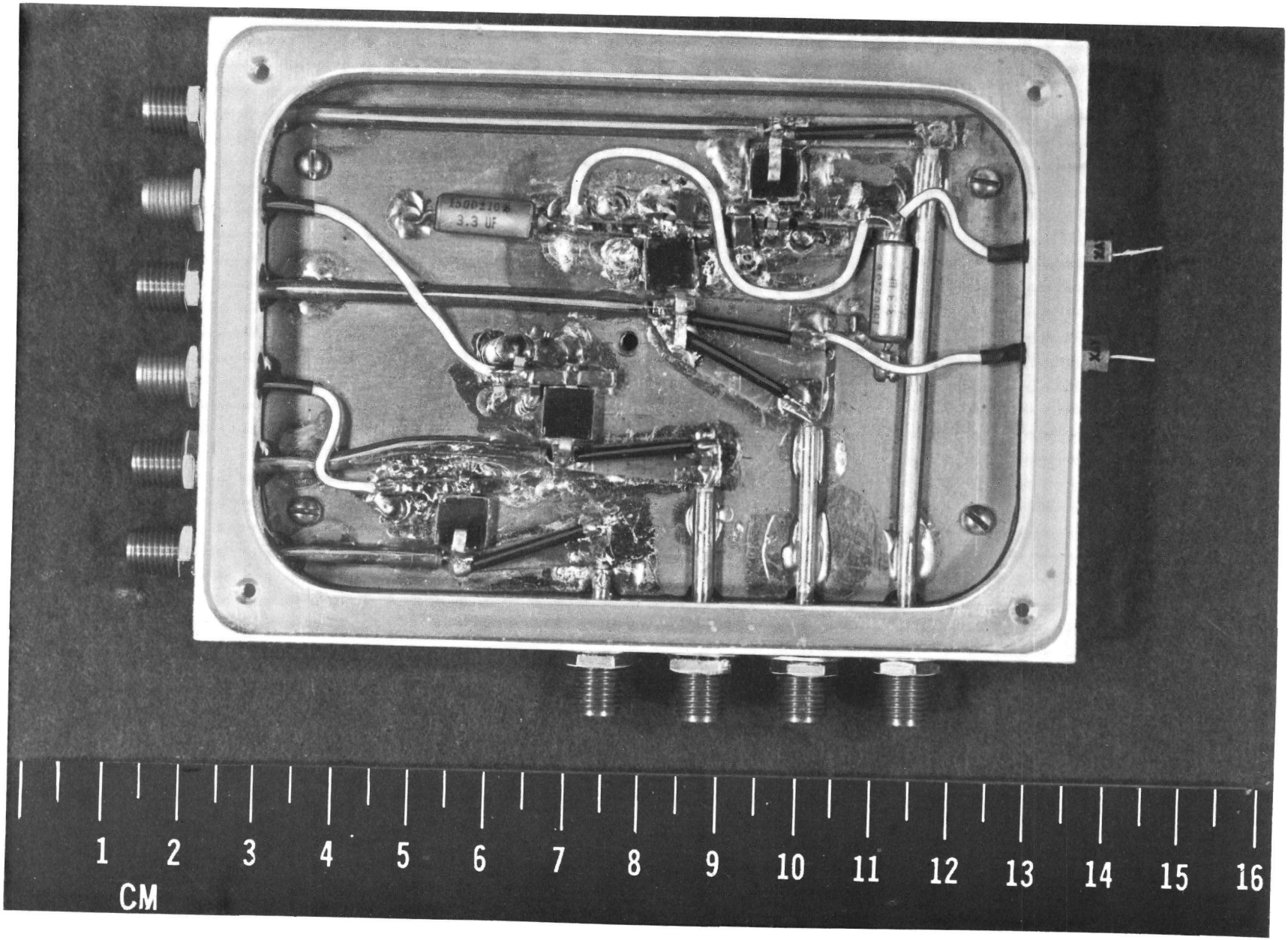

FIGURE 24 MODULE D OF THE ELECTRONICS ASSEMBLY –
BROADBAND LOAD MODULE

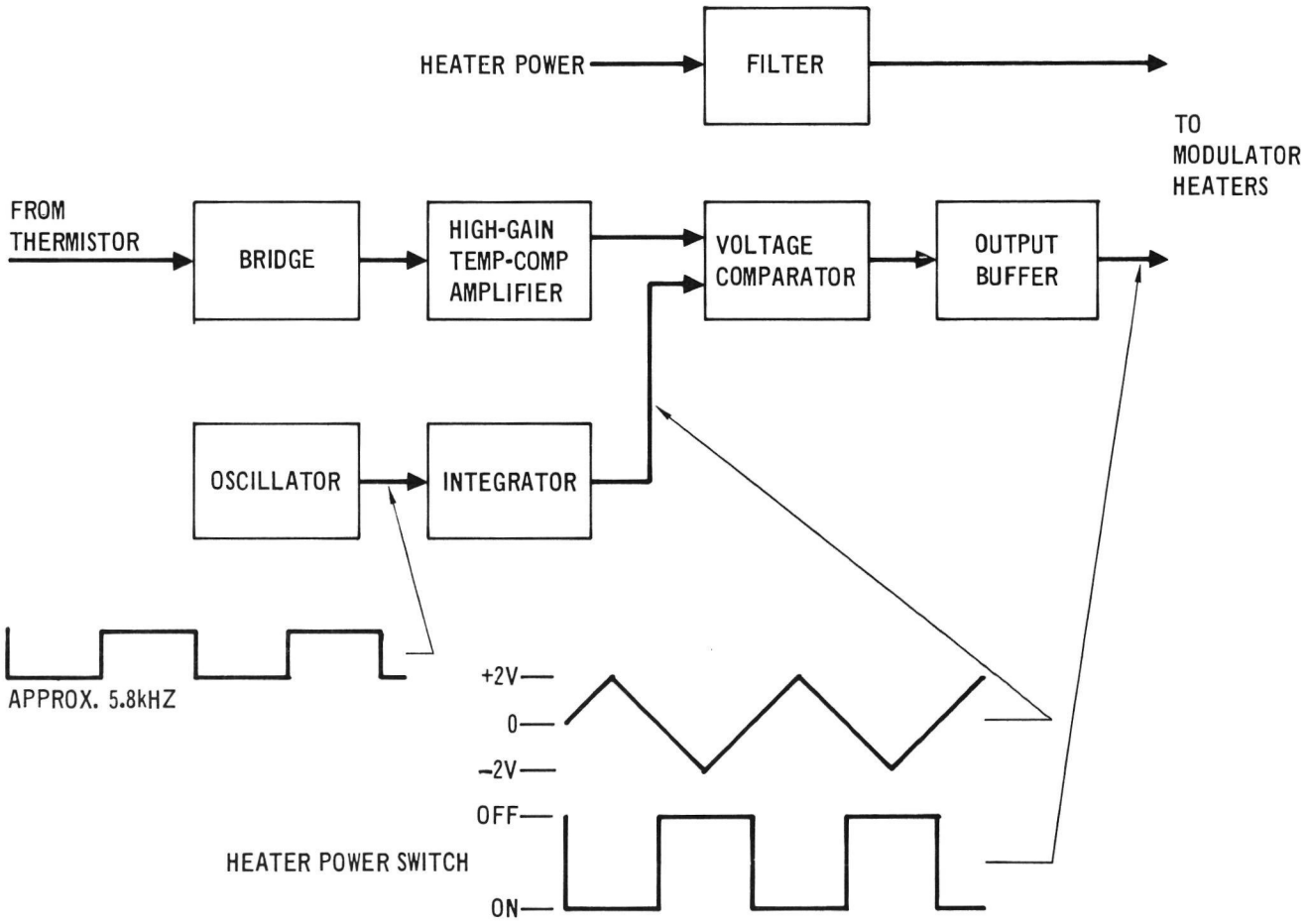

FIGURE 25 TEMPERATURE CONTROLLER BLOCK DIAGRAM

2.5.4 OPTICAL COMPENSATORS. The process of adjusting the crystal birefringence to the desired operating point is termed "optical compensation." Optical compensation produced by an applied voltage we have termed "electronic compensation," and optical compensation produced by a temperature change or differential has been termed "thermal differential compensation." Both types of optical compensation are used in the modulator fabricated for this program and operate in either an automatic mode or a manual mode.

The function of the automatic electronic compensator (AEC) is to compensate electrically for any rapid thermal effects not compensated for by the crossed axis crystals or for any rapid bias effects introduced by any dc bias level applied from the driver amplifier. The function of the manual thermal differential compensator (TDC) is to compensate thermally for the long term effects of these same parameters in such a way to preset the average AEC bias voltage at a predetermined value.

2.5.4.1 Automatic Electronic Compensation (AEC). The automatic electronic compensation, shown in Figure 26 and 27 operated the same as in the previous modulator units but has several circuit changes to provide a better signal-to-noise ratio, a gating method change, and a differential output to bias the independently matched crystals.

The detected laser pulses from the avalanche photodiode were first amplified well above the high frequency noise produced in the gate circuit by the modulation data. The output from the gate was filtered and amplified to operate the phase comparator. The output from the integrator amplifier was passed through the bias amplifier to the optical crystals.

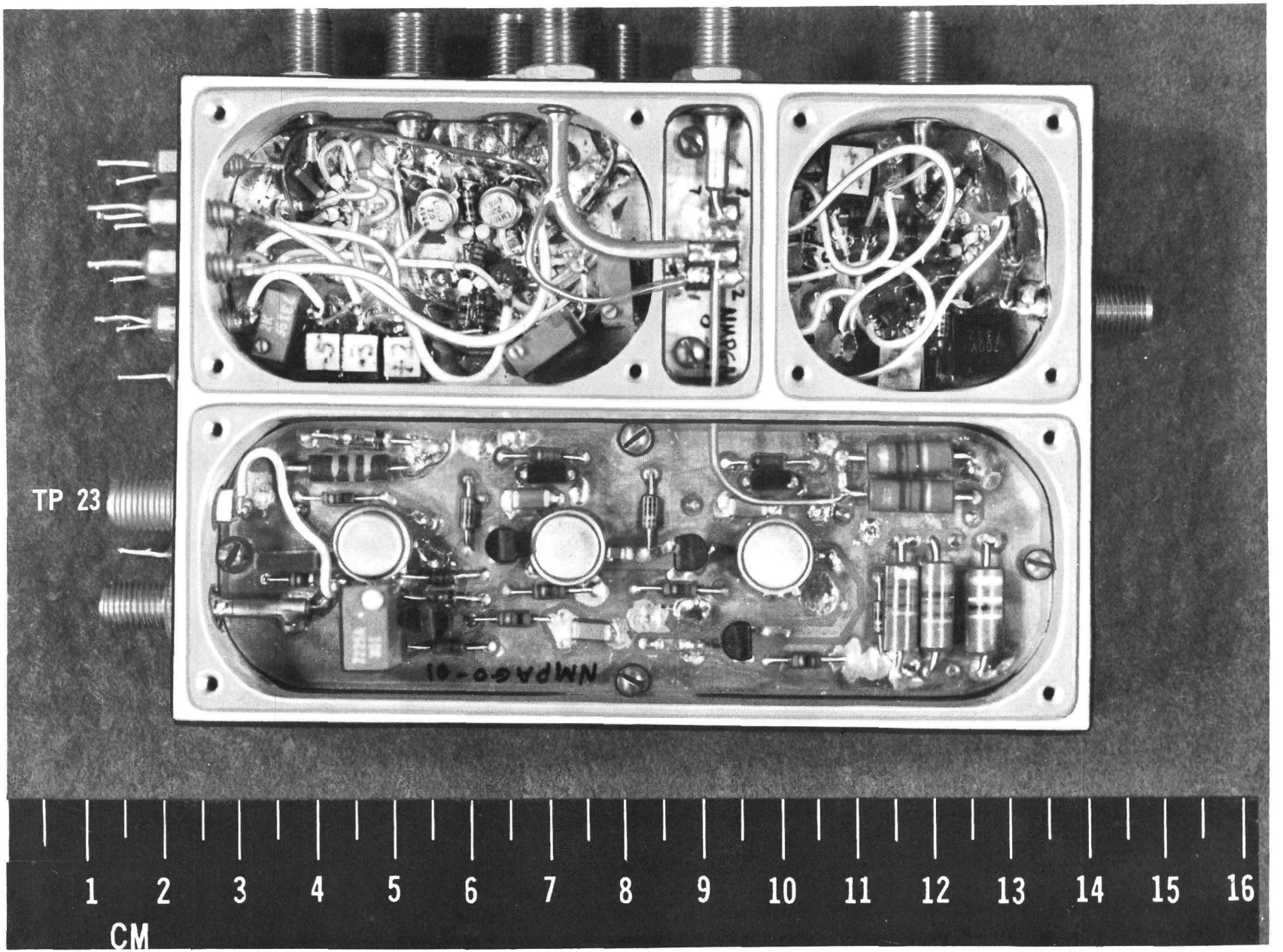

FIGURE 26 MODULE A OF THE ELECTRONICS ASSEMBLY – AUTOMATIC ELECTRONIC COMPENSATOR AMPLIFIER/GATE MODULE

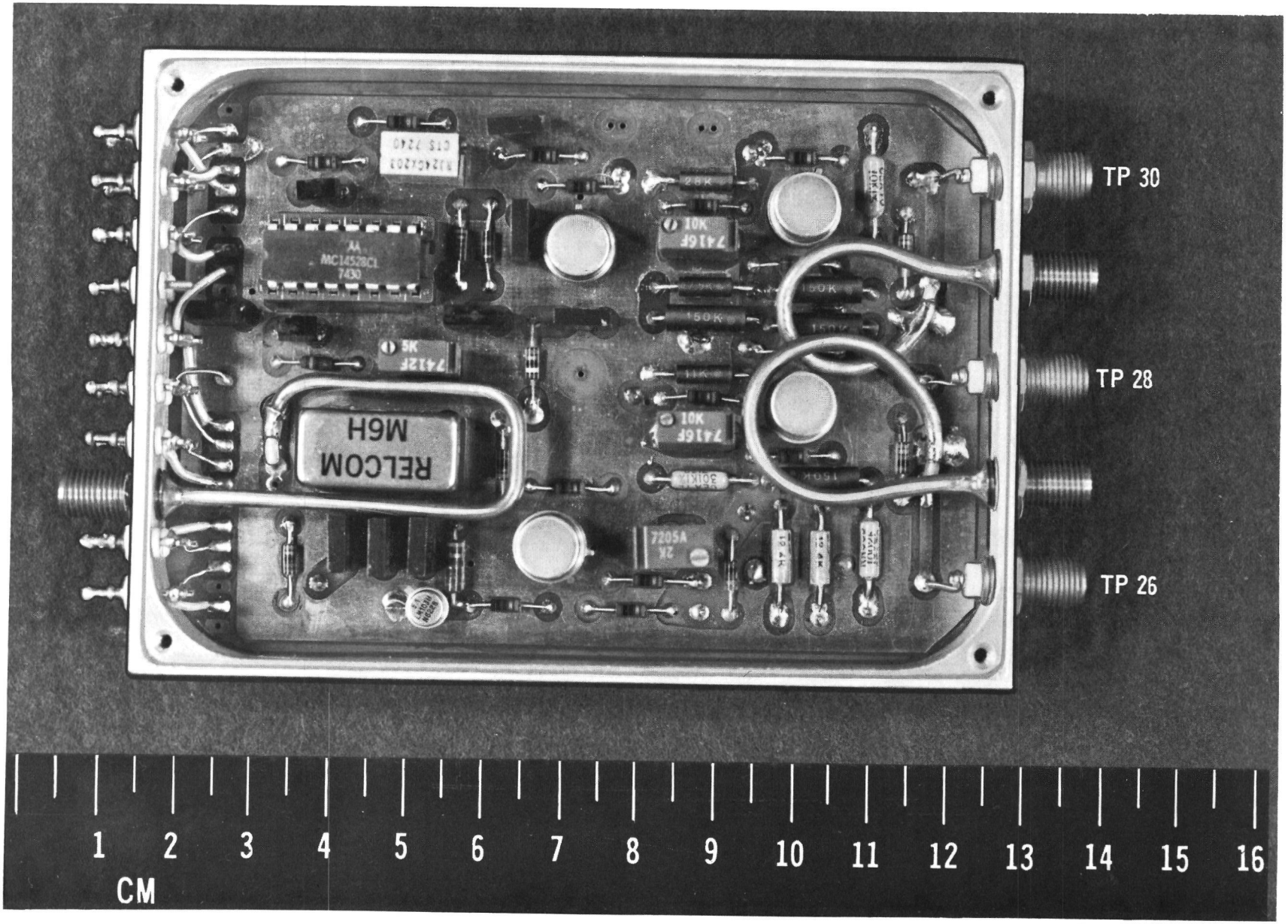

FIGURE 27 MODULE B OF THE ELECTRONICS ASSEMBLY –
AUTOMATIC ELECTRONIC COMPENSATOR OUTPUT MODULE

It was determined that 1% of the transmitted optical signal would be adequate for the compensator photodiode in the modulator with the PPBM format. Since both polarizations must be transmitted for PPBM, 1% of the transmitter optical signal was split off, analyzed, and focused into the compensating photodiode. Focusing the light on the photodiode was found to increase the diode output by a factor of 6 to 8 as compared to the breadboard approach of using unfocused light on the compensating diode. Thus, by focusing the 1% sample of the transmitted beam on the photodiode, the diode output was equivalent to the demonstrated operation of the double-pass PGBM modulator at only 15 to 20 milliwatts.

The AEC block diagram was included in the modulator functional block diagram in Figure 1. The basic theory of operation was to apply a low frequency (100 kHz) dither modulation to the laser beam at the modulator crystals. The laser output beam was then analyzed to recover the dither signal. The recovered dither signal was minimum at the desired operating point and increased as the bias point was changed in either direction from optimum; as the bias point changed in one direction from optimum, the recovered dither signal increased and was in-phase with the applied dither signal phase; as the bias was moved back through optimum and changed in the opposite direction from optimum, the recovered dither signal again increased but with the opposite phase relationship. Therefore, the recovered dither signal amplitude was the driving function of the electronic compensator, and the phase relationship controlled the direction of bias change. However, the data modulation to the modulator crystals was in the form of two distinct bias levels representing the binary "0's" and the second bias level represented the binary "1's". Therefore, the recovered dither signal was a composite signal made up of two distinct signals (the main difference being phase). One drove the bias in a direction to obtain a

minimum recovered dither signal when the crystals were modulated with binary "1's." Since the compensator circuits could not respond at rates equal to the data modulation, the resultant automatic compensator bias could be at some mean-point between the two. To prevent this ambiguous condition, the detected laser pulses, with the dither modulation, were passed through a gate circuit where the pulses representing the binary "0's" were passed unchanged, and the pulses representing the binary "1's" were inverted. Inverting the binary "1" pulses also inverted the phase of the dither modulation on the binary "1" pulses. The phase of the recovered dither signal component from the binary "1" pulses was now the same as the phase of the recovered dither signal component from the binary "0" pulses. Both recovered dither signal components now drive the crystal bias in the same direction to obtain a minimum recovered dither signal at the same point.

The dither signal was generated from the 100 kHz square wave logic oscillator by scaling, filtering, and buffering. The dither amplitude was scaled to an effective 4% of the modulator switching voltage (which produced approximately 1% modulation). The dither was then summed with the DC bias and applied through the broadband load to one crystal; since the dither was applied to only one crystal, the actual dither voltage required was double or 8% of the switching voltage. The oscillator and dither signal waveforms are shown in Figure 28 along with the dither reference signal which was also scaled down and buffered from the oscillator signal. The reference signal passed through an adjustable time delay circuit to provide phase alignment with the recovered dither signal phase, Figure 29; the recovered dither shown was taken from over range compensation to provide a large signal for clarity. A square wave reference signal was used to decrease the switching time of the phase detector and therefore decreased the phase detector sensitivity to small changes in phase alignment.

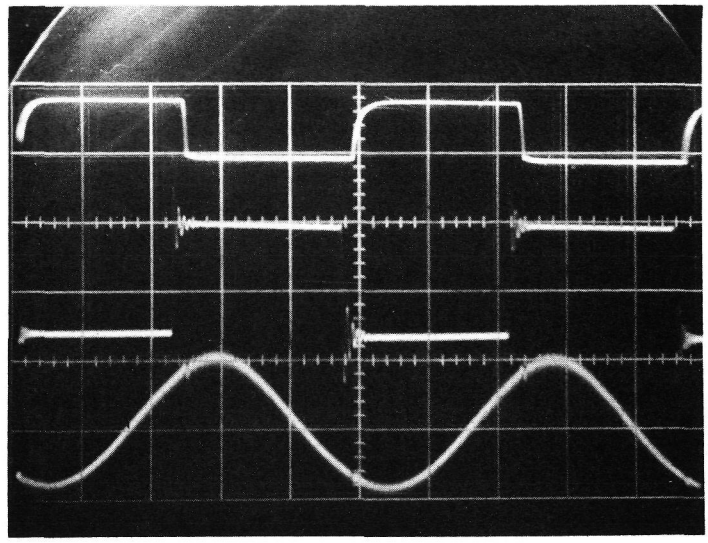

SYSTEM CLOCK 5V/DIV
OT-PIN 4

DITHER REFERENCE .5V/DIV
TP 28

DITHER SIGNAL 1V/DIV
TP 30

2μs/DIV

FIGURE 28 AUTOMATIC ELECTRONIC COMPENSATOR CLOCK AND DITHER WAVEFORMS

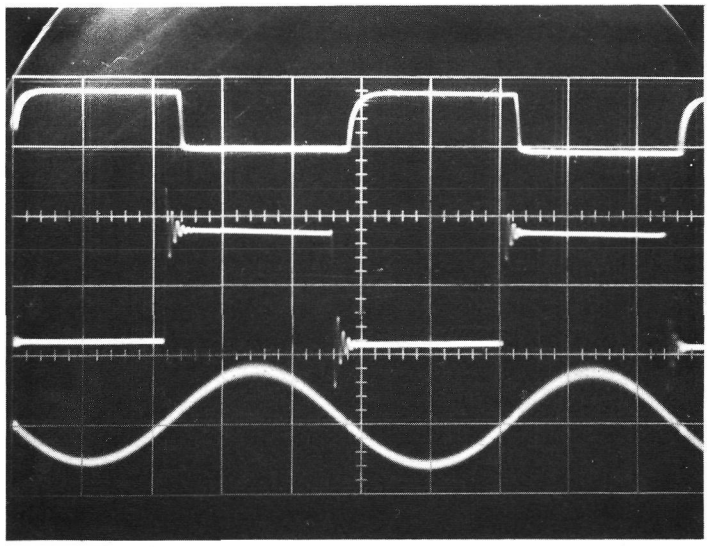

SYSTEM CLOCK 5V/DIV
OT–PIN 4

DITHER REFERENCE .5V/DIV
TP 28

RECOVERED DITHER .5V/DIV
IN PHASE
TP 23

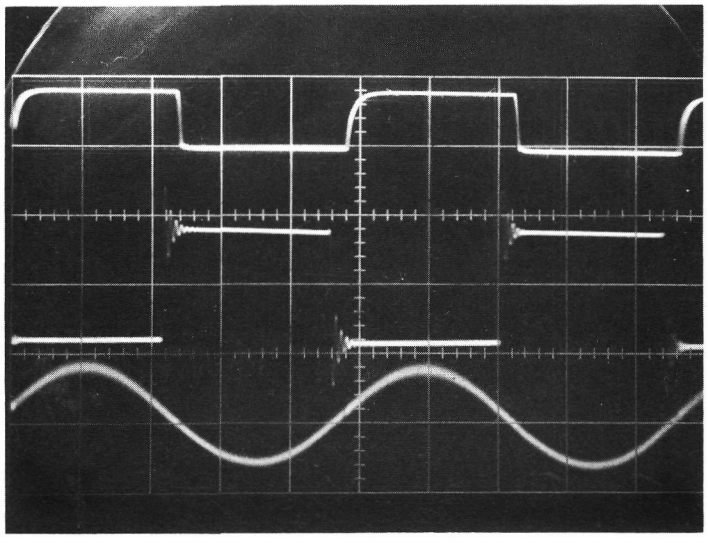

SYSTEM CLOCK 5V/DIV
OT–PIN 4

DITHER REFERENCE .5V/DIV
TP 28

RECOVERED DITHER .5V/DIV
OUT-OF-PHASE
TP 23

FIGURE 29 AUTOMATIC ELECTRONIC COMPENSATOR CLOCK AND RECOVERED DITHER WAVEFORMS

The dither frequency modulation and dither phase relationships are illustrated in Figure 30. The relative optical polarization of the laser beam output is plotted along the vertical axis and the applied modulator bias voltage along the horizontal axis; the resultant curve is referred to as the transmission curve. Points at the top of the curve represents bias voltages where the transmitted beam has linear vertical polarization; points at the bottom of the curve represents bias voltages where the transmitted beam has linear horizontal polarization; points in between represents bias voltages for some degree of elliptical polarization which can be resolved, with a polarization analyzer, into both vertical and horizontal polarization components. With the DC bias voltage applied at point V_b (as shown to represent a binary "0" level) the transmitted beam had linear horizontal polarization; when the DC bias voltage was switched to V_d (to represent a binary "1" level) the transmitted beam had linear vertical polarization. The same results could have been obtained by switching the DC bias voltage to point V_e (V_d minus V_b or V_b minus V_e represents the modulator switching voltage). When the DC bias voltage was changed, a small amount back and forth about the desired operating point, V_b, (as indicated by the low frequency dither signal superimposed on the DC bias) the transmitted beam changed a small amount from linear horizontal polarization and became slightly elliptically polarized. When the DC bias was changed either direction from nominal, the modulation goes through one complete cycle (linear to elliptical to linear polarization) for each half cycle of the dither signal on the DC bias.

Now for the sake of discussion, let's say a temperature change caused the modulator crystal characteristics to change so that V_a was now the required bias voltage for linear horizontal polarization (again for the sake of discussion and clarity,

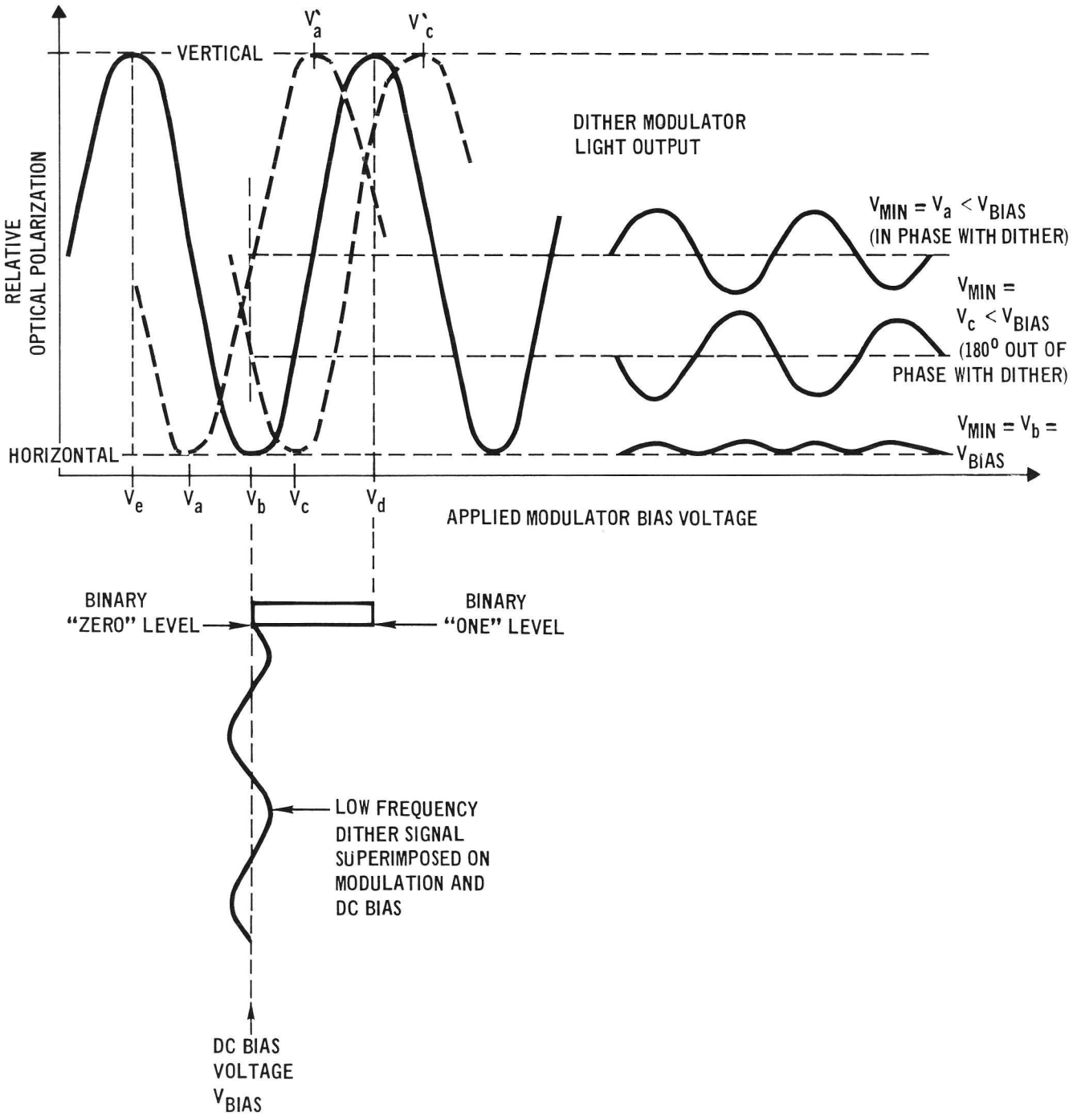

FIGURE 30 DITHER FREQUENCY PHASE RELATIONSHIPS
IN AUTOMATIC ELECTRONIC COMPENSATOR

the amount of change was exaggerated). With the bias voltage still at V_b, the operating point shifted up the positive slope of the transmission curve to point "X", where the transmitted beam was elliptically polarized; positive swings of the dither signal on the bias voltage caused the polarization to move toward the linear vertical polarization side of the curve; negative swings of the dither signal caused the polarization to move toward the linear horizontal polarization side. The resulting transmitted polarization was then dithering back and forth at the dither signal rate. When the crystal characteristics change in the other direction so that V_c was the required bias voltage for linear horizontal polarization, the operating point shifted up the negative slope of the transmission curve to point "Y". The transmitted beam polarization was basically the same as described above except the polarization dithers back and forth with a 180° phase relationship from that described above. The automatic electronic compensator (AEC) detects this phase relationship with respect to the applied dither signal to control the bias direction change.

Now the same analysis could be made around the binary "1" bias level at point V_d. However, the operating point "X'" was on a negative slope of the transmission curve in place of a positive slope as point "X" is; point "Y'" was also on the opposite slope for the same shift in crystal characteristics. Therefore, the corresponding polarization dither also had the opposite phase relationship which, when applied to the same AEC as above, produced compensation in the wrong direction. This was the reason a gate circuit was required, to invert the phase of the dither information that was generated during the binary "1" level. All of the recovered dither information did then provide compensation to the single desired point.

The laser beam was now polarization modulated. One percent of the optical pulse amplitude was split from the main beam for the AEC operation. The 1% beam was passed through a polarization analyzer where the polarization modulation for each pulse was resolved into both horizontal and vertical components. The dither modulation now showed up as amplitude modulation, as illustrated in Figure 31, where a "1-0-1" type modulation format was used to represent data modulation. For simplicity, only a few pulses are shown per dither cycle. These analyzed optical signals were analogous to amplitude modulated RF waveforms. The vertical polarization component was not used. The horizontal polarization component was focused onto a photodiode where the optical pulses were converted to electrical pulses. Ideally, only every other pulse (or the binary "0" pulses) appeared as shown in waveform 4 in Figure 31; however, due to the finite extinction ration, a small part of the binary "1" pulse was also present, as illustrated in waveform 5, Figure 31. Note that the low frequency dither modulation components on these two waveforms are 180° out-of-phase with respect to each other as explained above. Therefore, the dither component in waveform 5 must be inverted for correct automatic compensation.

The detected pulses from the photodiode were then amplified by a pulse amplifier that had a low frequency cut-off around 100 MHz; this cut-off point eliminated the baseband frequency component of the recovered dither signal (100 kHz) and passed only the upper frequency side-band information. The baseband frequency components were eliminated because their phase shift through the amplifier and gate circuits could introduce a timing problem for gating the desired dither components. The photodiode frequency spectrum output is shown in Figures 32 and 33. Figure 32 is the broadband spectrum with and without the six-stage PN code data modulation; the large power points are the fundamental second, third, and fourth frequency harmonics. The time reference was expanded in Figure 33 to

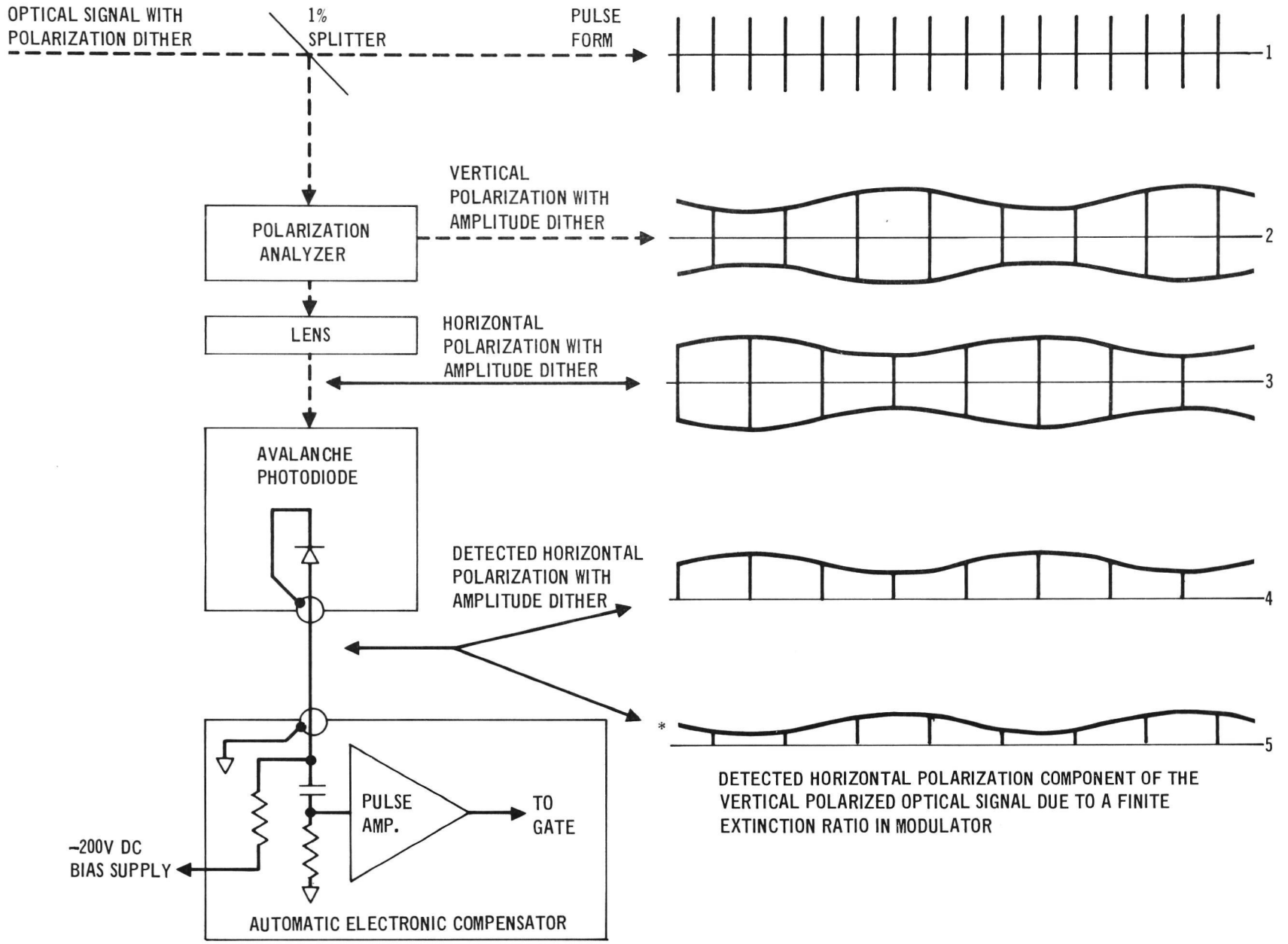

FIGURE 31 MODULATOR COMPENSATOR DITHER ANALYSIS WITH ONE-ZERO-ONE MODULATION

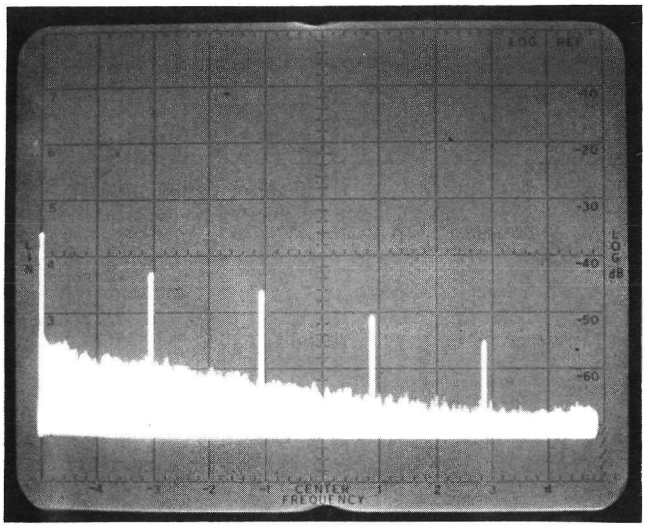

6–STAGE PN CODE DATA MODULATION

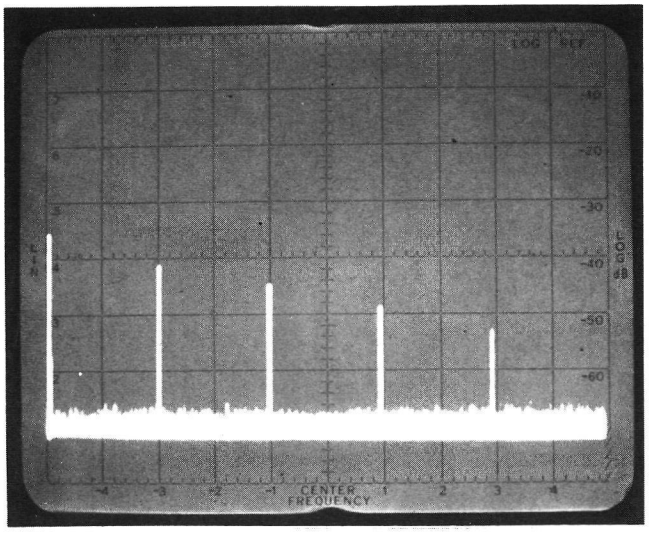

ALL ZERO DATA MODULATION

FIGURE 32 PHOTODIODE FREQUENCY SPECTRUM OUTPUT

200 MHz/DIV
CENTER POINT 1 GHz REFERENCED AT –4 dBm

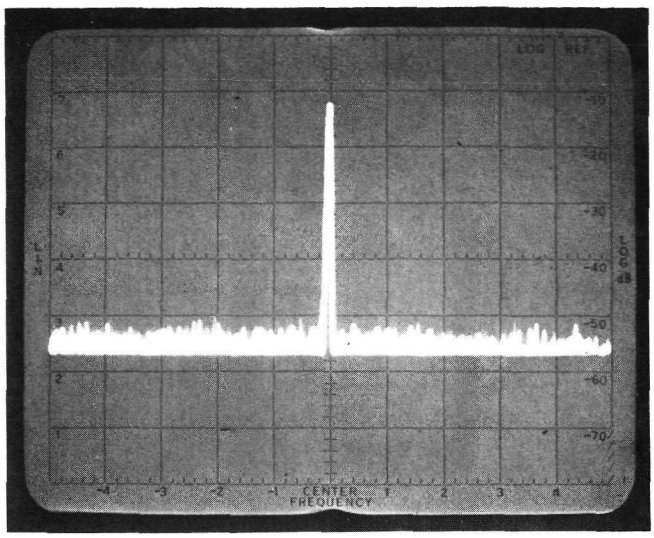

COMPENSATED CORRECTLY

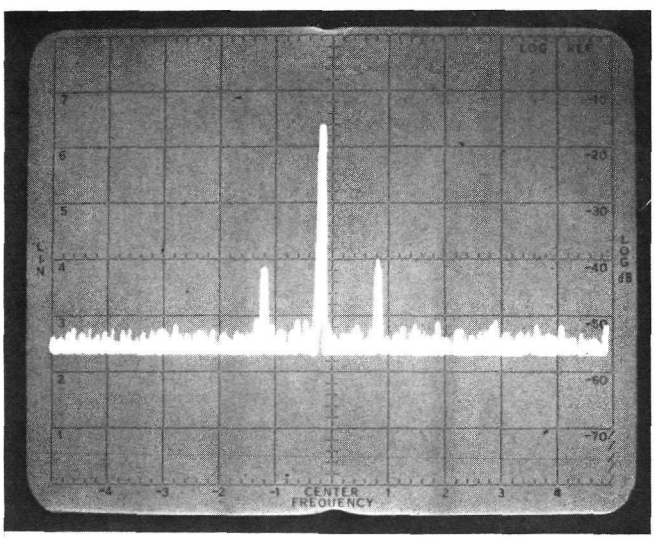

COMPENSATED OVER RANGE

FIGURE 33 PHOTODIODE FREQUENCY SPECTRUM OUTPUT

100 kHz/DIV

CENTER POINT 400 MHz

REFERENCED AT -34 dBm

show the dither side-bands on each side of the fundamental (400 MHz) signal. When compensating, the dither component was too small to see (down over 46 dB from fundamental); the second picture is with the compensator over range to illustrate the dither side-bands. Figure 34 shows the same two conditions (as Figure 33) at the pulse amplifier output; here the side-band can be seen during compensation; the over range condition also contained second and third harmonics.

The gate function is illustrated in Figure 35. The pulse amplifier output was applied to one gate input; the corresponding driver waveform was applied to the second gate input and timed to arrive at the same time as the pulses from the pulse amplifier. The pulses corresponding to driver binary "0's" were passed unchanged, the pulses corresponding to driver binary "1's" were passed with inverted polarity. Note the dither frequency component was also inverted. Now both dither frequency components have the same phase relationship and produced a single compensation point.

Because the gate was a double-balance-mixer, it was transformer coupled and therefore, had frequency limitations below 100 kHz. Modulation data with frequency components below 100 kHz caused the automatic compensator operation to degrade because of improper gating action. To avoid this problem, the modulation data was changed from binary coded data to Manchester coded data where the effective low operating frequency component was one-half the fundamental frequency (400 MHz) or 200 MHz. Then the lower frequency components of the modulation data have no affect. The Manchester code drive waveform is illustrated in Figure 36.

2.5.4.2 Manual Electronic Compensator. The manual compensator (Figure 37) provided bias for the modulator when automatic operation was not desired. The manual compensator was used to set the modulator for maximum extinction ratio when

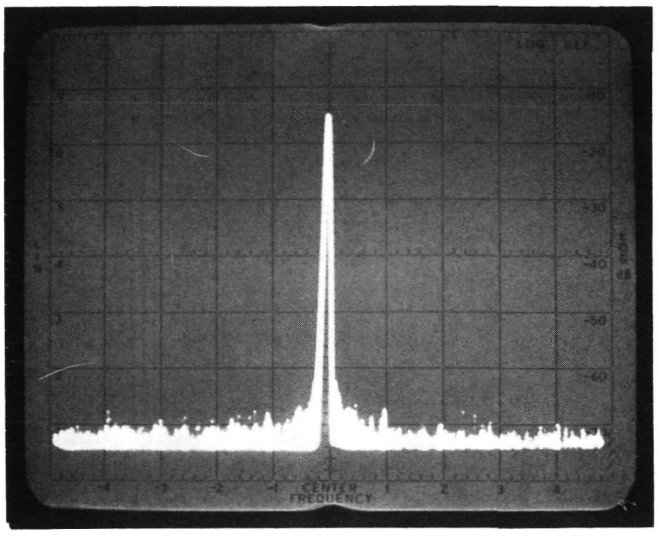

COMPENSATED CORRECTLY

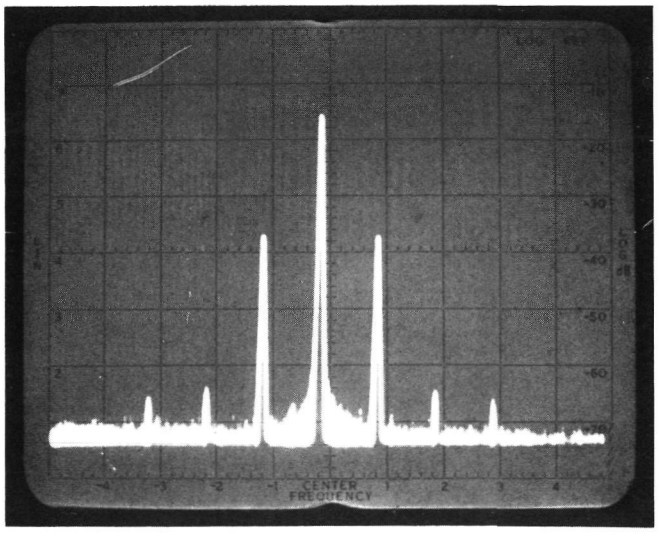

COMPENSATED OVER RANGE

FIGURE 34 PULSE AMPLIFIER FREQUENCY SPECTRUM OUTPUT

100 kHz/DIV

CENTER POINT 400 MHz

REFERENCED AT -14 dBm

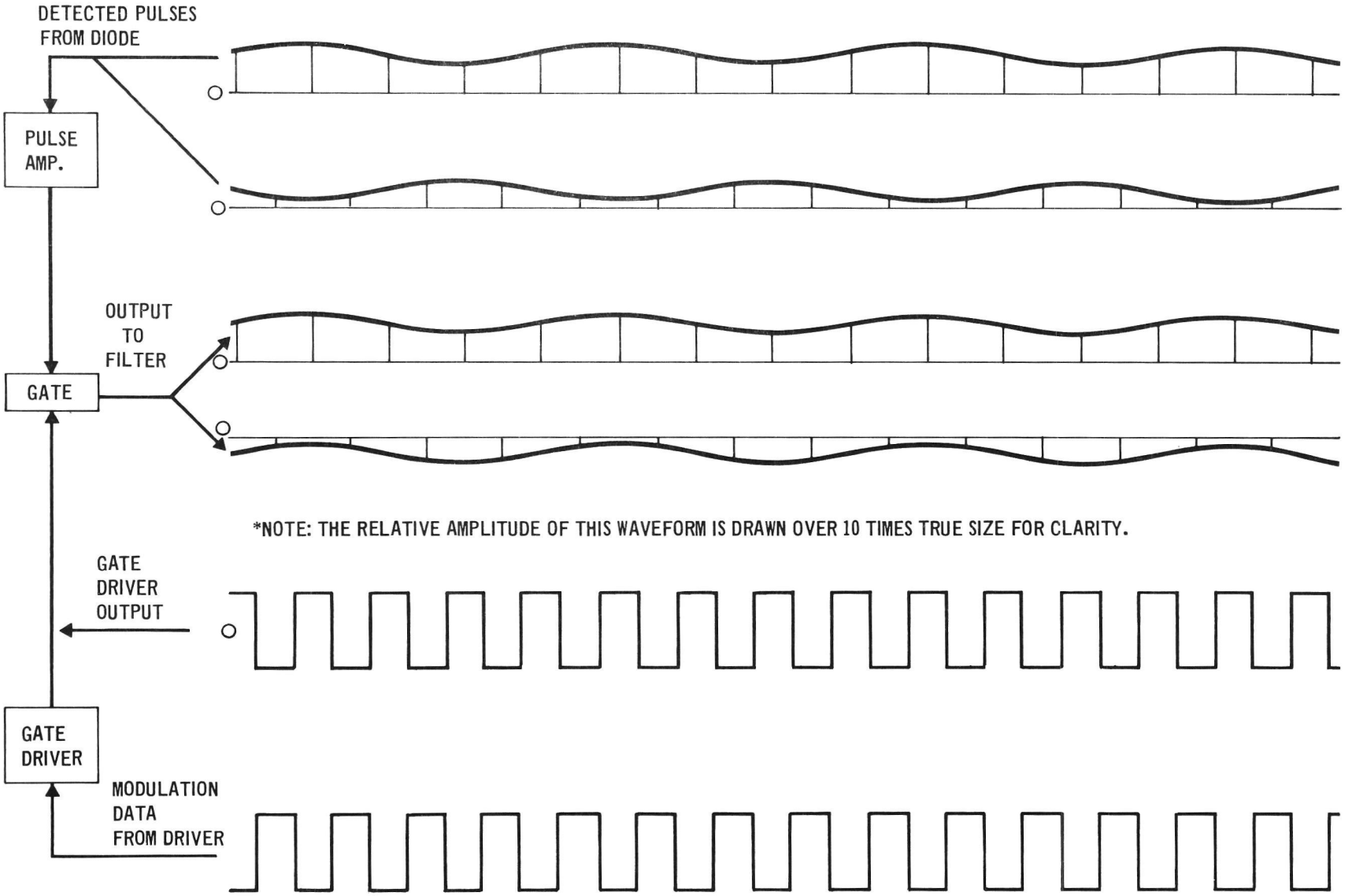

FIGURE 35 MODULATOR COMPENSATOR GATE ANALYSIS

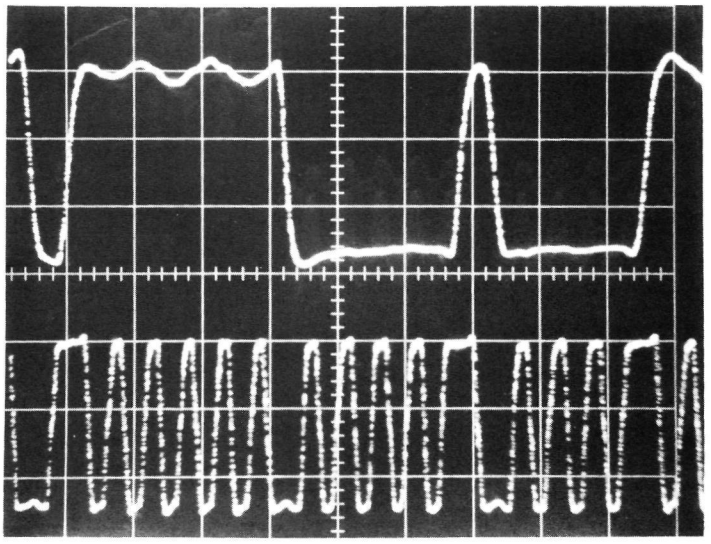

MODULATOR
DRIVER NO. 36

MANCHESTER
CODE

FIGURE 36 MANCHESTER DRIVE WAVEFORM VS.
MODULATOR DRIVER WAVEFORM

VERTICAL: 10V/DIV
HORIZONTAL: 5 ns/DIV

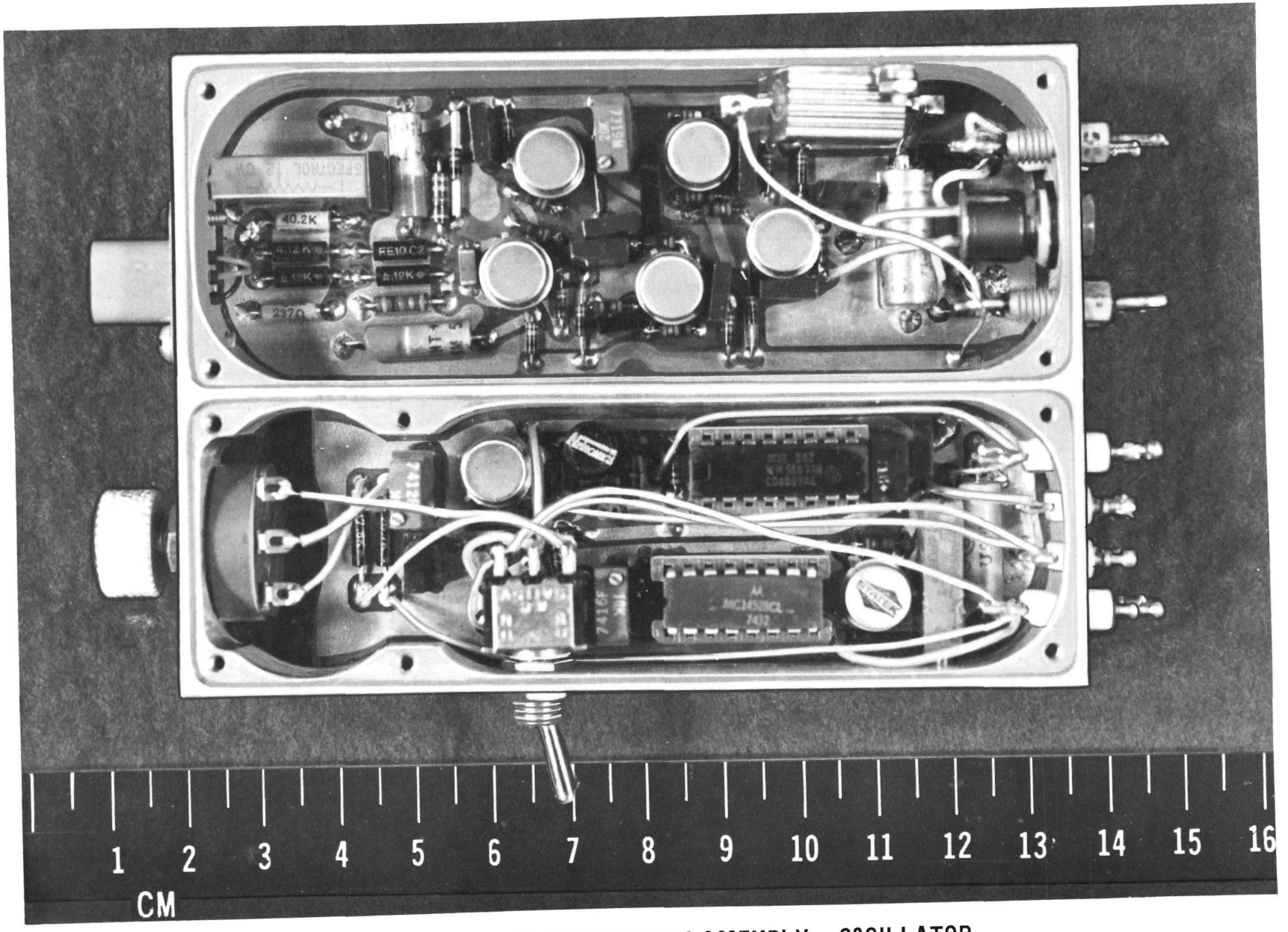

FIGURE 37 MODULE OF THE ELECTRONICS ASSEMBLY – OSCILLATOR MANUAL COMPENSATOR AND TEMPERATURE CONTROLLER MODULE

operating with a data input. In addition, the manual compensator was used to measure the static extinction ratio of the modulator by biasing the crystals first for minimum and then for maximum transmission with the output polarization splitter cube in the beam path.

The manual compensator provided a DC output which was used to drive the bias voltage amplifier. The amplifier which was also used for automatic compensator operation, controlled the voltage applied to the modulator crystals for compensation purposes. A compensator select switch located on the manual compensator module was used to select the desired mode of compensation, and the manual bias adjustment was made with the control located on the end of the manual compensator module. The range of bias voltage provided by the manual compensator was approximately the same as that provided by the AEC -15 to +55 Vdc (over $\pm$60 Vdc differential).

2.5.4.3 Manual Thermal Differential Compensator. The manual thermal differential compensator (TDC) (Figure 1) was used in conjunction with either the automatic or manual electronic compensator to adjust the modulator crystals to the desired operating point. Although the end result of using either the thermal differential or electronic compensator was the same, i.e., adjusting the modulator to obtain maximum extinction ratio, the methods and reasons were different.

The TDC was added to the modulator units as a modification designed to improve modulator electronics compensator operating stability. The function of the TDC was to bias the modulator so that the bias voltage produced by the electronic compensator resulted in zero average field across the modulator crystals. This was the condition for which optimum voltage stability occurs and therefore maximum extinction ratio maintained over a given test period.

The term thermal differential compensation arose from the fact that this compensation technique utilized the temperature dependence of the birefringence of $LiTaO_3$ to obtain optical compensation. Normally, in a two crystal crossed axes modulator configuration both modulator crystals were maintained at a uniform temperature inside a boron nitride oven core which was heated by two balanced heater coils located at opposite ends of the core. By intentionally unbalancing the heaters a precise temperature differential was created within the oven. This temperature differential caused a change in the birefringence of one crystal with respect to the other and thus produced a net birefringence change which was a function of the differential. The heater unbalance was created by a variable resistance connected in parallel with one of the heaters and adjusted for the desired unbalance. Although a TDC compensation range equivalent to only plus or minus one fringe (full switching) was required, the actual available range was four times that amount.

2.6 MODULATOR LABORATORY POWER SUPPLY. The power supply package consisted of commercial regulated power supply modules assembled in a chassis with front panel control. The chassis and front panel fit into a standard 19-inch equipment rack. A block diagram of a power supply is shown in Figure 38. Table V lists all the voltages provided for the 1.06μm wideband modulator.

Eleven voltages were provided for the operation of the modulator driver, automatic electronic compensator, and temperature controller, as listed in Table V. Each supply was voltage regulated and current limited. Protection (crowbar) circuits with manual reset capability were provided for circuits which might be damaged by overload due to operator error. Power supply controls included an oven temperature selector switch for modulator warmup and cool down, an on-off switch for power for the photodiode used in the automatic compensator circuit, an on-off switch for driver final stage output which can have either an operational output or a DC level output, and reset buttons for the protection circuits.

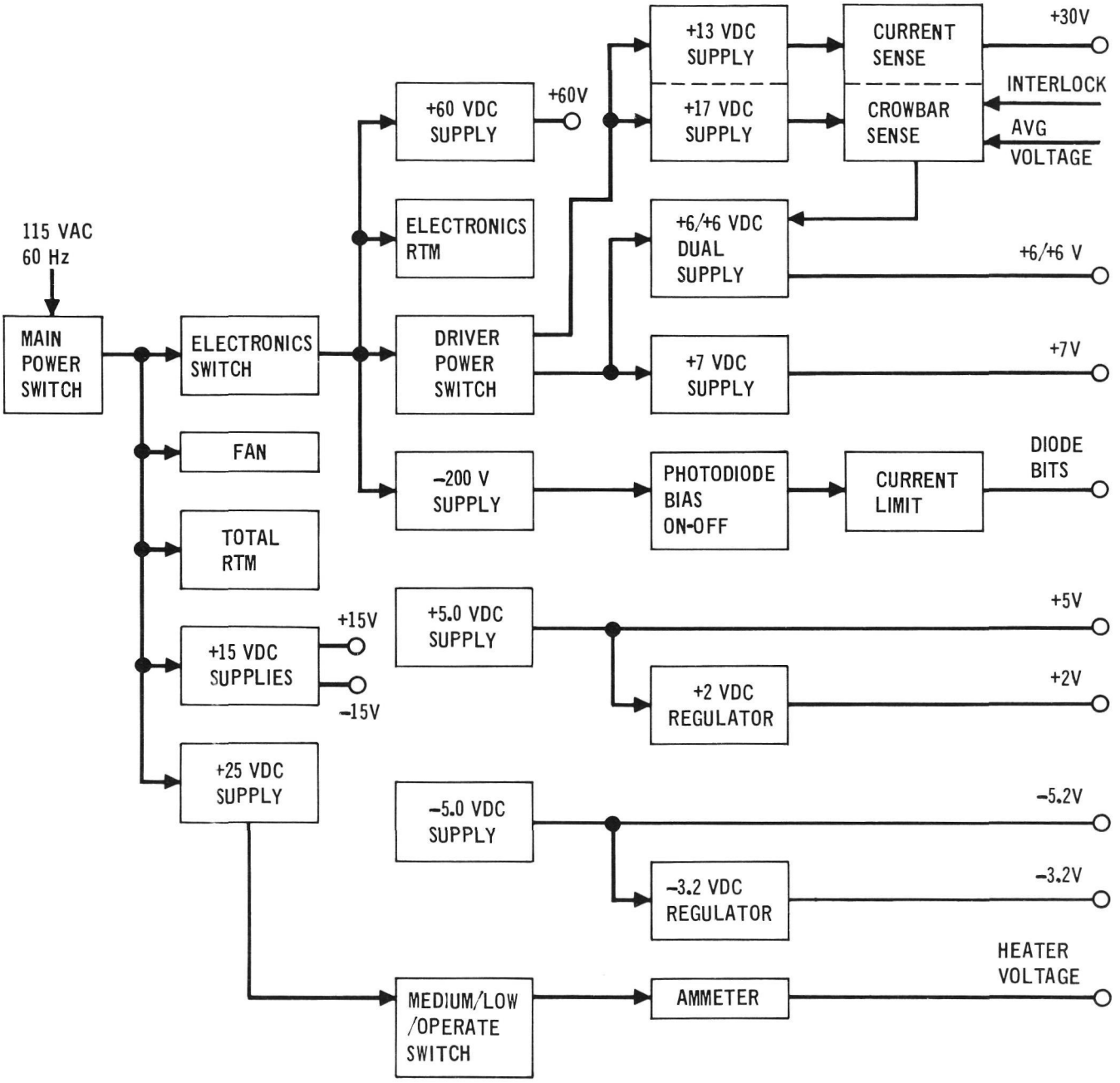

FIGURE 38 POWER SUPPLY BLOCK DIAGRAM

TABLE V

Power Supply Voltages

	+2.0V dc	Regulated, for automatic compensators and modulator drivers
	-3.2V dc	Regulated, for automatic compensators
	+5.0V dc	Regulated, for automatic compensators
	-5.2V dc	Regulated, for automatic compensators and modulator drivers
	+15.0V dc	Regulated, for automatic compensators, temperature controller
	-15.0V dc	Regulated, for automatic compensators, temperature controller
*	+7.0V dc	Regulated, for modulator driver buffer stage
*	+6.0V dc	Regulated, for modulator driver Q grounded base stage
*	+6.0V dc	Regulated, for modulator driver $\overline{Q}$ grounded base stage
*	+30.0V dc	Regulated, for modulator driver output
	+25.0V dc	Regulated, for temperature controller
	+60.0V dc	Regulated, for automatic compensator
	+200.0V dc	Regulated, for silicon photodiode for automatic compensator

*Note: These supplies will be adjusted as required to meet the individual driver needs.

2.7 INTERCONNECTIONS. There are three main interconnections as shown in Figure 39. Since the modulator assembly was located on a different mainstructure than the electronics to reduce the thermal loading and weight on the modulator structure, the package must interconnect via shield cables. The interconnection cable length from optics package to electronics was 1.33 meters. The modulator electronics have modulation data input, a synchronous clock input, and modulator laboratory power supply input. The modulator laboratory power supply was powered by 115 Vac, 60 Hz input.

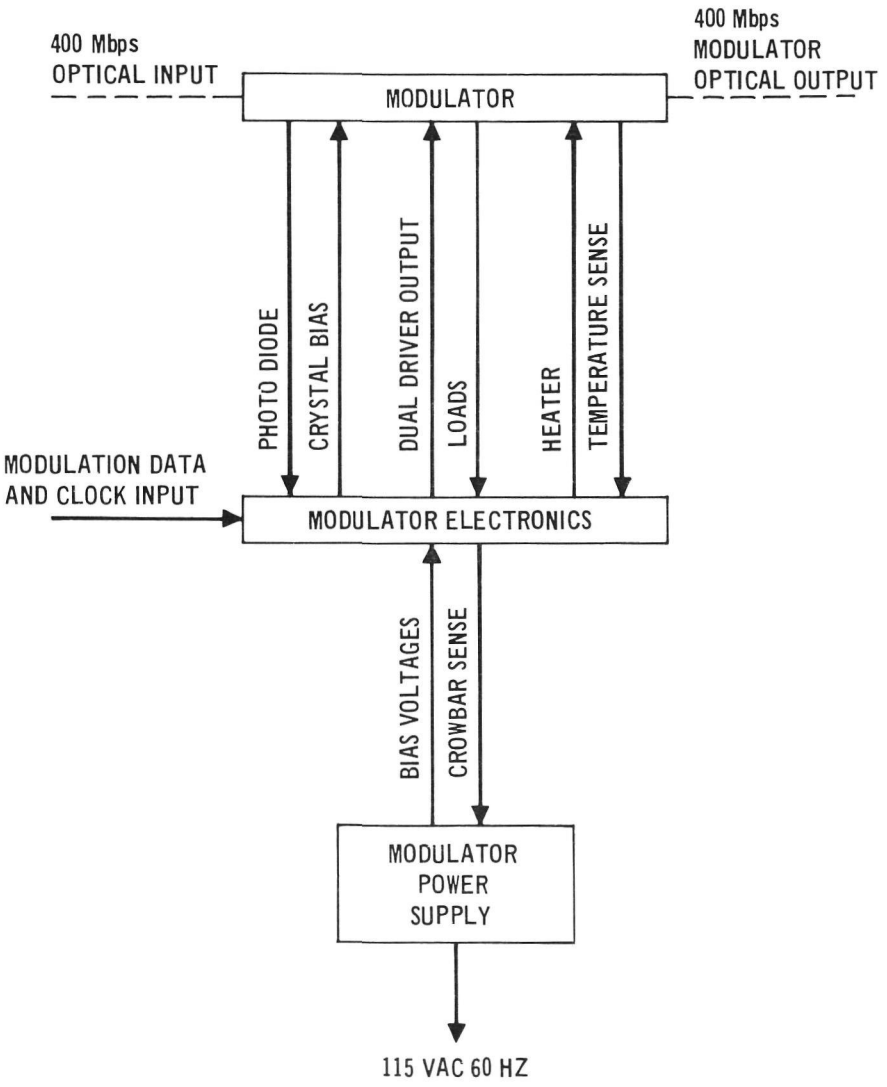

FIGURE 39 MODULATOR ELECTRONICS INTERCONNECTION DIAGRAM

3. MODULATOR INTERFACE SPECIFICATIONS

The interface specifications for the 1.06 Micrometer Wideband Laser Modulator are given in Table VI . These include the optical input, electrical input, optical output, mechanical interface and thermal interface.

MDAC-E designed a broadband laser modulator which consisted of an electro-optic modulator assembly and an electronics assembly interconnected with one and one-third meter long electrical shielded cables. The electrooptic modulator assembly included lithium tantalate crystals mounted in a temperature controlled enclosure with input and output beam forming optics, and a broadband electrical matching network to couple the driver output to the electrooptic crystals. The electronics assembly included a dc coupled modulator driver, temperature controller, automatic electronic compensator, manual electronic compensator and manual thermal differential compensator. The broadband laser modulator required only a laboratory power supply, input optical beam, and a low level signal source for operation. The broadband laser modulator was designed to the specifications given in Table III.

TABLE VI

Interface Specifications

Optical Input	
Wavelength	1.06 μm TEM_{∞}
Beam Diameter	~ 1 mm
Beam Divergence	2.5 mrad
Beam Ellipticity	$\leq$ 11:10
Polarization	Vertical
Polarization Purity	$\geq$ 200:1
Power	100 mW
Power Variation	$< \pm 5\%$
Mode-Lock Pulse Repetition	400 Mpps
Pulse Width	$\leq$ 200 ps
Beam Input Position	11.5 cm above modulator baseplate

Electrical Input

Modulation Format	Pulse gated binary modulation Pulse polarization binary modulation
Data Rate	10^4 to 4 x 10^8 bits per second
Data Duty Cycle	30%-70%
Input Impedance	50 ohms resistive (nominal)
Binary 1 Signal Level	-0.8 volt $\pm$0.1 volt
Binary 0 Signal Level	-1.6 volts $\pm$0.1 volt
Timing accuracy with respect to laser pulse timing	$\leq$ 250 ps peak-peak
Power Supply Input	120 volts, 60 Hertz

Optical Output

Static Extinction Ratio	50:1
Dynamic Extinction Ratio	20:1
Optical Transmission	$\geq$ 70%
Beam Diameter	1.2 mm
Beam Divergence	2.5 mrad
Total Power Dissipation	$\leq$ 45 watts
Weight	$\leq$ 2.0 kg
Volume	$\leq$ 2 x 10^3 cm^3

Mechanical Interface

Modulator Optics Package Dimensions: 24.2cm x 7.0cm x 11.4cm

Overall Modulator Dimensions: 24.2cm x 7.0cm x 17.8cm (including baseplate)

Modulator Electronic Dimensions: 17.7cm x 10.8cm x 7.6cm

Modulator Electronics Dimensions: 17.7cm x 13.4cm x 8.3cm (including baseplate)

Modulator Power Supply Dimensions: 54.5cm x 52.1cm x 40.5cm

Interconnect Cable Length: 5 meters

Separation of Modulator Electronics from Optics Package: 1.3 meters

Thermal Interface

Ambient Temperature 75° $\pm$10°F

4. PHYSICAL DESCRIPTION

A cutaway drawing of the modulator assembly was shown in Figure 9, and the nominal input and output optical beam locations were given in the figure. The modulator baseplate was a Huber camera mount and had provisions on each corner for clamping it to the table top. A top view photograph of the modulator with all components in place is shown in Figure 40. This view gives a perspective of the entire modulator. Close up photos of various portions of the modulator are included in the following pages to illustrate the location of controls, indicators, and test points.

4.1 MODULATOR MECHANICAL DESIGN. The 1.06 μm wideband modulator was composed of two major components (as shown in Figure 41) and a laboratory power supply package. (1) The modulator assembly which consisted of the oven assembly, an optics tail assembly, and two lens translators. (2) The electronics assembly which consisted of the modulator driven, load box, temperature controller, thermal differential compensator and both manual and automatic electronic compensators. (3) The laboratory power supply package which consisted of the commercial power supplies and circuit protection circuits for the modulator electronics. The separation of the laser modulator into two major assemblies permitted the electrooptic modulator assembly to be precisely aligned in the optical path of the laser beam and transmitter optics, while the electronic assembly was conveniently located with the remainder of the transmitter electronics.

4.1.1 Modulator Assembly Package. The modulator was attached to the "L" bracket which was mounted to the Humber camera mount for ease of modulator alignment by means of three mounting ears. The mounting ears securing the modulator subassembly were integral to the oven housings as shown in Figure 42.

The optics tail assembly and lens translator assemblies were secured to the ends of the oven housing via long bolts that fasten into threaded holes in the end faces of the housings, as shown in Figure 43. Optical alignment (in the direction perpendicular to the light beam) was maintained at the optics tail-to-oven

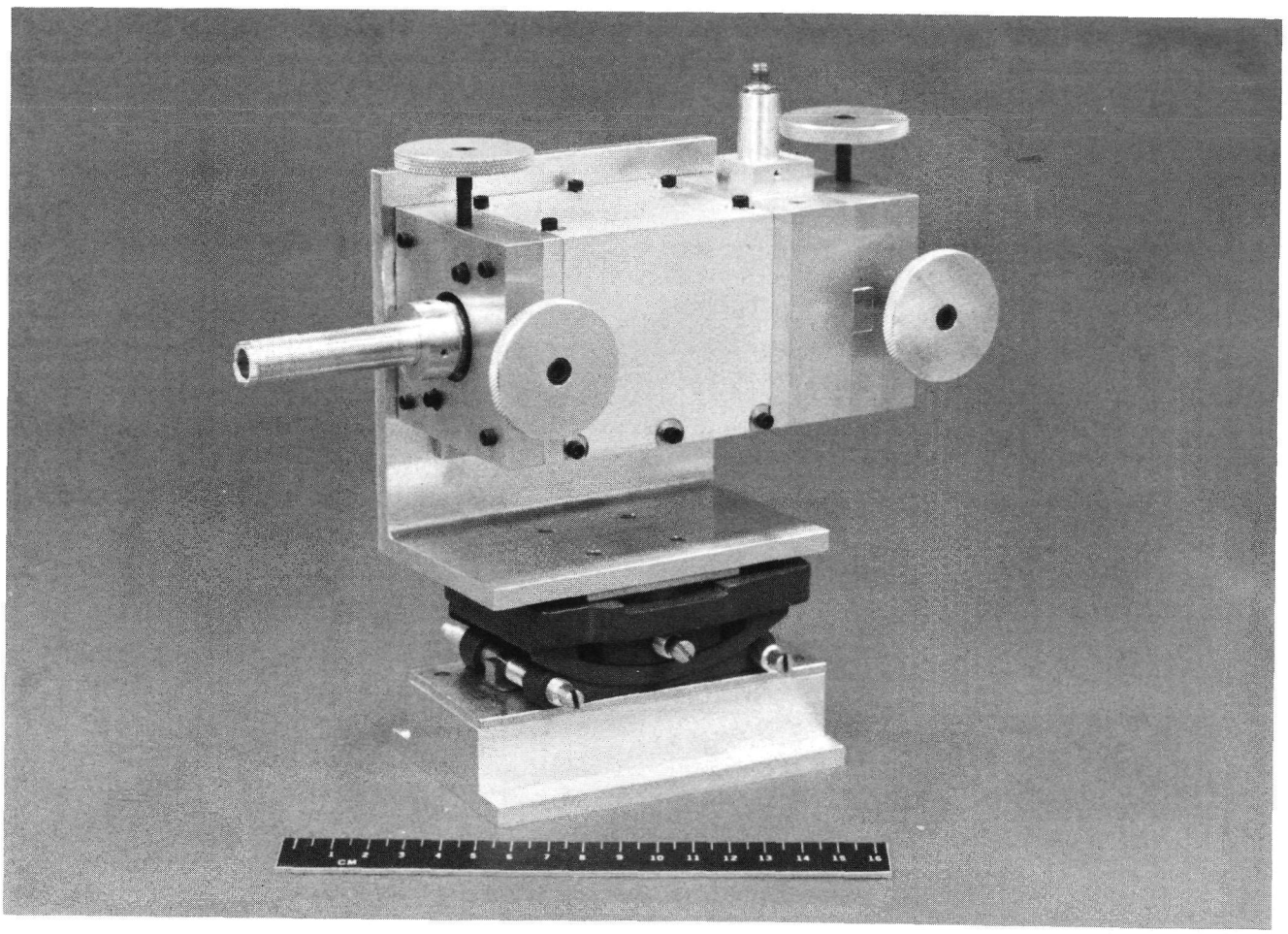

FIGURE 40 COMPLETED MODULATOR

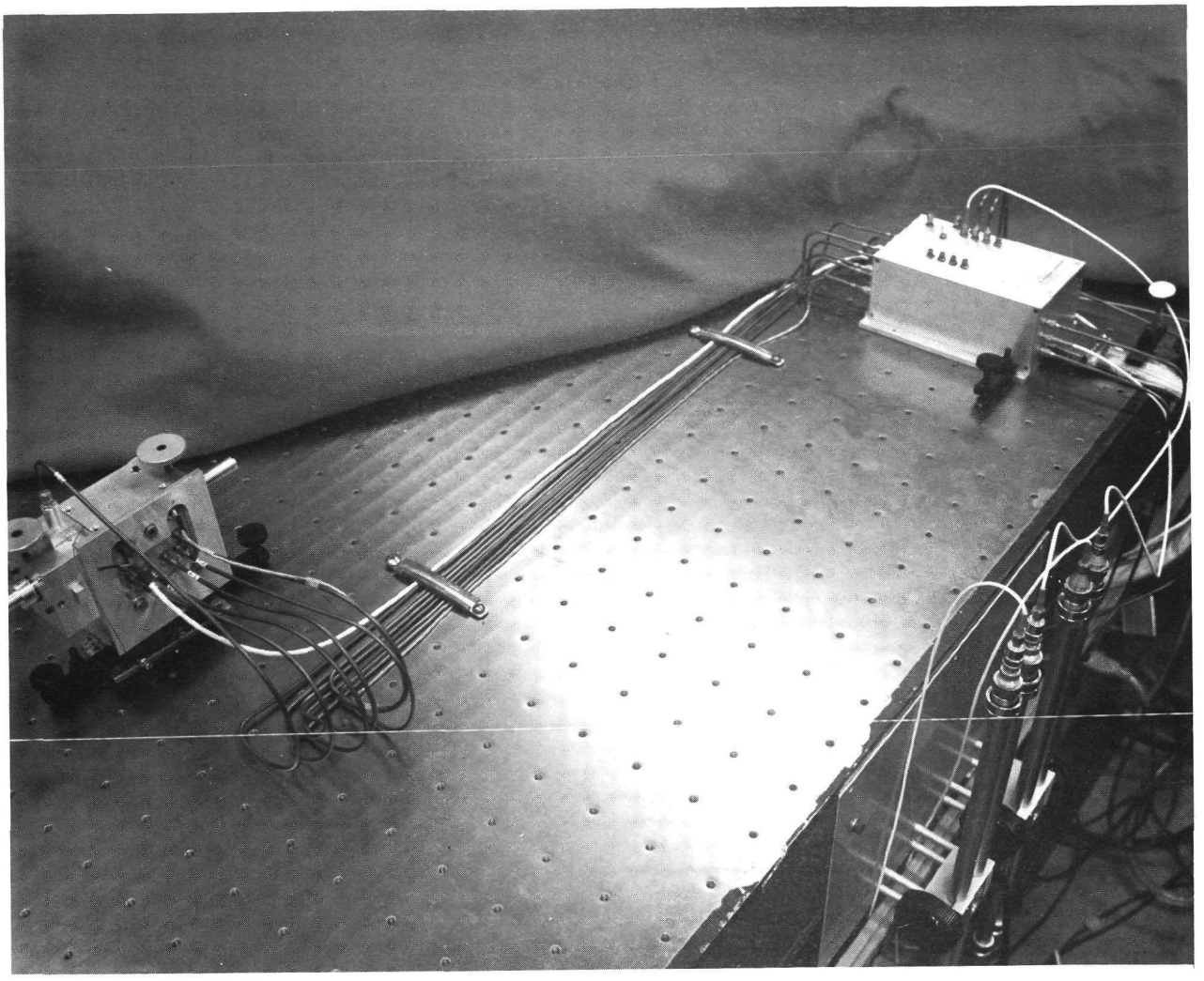

FIGURE 41 ASSEMBLED MODULATOR ASSEMBLY

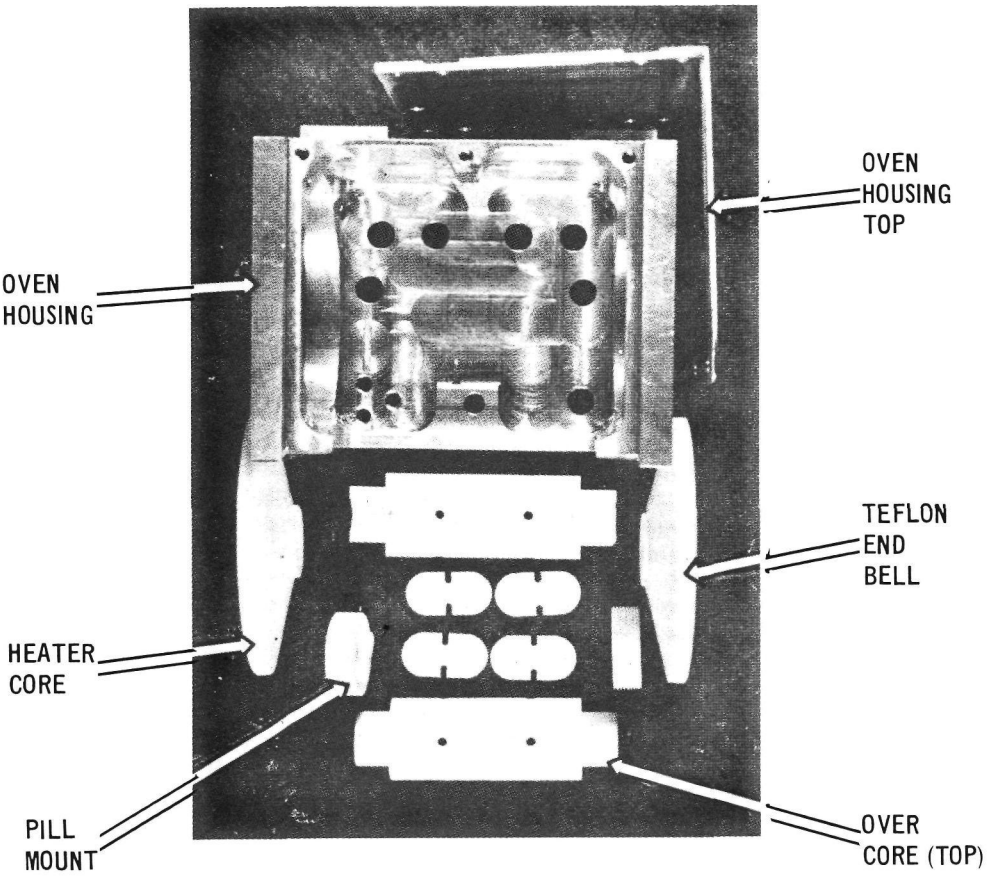

FIGURE 42 OVEN HOUSING COMPONENTS

interfaces, the lens translator-to-oven interfaces, and the lens translator-to-optics tail interfaces by a precision machined cylinder extending from the housing of one part into a precision slip-fit hole in the housing of the adjacent part, (see Figures 42, 43).

Photographs showing the front and back view of an assembled modulator is shown in Figure 44. The dimensions of the modulator assembly were 9.8 cm x 6.4 cm x 24.1 cm (including the lens holders) and the assembly weighed approximately 1.14 kg.

4.1.2 Electronics Assembly Package. The packaging approach for the modulator electronics package incorporated the elements of minimum volume and weight within the constraints of flexibility and maintainability. Consistent with this approach, the modulator electronics was packaged in a single unit made up of our modules arranged as shown in Figure 45. Photographs of the assembled unit are seen in Figure 46. The dimensions of the assembled electronic package were 18.4 cm x 10.8 cm x 7.6 cm and the assembly weighed 2.11 kg. The packaging techniques used in a given module were governed by considerations such as signal propagation, VSWR, cross-talk, power dissipation, as well as maintainability and flexibility. Planar construction using double side circuit boards was used to obtain maximum ground plane, which minimized crosstalk.

The circuit layouts were optimized to minimize signal propagation times, and coaxial interconnections were used where required for noise sensitive signals. Good EMI design and power grounds were incorporated in the layout to eliminate conductive and radiative interference between circuits. Adequate heat dissipation paths were included as a result of a thermal analysis of each module to ensure that all components operate well below their maximum safe temperature.

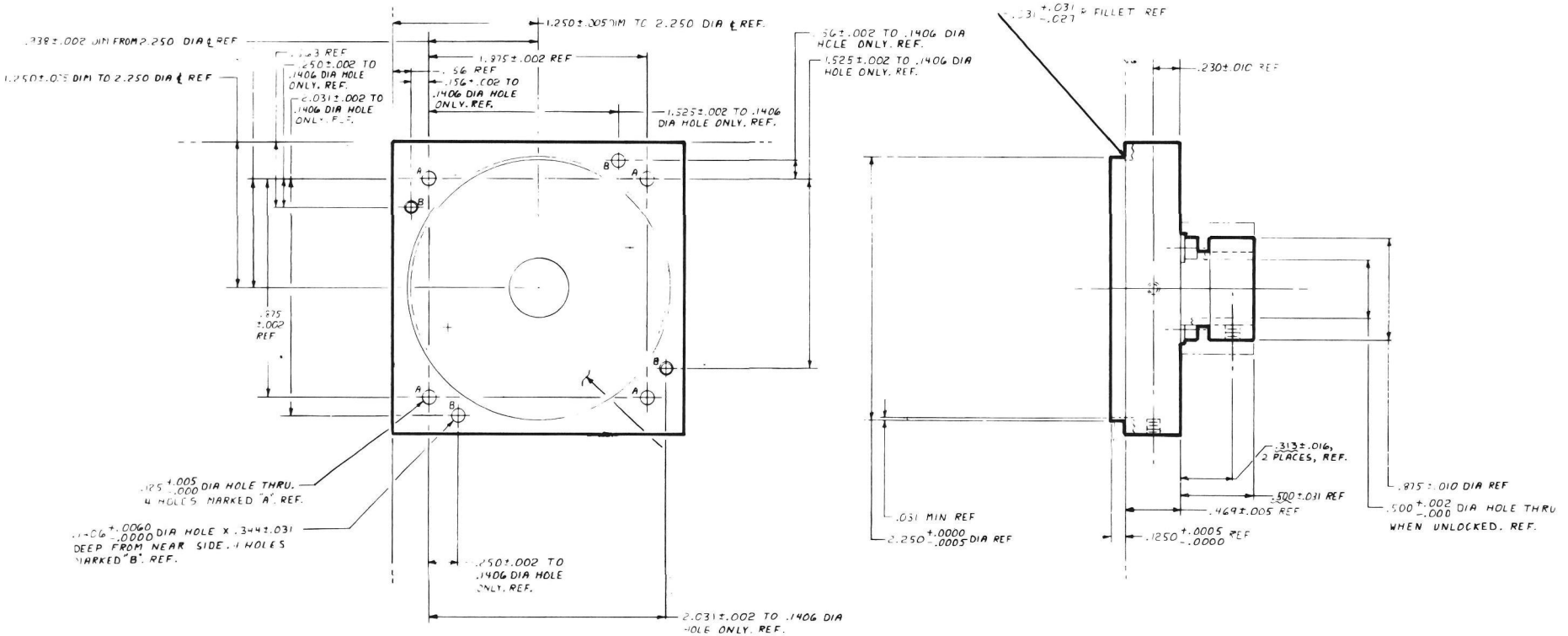

FIGURE 43 LENS TRANSLATOR

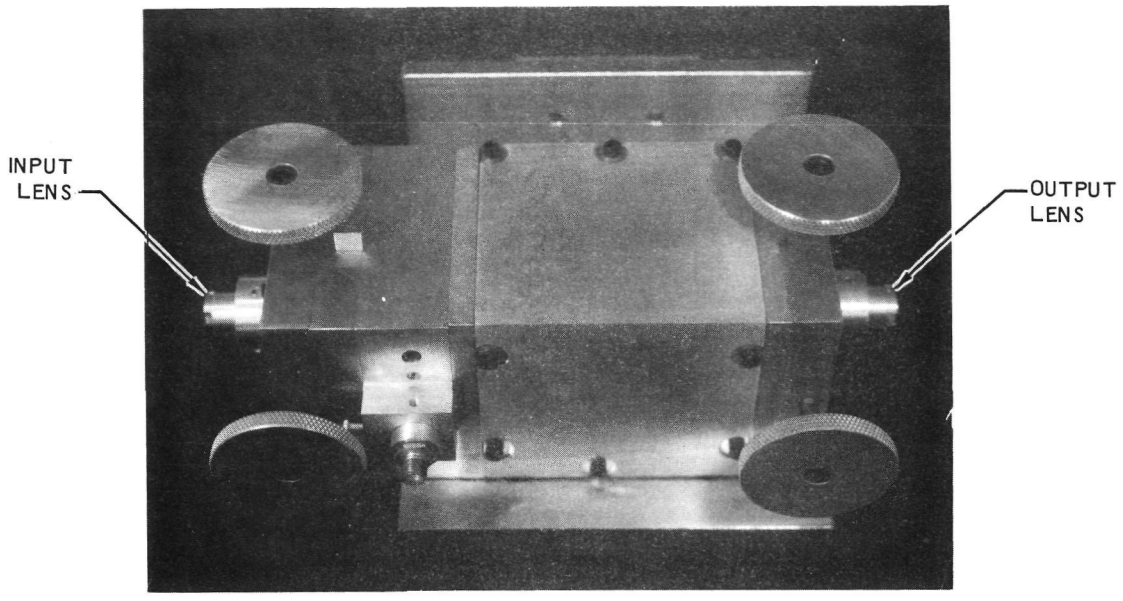

(A) FRONT VIEW OF MODULATOR SUBASSEMBLY SHOWING LENS, OVEN HOUSING CONTAINING CRYSTAL OVEN CORE, OPTICS TAIL AND TRANSMITTED FORMAT CHANGER.

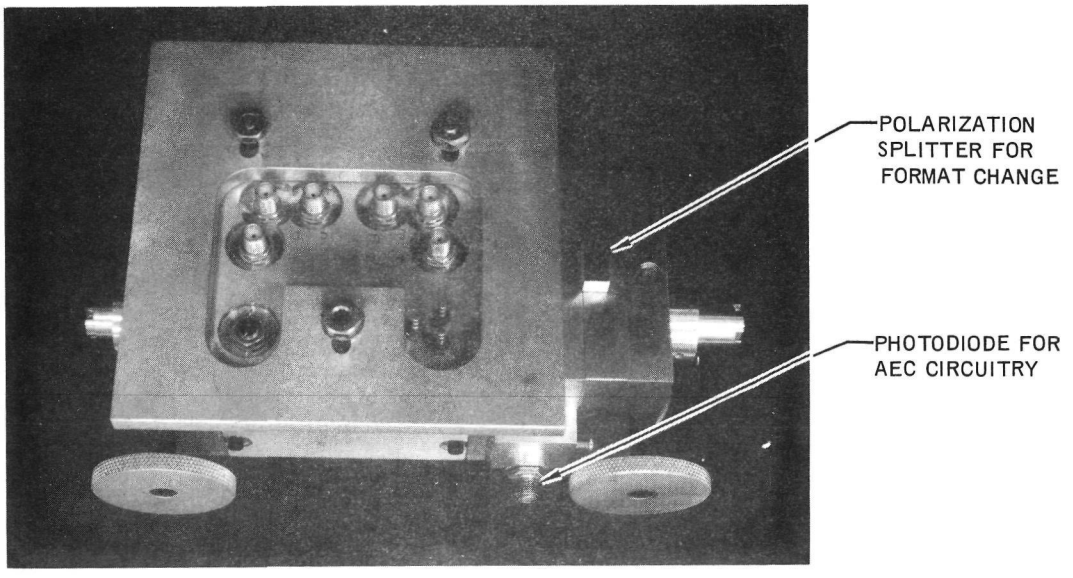

(B) BACK VIEW OF MODULATOR SUBASSEMBLY SHOWING ELECTRICAL INPUT CONNECTIONS

FIGURE 44 PHOTOGRAPH OF MODULATOR ASSEMBLY COMPLETED

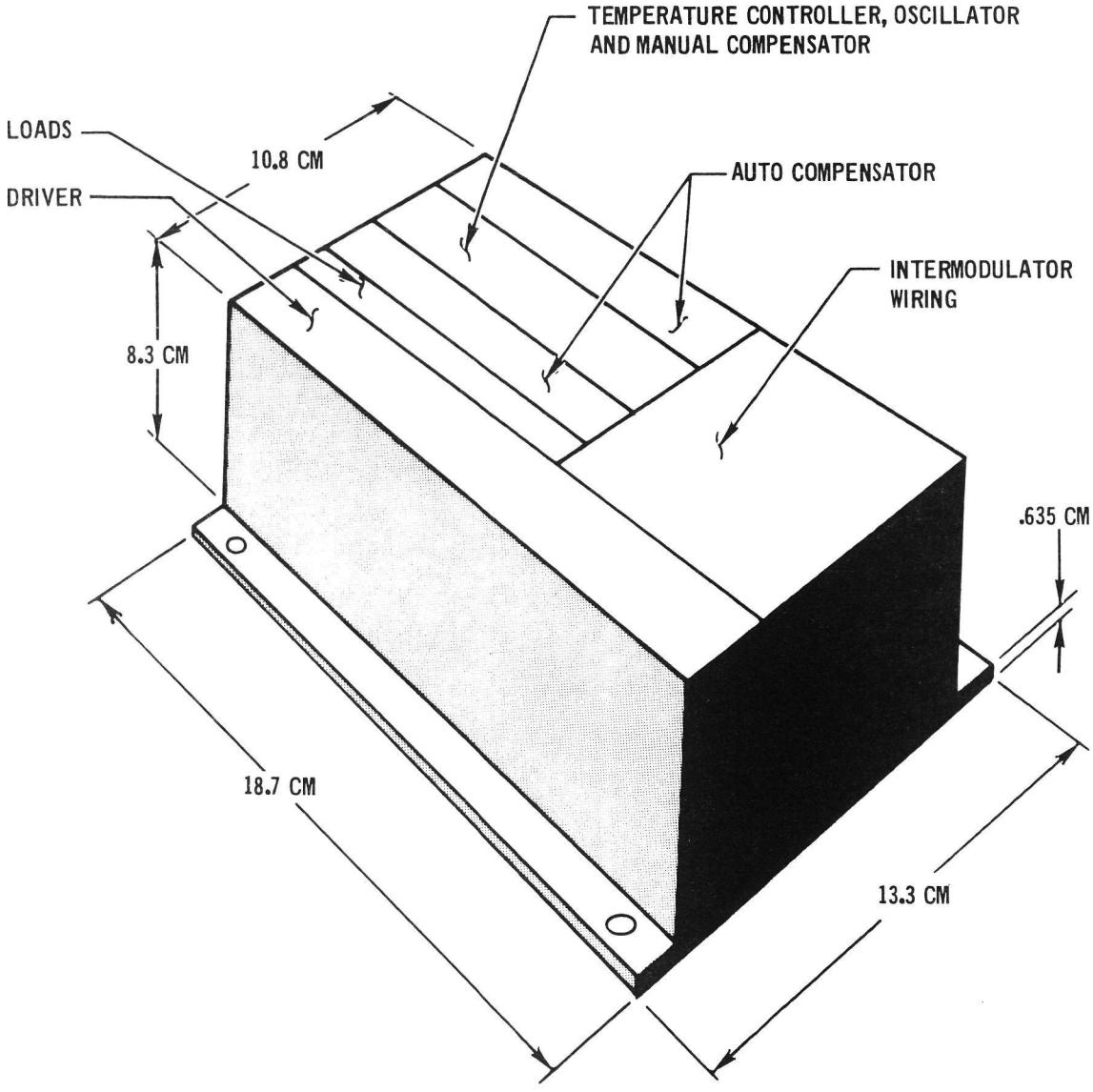

FIGURE 45 ELECTRONIC ASSEMBLY OUTLINE DRAWING

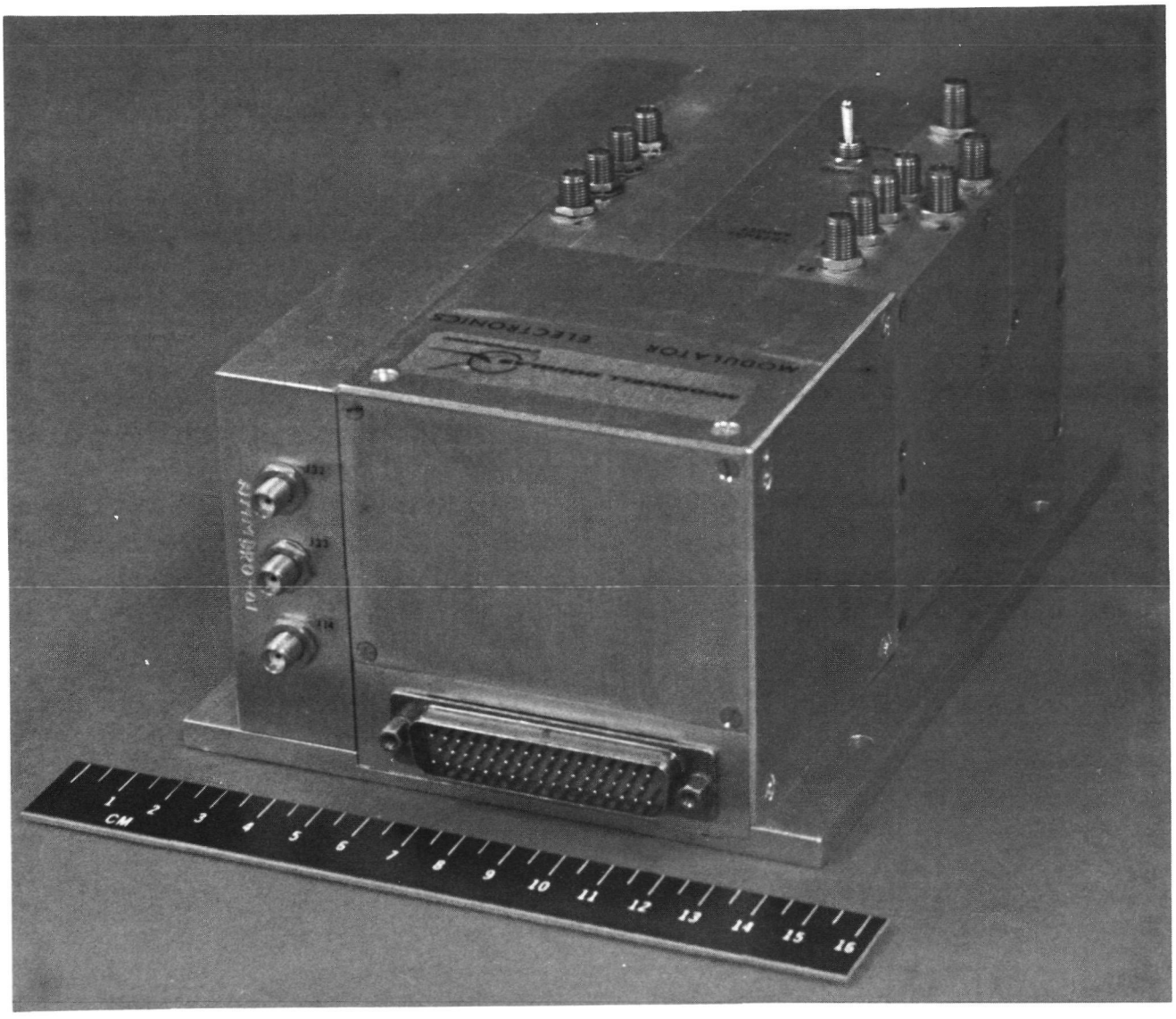

FIGURE 46 ELECTRONICS ASSEMBLY

Controls located on the modulator units include the manual/automatic electronic compensator selector switch, the manual electronic compensator bias adjust potentiometer, the manual thermal differential compensator adjust potentiometer and the temperature controller oven temperature adjust potentiometer.

The manual/automatic electronic compensator selector switch and the manual thermal differential compensator (TDC) adjustment are shown in Figure 47. Minimum thermal differential was produced for full counterclockwise rotation of the control and maximum thermal differential was produced by full clockwise rotation. When operating in the automatic electronic compensator mode, a clockwise rotation of the TDC control caused the automatic electronic compensator to produce an increase in bias voltage applied to the first (input) crystal.

The compensator selector switch is a two position switch for selecting either the automatic or the manual electronic compensation mode. The manual control shown in Figure 48 is inoperative in the automatic mode. The control had a bias voltage range of -15 Vdc to +55 Vdc for each bias output or a differential output over $\pm$60 V. The bias to the first (input) crystal (Test Point 26) moves to +60 V with respect to the second (output) crystal (Test Point 30) when the manual adjust was rotated clockwise, and to a -60 V when the manual adjust was rotated counterclockwise. These modes of operation are further described in Appendix I.

The oven temperature adjustment also shown in Figure 48 had been preset to produce a temperature of 150°C in the modulator oven. If some other operating temperature is desired, a clockwise rotation of the control increases oven temperature and a counterclockwise rotation decreases oven temperature. A thermocouple or other temperature monitor attached to the oven core is required when resetting the oven temperature in order to avoid possible overheating of the crystals.

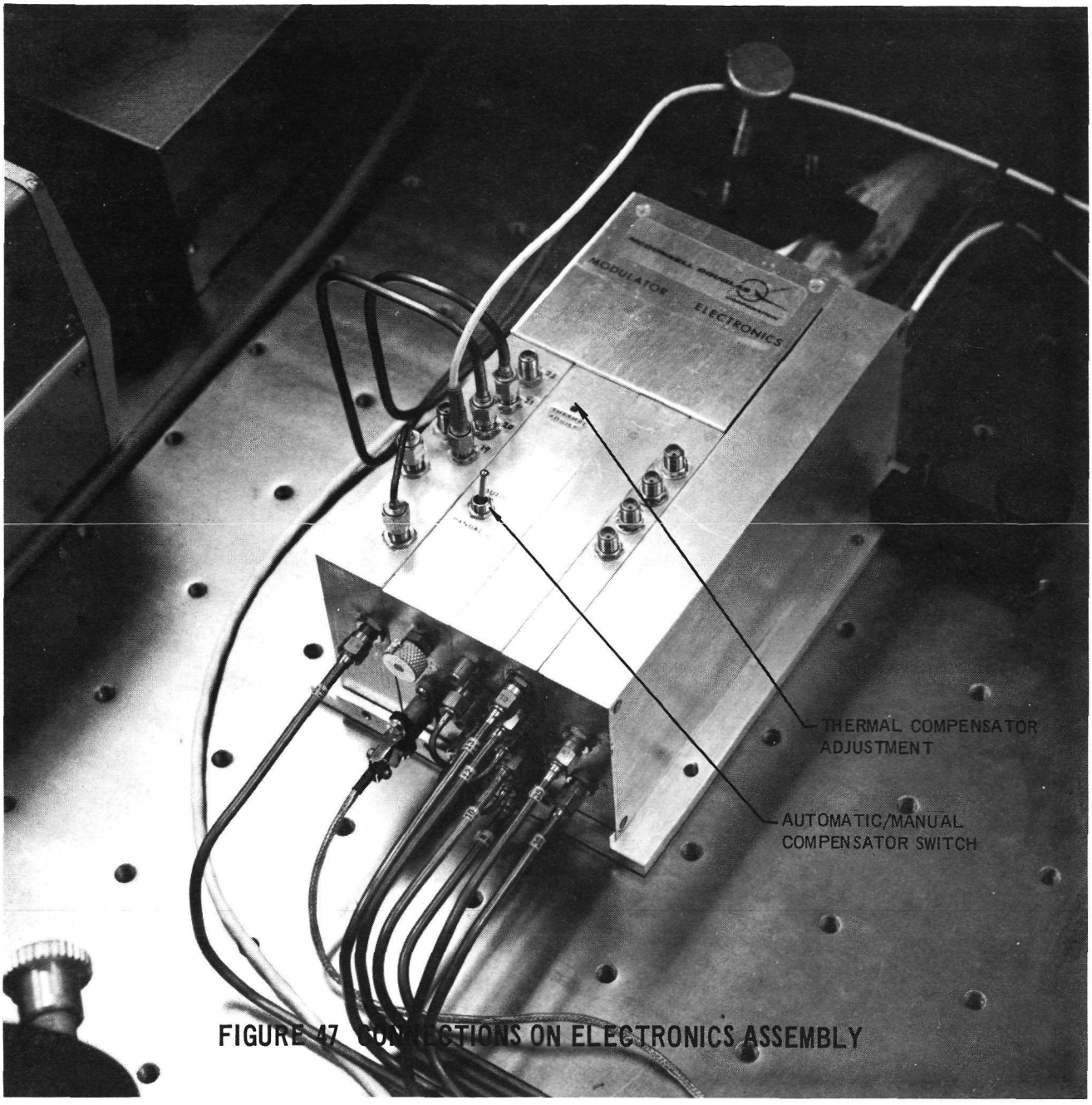

FIGURE 47 CONNECTIONS ON ELECTRONICS ASSEMBLY

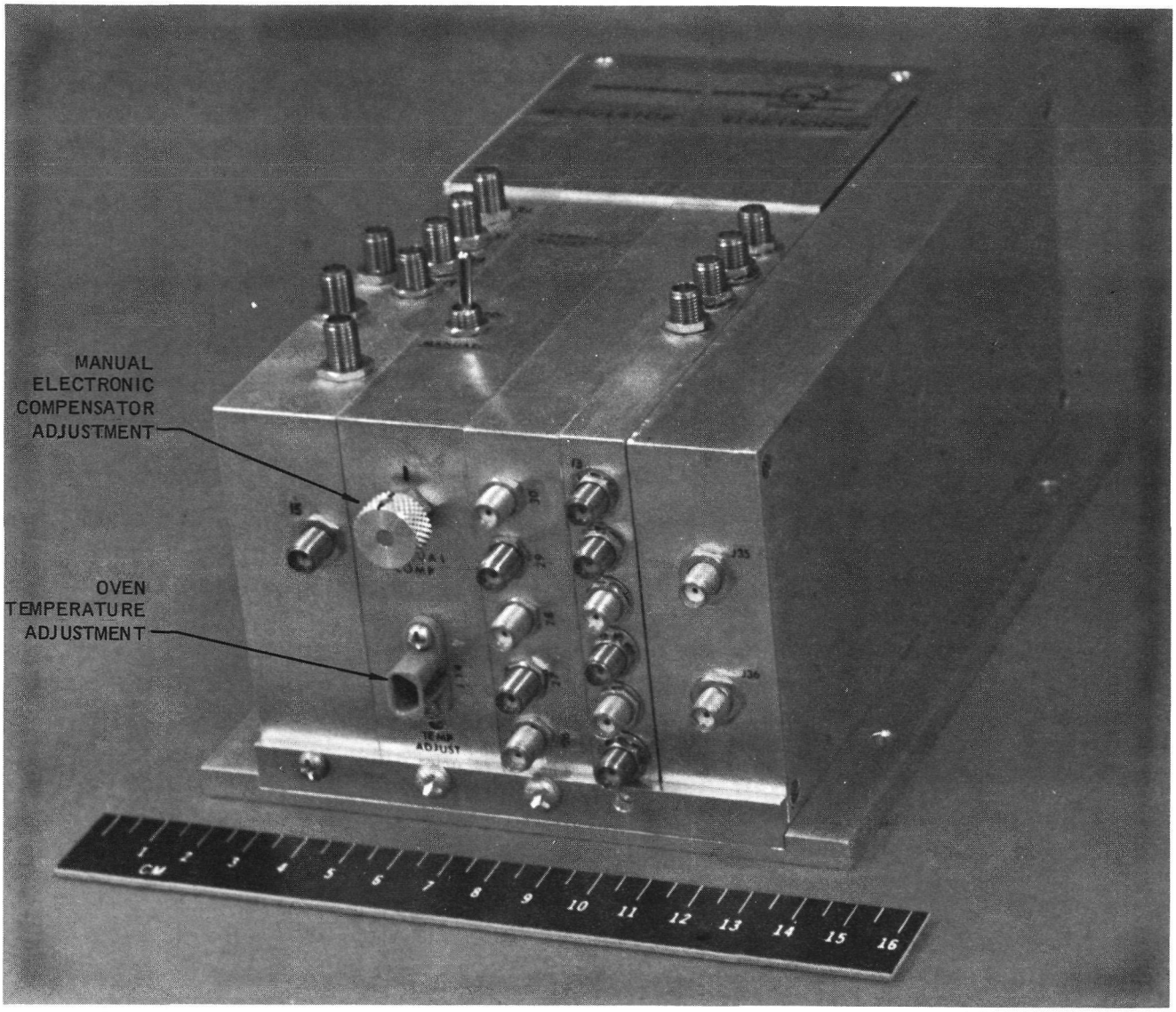

FIGURE 48 CONTROLS ON ELECTRONICS ASSEMBLY

4.1.3 Modulator Laboratory Power Supply. The packaging approach for the power supply incorporated off-the-shelf commercial equipment where available and minimized the special design. The off-the-shelf equipment included the cabinet, racks, panels, and power supplies except for the +2 volt and -3.2 volt regulators. The special design included: the panel layout and printing, +2 volt and -3.2 volt regulated voltages from the +5 volt and -5.2 volt supplies respectively, the driver sense and crowbar protection circuits, and the photodiode current limit circuit.

The controls are on the front panel. The main power switch controls power off or on; when on, the total running time meter (viewed through the rear door), the fan, and the heater voltages ($\pm$15 and +25 volts) are on and operating. A heater low, medium, and operate switch places current limiting resistors in the heater circuit to change the modulator crystals, the medium heat position is used for modulator turn-on and the low heat position is used for modulator turn-off as described in Appendix I. The electronics off-on switch then provides power for all the modulator electronics including the automatic electronic compensator photodiode bias and the final output stage of the modulator driver. Both of these circuits also have their own respective off-on switches so that they may be turned off without affecting the other circuits. The electronics running time meter runs when the electronics switch is on.

The photodiode bias switch in the on position provided the bias voltage for the automatic electronic compensator photodiode. A dc power supply was used to eliminate the need for batteries with their finite lifetime. When manual electronic compensation was used, there was no need for the photodiode bias. Therefore, bias the output supply was switched to the off position.

The driver power and output stage switches serve two distinct purposes: turn the output section of the driver to operate for system

performance (both switches in operate), or turn on only the output stage voltage to the operate or the average voltage levels.

The protection (crowbar) circuit trouble light (red) indicator and the protection circuit reset button were associated with the bias voltages applied to the modulator driver. When the protection circuit sensed an overload or trouble condition associated with modulator driver, critical bias voltages were immediately removed, and the crowbar light glowed. The purpose of the protection circuit was to prevent damage to the modulator driver due to operator errors such as an incorrect electrical input condition or an accidential shorting of some bias voltage while probing the driver during tests. The crowbar reset switch resets these supplies when pressed and released; if crowbar conditions still exist, the lights return on after approximately 50 ms. At initial driver power turn on, the crowbar lights had approximately one second delay before turning on if crowbar conditions exist although the crowbar came on within 150 ms. Fuses for various groups of power supplies are located on the rack back panels accessible through the rear cabinet door.

A front view of the assembled laboratory power supply is shown in Figure 49. The power supply voltage test points are readily seen on the power supplies front panel. The weight of the laboratory power supply was approximately 54.5 kg. The power supply dimensions were 54.6 cm x 52.1 cm x 40.6 cm. It must be emphasis that this is only a laboratory power supply.

4.2 TEST POINTS. Test points were provided on the modulator power supplies for observing the dc levels provided. The power supply regulators boards were marked with the nominal voltage value of the regulator; the voltage test points were located on the front of the power supply chassis as shown in Figure 49.

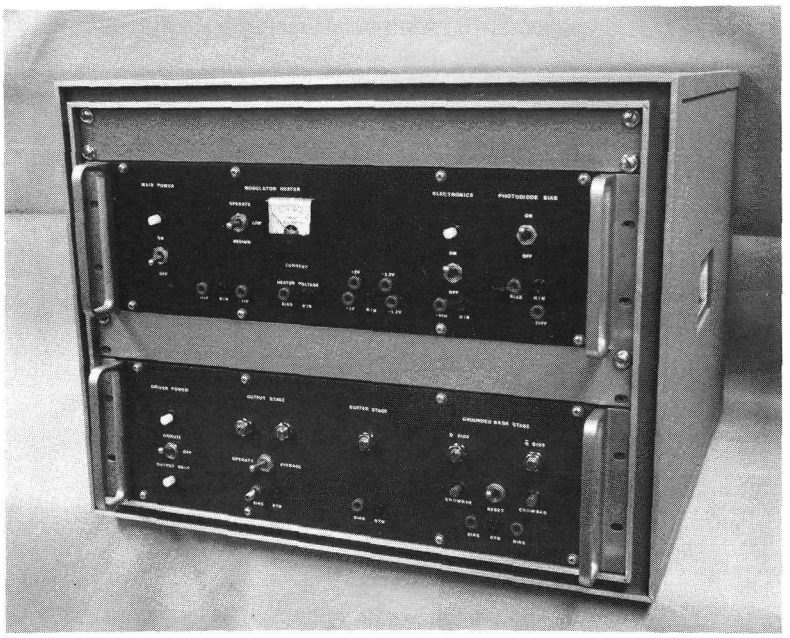

FIGURE 49 MODULATOR ELECTRONICS LABORATORY POWER SUPPLY

On the modulator electronics package tests points were provided for observing operation of the modulator driver and the automatic electronic compensator. Figure 47 and 48 show all of the coax test points except one which was accessible by removing the cover plates over the interconnect area. The test point names and numbers are listed in Table VII. Performance waveforms from the modulator unit test points are given in Section 5.

4.3 CONNECTOR DEFINITION AND GROUNDING. All electrical signal interfaces for the modulator unit were made with SMC connectors. The outer conductors of these connectors were grounded to the chassis of the unit in which they were located. The power to the modulator electronics was made through five twisted and shielded cables. The shields carried no current and were grounded on one end only. The power returns for each of these five cables or groups of power supplies were not connected together or to chassis at the power supply but were connected to a common point ground and to the electronics package chassis within the electronics package. The power supply chassis was connected to earth ground through the 115 V 60 Hz power cable third wire safety ground. The modulator electronics package had no direct electrical connections to earth ground but was grounded through the mounting and heat sink structure at the point of usage. Two supplies had remote sensing at the electronics package through twisted pair shielded cables. Note the power supply should not be turned on without the connection made to the electronics package or a suitable jumper plug installed.

Heater power from the electronics packages to the modulator assembly branched out of this same power cable. The temperature controller thermistor sense leads were through a separate connector and twisted shielded cable for maximum isolation.

4.4 POWER REQUIREMENTS. The modulator laboratory power supply required an capability of 120 V, 60 Hz, and 1.5 A maximum current. Table XIII in Section 5 gives a breakdown of voltages and powers supplied by a given regulator, or received by a given subunit, as well as total power required for the 400 Mbps modulator unit.

TABLE VII

MODULATOR ELECTRONICS PACKAGE TEST POINTS

T/P	MODULE LOCATION	TEST POINT NOMENCLATURE
4	Load	Driver C1 Load
5	"	Driver C2 Load
6	"	Driver L1 Load
7	"	Driver L2 Load
18	Amplifier/Gate	Gate Output
22	"	Gate Drive
23	Amplifier (Internal)	Error Amplifier
26	Compensator Output	Bias Amplifier Output 1
28	" "	Phase Reference Voltage
30	" "	Bias Amplifier Output 2

5. PERFORMANCE TESTS

All of the hardware on this program was subjected to a variety of tests at modulator components, modulation unit and complete modulator levels. The results of the tests are documented in this section.

5.1 MODULATOR UNIT AND COMPONENT EVALUATION TESTS. Complete tests were performed on each of the 400 Mbps modulator units built. Because the two fabricated modulator oven cores were nearly identical, most of the test results were the same for both units except that oven core number 2 was better in overall performance. In the tests described below, the results are given and the test difference are stated with appropriate explanations.

5.1.1 Optical Components. The pellicles which were to have been used to split off 1% of the modulator crystal transmitted light for the automatic electronic compensator photodiode signal input were checked for transmission and reflection at 45° using the 1.06 μm Bausch and Lomb monochromatic light source. Table VIII gives the results of the measurements. As these measurements show, neither of the pellicles met the required specifications. Therefore, pellicle #1 was returned for replacement while keeping pellicle #2 as a backup for the program. The reason pellicle #2 did not meet specifications was that the coating was not of the correct thickness for the proper 1% reflection; however, a more serious problem was seen in the increased transmission loss. The problem was discussed with the supplier and it appeared that separation of the 1.06 μm AR coating from the pellicle substrate was the major reason for the additional loss. This separation occurred when mounting the AR coated pellicle from a 75 mm diameter pellicle ring to the required 12.5 mm diameter ring. The reason to transfer the AR coated pellicle was to insure that the entire 12.5 mm diameter pellicle was uniformly coated. The method used to achieve this was to AR coat a larger pellicle and then transfer to the smaller pellicle ring. The transfer method was necessary since in AR coating the pellicle on the back side, where the ring was shadowing the

TABLE VIII

Pellicle Performance Values

Pellicle	Transmission	Reflection	Polarization
#1 (Frosted A-R Coating)	92.2%	1.5%	"P"
	92.8%	2.4%	"S"
	92.6%	2.2%	Unpolarized
#2 (Appeared to be a Better A-R Coating)	97.4%	1.0%	"P"
	97.8%	1.8%	"S"
	97.6%	1.6%	Unpolarized
#3 (Replacement for Pellicle #1)	98.1%	1.7%	"P"
	98.5%	0.8%	"S"
	98.5%	1.1%	Equal Amplitude Orthogonal Waves

TABLE IX

Polarization Beamsplitter Performance Data

Cube	"P" Polarization		"S" Polarization	
	Transmission	Extinction Ratio	Transmission	Extinction Ratio
#1	97.7%	266:1	97.5%	207:1
#2	98.0%	--	--	--
#3	97.6%	320:1	98.0%	257:1
#4 Replacement for Cube #2	98.5%	666:1	97.7%	337:1

pellicle. If this transfer was not done the pellicle would not be uniformly coated and perhaps not coated at all around the periphery.

A pellicle was used in the optics tail to prevent double reflected spots which occurred with a thicker disc. Previous work had shown that if the coating did not separate from the pellicle during remounting, or immediately thereafter, it did not degrade.

The best of the two pellicles was kept and the other returned for replacement. The replacement pellicle was received and evaluated. The transmission and reflection of the pellicle (3) was measured with linearly polarized light using a polarizer and the 1.06 μm Bausch and Lomb monochromator light source. Table VIII gives the results of the measurements. As these measurements show, the pellicle did not meet our 1% reflection specifications, however, it was very close and was acceptable. The replacement pellicle had 98.5% transmission and 1.1% reflection at 45° incidence with linearity polarized light containing equal components of the "s" and "p" polarization. This pellicle was used in the optics tail of the fabricated modulator.

Three beamsplitter cubes were received and evaluated to determine "p" and "s" polarization transmission and their respective extinction ratio. One of these polarization splitter cubes was to be used in the optics tail to provide a polarized input photodiode signal for the AEC circuitry and another cube in the optics tail for PGBM format operation. Table IX lists each beamsplitter cube transmission and extinction ratio for each polarization. These measurements were made using the Bausch and Lomb monochromatic light source with a focused 3 mm spot. It was seen that the polarization beamsplitter cube #2 was no good. Cube #2 evidently did not have a polarization splitter coating. The cubes were 1.06 μm AR coated on four sides of the cube to minimize 1.06 μm

reflections. The cube was composed of two 90° prisms. The base of the prisms were coated to transmit the "p" polarization and reflect the "s" polarization.

The two prisms were then optically contacted together. Once assembled, the beamsplitter either transmitted the beam or reflected the beam 90° with respect to the incident beam, depending on input polarization. The reflected beam was denoted as "s" polarization and the transmitted beam was "p" polarization. Cube #2 was replaced by the supplier. The replacement cube #4 was very good in both optical transmission and extinction ratio properties for both "p" and "s" polarization. This cube was used in the optics tail for the modulator transmitted PGBM optical signal.

As seen in Table IX, the "p" polarization, which was the one of interest for use in the optics tail for PGBM data transmission for the AEC circuitry transmitted 97.7% of the input 1.06 μm optical beam.

Antireflection (AR) coated 1.06 μm 84.2 mm focal length lenses were used in the delivered modulator as the input and output lenses. The lenses were checked for transmission by using a 1.06 μm laser and a photodetector. The optical power was measured with and without the lens in the beam to determine the transmission. The transmission was determined to be 99.1%; this was an average of five measurements. The focal length was measured by focusing a collimated 1.06 μm laser beam and measuring the physical length from the lens to the beam waist and it was determined to be 84.4 mm.

Optical transmission measurements of a 1.06 μm antireflectance coated bulk crystal were made using a 1.06 μm laser, a Bausch and Lomb monochrometer set for 1.06 μm light output, and a Beckman DK-2 spectrophotometer. Figure 50 is an optical transmission plot of the

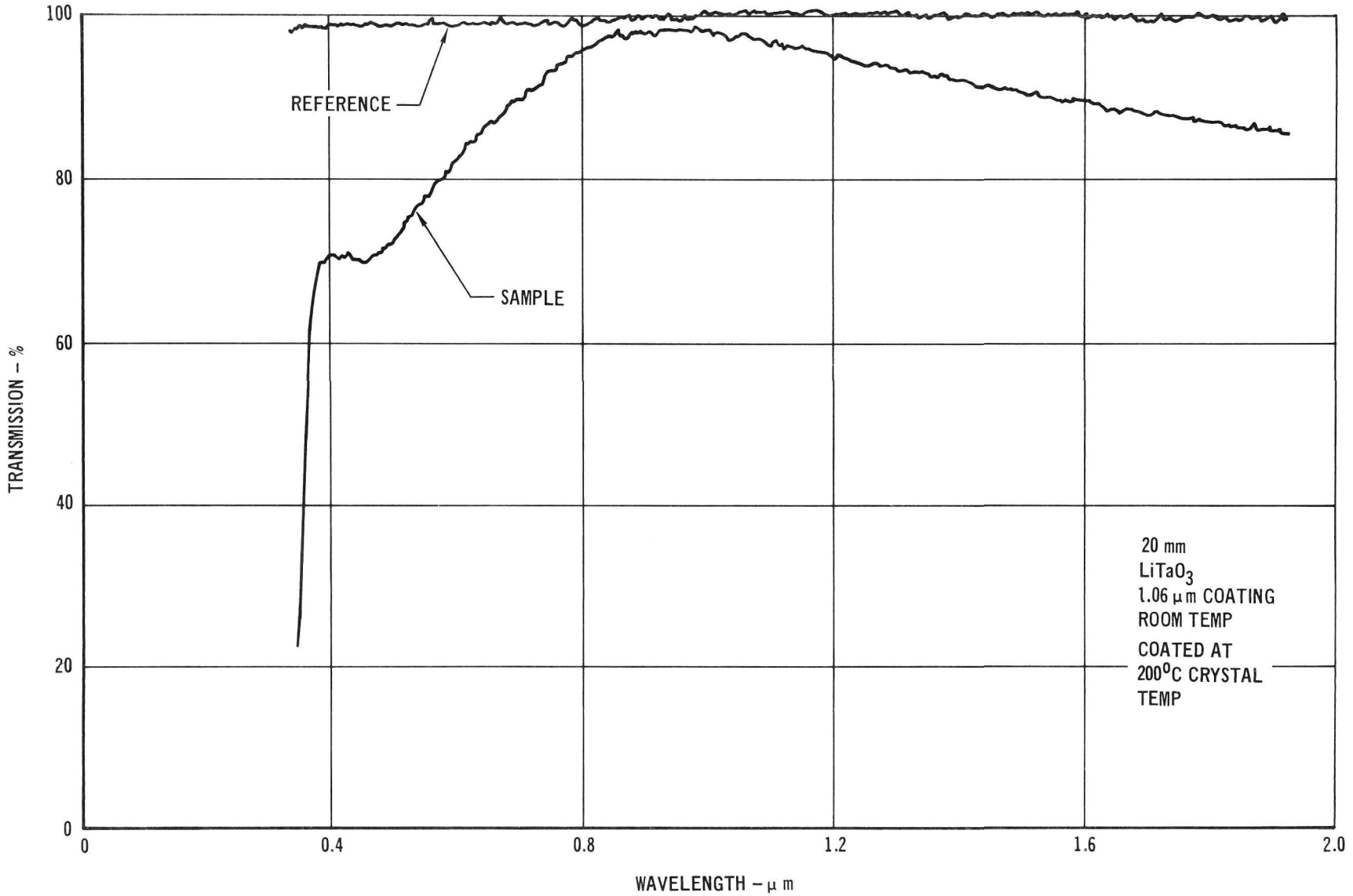

FIGURE 50 TRANSMISSION OF AR COATED $LiTaO_3$ SLAB

1.06 μm AR coated $LiTaO_3$ slab. This wavelength versus transmission plot was taken using a Beckman DK-2 spectrophotometer. It is seen that the transmission at 1.06 μm is 98%. However, the crystal did not have a correct AR coating thickness for optimum 1.06 μm transmission. This was the result of the coating personnel assuming that the thickness of the coating should double when coating for 1.06 μm as compared to 0.53 μm. However, the thickness more than doubles since the index of refraction of $LiTaO_2$ changes as a function of wavelength. This was not a serious problem as the index of refraction was known for 1.06 μm and only required that the coating thickness account for the index change. This correction was made in the remainder of the AR coating. The transmission of the AR coated slab was measured with a 1.06 μm Nd:YAG laser source and was 98.2%. When measured with the Bausch and Lomb monochrometer set for the 1.06 μm source it measured 98% transmission. The bulk crystal transmission was better than 98% when the $LiTaO_2$ crystal was AR coated correctly for 1.06 μm light.

Several $LiTaO_3$ modulator size crystals were evaluated to determine what minimum size should be used in the modulator for optimum transmission and extinction ratio. The modulator crystal sizes used were 0.25 mm x 0.20 mm cross section, 0.27 mm x 0.20 mm cross section, and crystals with 0.27 mm x 0.27 mm cross section tapered to 0.27 mm x 0.23 mm cross section. The best transmission achievable was 71.5% for the tapered crystal using a 1.06 μm Nd:YAG laser source. The static extinction ratio for this crystal was only 40:1. However, the crystal was neither strain relieved nor AR coated.

From this data it was decided that the modulator would be fabricated from crystals with a cross section of 0.27 mm x 0.27 mm tapered to 0.27 mm x 0.23 mm. The crystals were tapered in the c-axis which minimized the switching voltage while maximum optical performance for this modulator crystal size. The switching voltage for this particular modulator using the above size crystals would

be 28 Vdc. Having determined the crystal modulator size to be used, fabrication of the modulator crystals proceeded.

The improved antireflection SiO_2 coating was reliably deposited on $LiTaO_3$ of correct thickness for minimum reflectivity. An optical reflectivity of less than 0.1% using the SiO_2 AR coating deposited on $LiTaO_3$ with a 1.06 μm laser beam was measured. Finally, as mentioned beforehand, the film stability appeared to be better than ThF_4 which was the only other known single layer quarter wave material match for $LiTaO_3$ currently feasible.

5.1.2 Laser Interface Parameters. The input laser beam parameters from our 1.06 μm Nd:YAG test source were measured and it was found that the laser output beam had a divergence of 2 mrad with a beam diameter of 3 mm measured at the modulator input lens. The input beam diameter was much too large for optimum transmission, since for diffraction-limited focusing, the beam diameter should be 1 mm. Therefore, lenses were placed in the optical path to obtain the proper beam waist at the modulator input lens for a confocal matching optical beam parameter of the laser to the modulator. After proper lens positioning, the laser beam was scanned and recorded using a Gamma Scientific scanning photometric microscope. The beam shape was Gaussian with a TEM_{∞} mode. The beam diameter was measured to be 1.05 mm which was adequate for modulator performance evaluations.

5.1.3 First Oven Core Crystals. The first attempt to solder electrodes to a crystal was unsuccessful; however, this was because the vacuum system was not working properly and the copper electrodes oxidized. The crystal was not held in the soldering mount tight enough for entire crystal face coverage. These problems were corrected before the next fabrication attempt.

5.1.4 Second Oven Core. Two modulator crystals were AR coated with SiO_2 for 1.06 μm utilizing the same conditions as described earlier. Reflectivity was measured for each crystal and was found to be less than 0.1% per surface. One modulator crystal had transmission of 94% using a 1.06 μm laser beam with an input beam diameter of 1.05 μm. This modulator crystal was however larger than that determined to be used in the fabricated modulator. The input beam diameter was measured using a Gamma Scientific scanning photometric microscope. Using this technique, the beam diameter was measured to an accuracy of 0.05 mm. The other modulator crystal appeared to have a pyroelectric strain frozen in it as the transmission (~ 85%) was not as good as the first crystal. This strain was removed by heating the crystal. When heated the transmission increased to ~ 88%. This second crystal was the same size as that chosen for the fabricated modulator. Therefore it was decided that the crystals would be electroded. The second modulator crystal pair was soldered to copper electrodes. The crystals had the same transmission values as they did before soldering, namely ~ 94% and ~ 85%. The electroded crystal pair was then mounted in boron nitride pills. After pill mounting the transmission was again checked before outgassing and was the same as previously measured. The pill mounted crystals were then outgassed in a vacuum chamber of 10^{-6} torr at 150°C for 48 hours each. After the outgassing procedure, both crystal transmissions had decreased to ~ 20%. The crystals were then examined using a microscope and minute cracks were found along the optical crystal length. There were numerous interior crystal cracks propagating parallel to the electroded C-face and along the optic axis. The modulator crystals were unusable due to poor transmission properties. Several evaluations were conducted to determine the cause of crystal breakage. The first time that the pill mounted crystals had been heated to 150°C was during the outgassing procedure. An electroded crystal was temperature cycled to determine if the copper's thermal expansion, or warping, was the reason for crystal breakage. Other areas studied were the pill mounts, mounting procedure, RTV cementing, and pressure applied

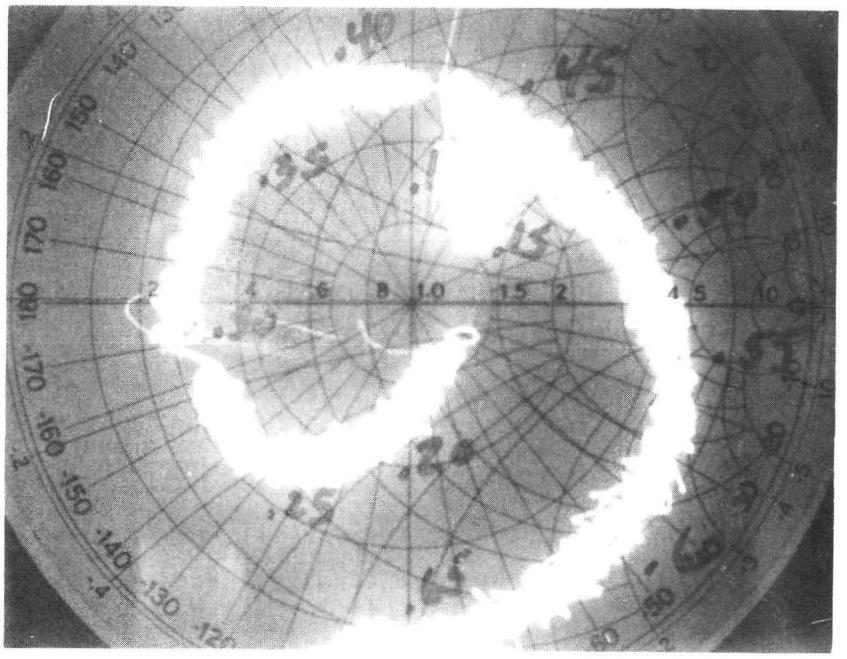

a) FLAT MOUNTED CRYSTAL
<9% FROM 100 MHz TO 650 MHz

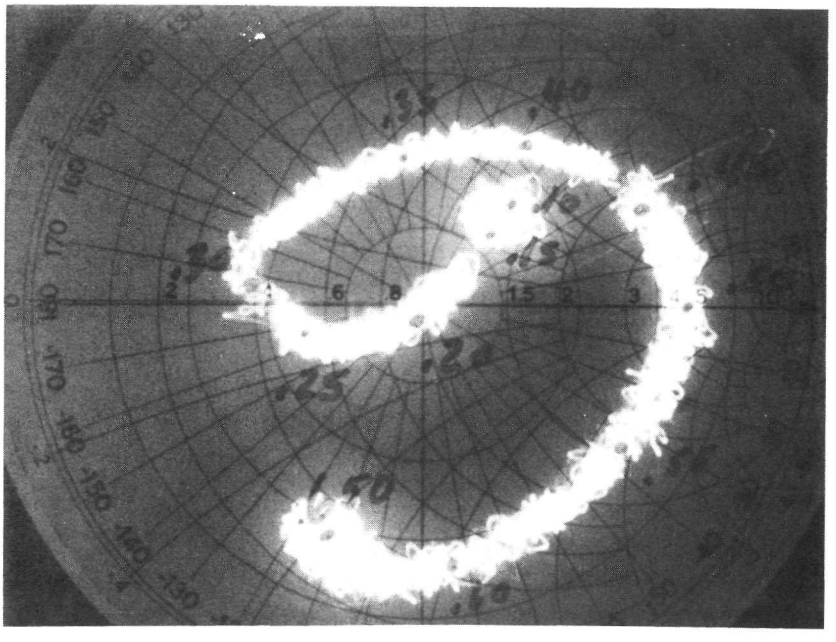

b) STEP MOUNTED CRYSTAL
<8% FROM 100 MHz TO 650 MHz

FIGURE 51 POLAR DISPLAY OF REFLECTION COEFFICIENTS OF CRYSTAL MATCHING NETWORK

FULL SCALE:10%

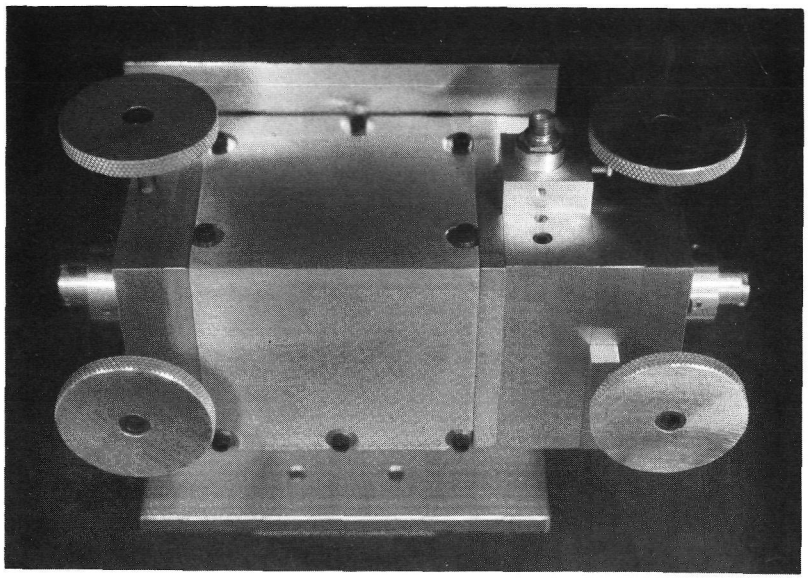

(A) FRONT VIEW OF MODULATOR SUBASSEMBLY SHOWING LENS, OVEN HOUSING CONTAINING CRYSTAL OVEN CORE, OPTICS TAIL AND TRANSMITTED FORMAT CHANGER.

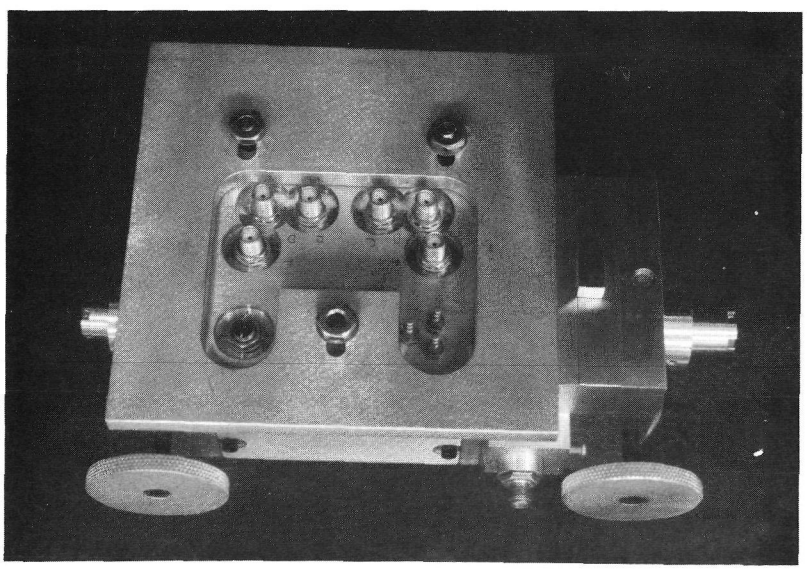

(B) BACK VIEW OF MODULATOR SUBASSEMBLY SHOWING ELECTRICAL INPUT CONNECTIONS

FIGURE 52 PHOTOGRAPH OF MODULATOR ASSEMBLY COMPLETED

PGBM and PPBM modulation formats, and the input and output lens holder with lens translators. All of the components composing the modulator assembly were mounted on a L-shaped bracket which was mounted and aligned in an optical beam on a Huber camera mount.

After the beam input interface parameter was corrected and recorded, the modulator was then heated to 150°C and aligned in the 1.06 μm optical beam path. When the modulator had been optimally aligned, the optical transmission was measured and found to be 56.9%. This measured value included the losses from the two 1.06 μm AR coated lenses (input and output lenses), two AR coated lithium tantalate crystals'(which are small aperture crystals) and the AR coated pellicle which splits off > 1% of the beam for the AEC photodiode signal. This value was lower than expected due to beam diffraction which was readily seen at the modulator output. This low transmission value was the result of small aperture crystals. It was believed that this transmission value will improve with larger aperture crystals that were being fabricated. The modulator had a static extinction ratio of 88:1 for the small aperture crystal pair. Therefore, the measured static extinction ratio exceeded the goal of 50:1, however, the 70% transmission goal had not been achieved.

After the electronics assembly was integrated with the modulator assembly and all interface parameters optimized, the dynamic performance data was obtained. The modulator was operated in both electronic compensation modes (automatic and manual) with similar results in modulation performance. The 400 Mbps 63 bit PGBM format dynamic extinction ratio was 18.3:1 worst case with an average extinction ratio of 30:1 or greater. Figure 53 shows photographs of the 63 bit 400 Mbps PGBM modulator output signal. The baseline shift is a function of the time constant for the photodetector. The range of timing adjustment between the optical pulses and the driver input signal measured ±300 ps. This dynamic performance data, using the small aperture crystals, was good and had considerable timing flexibility.

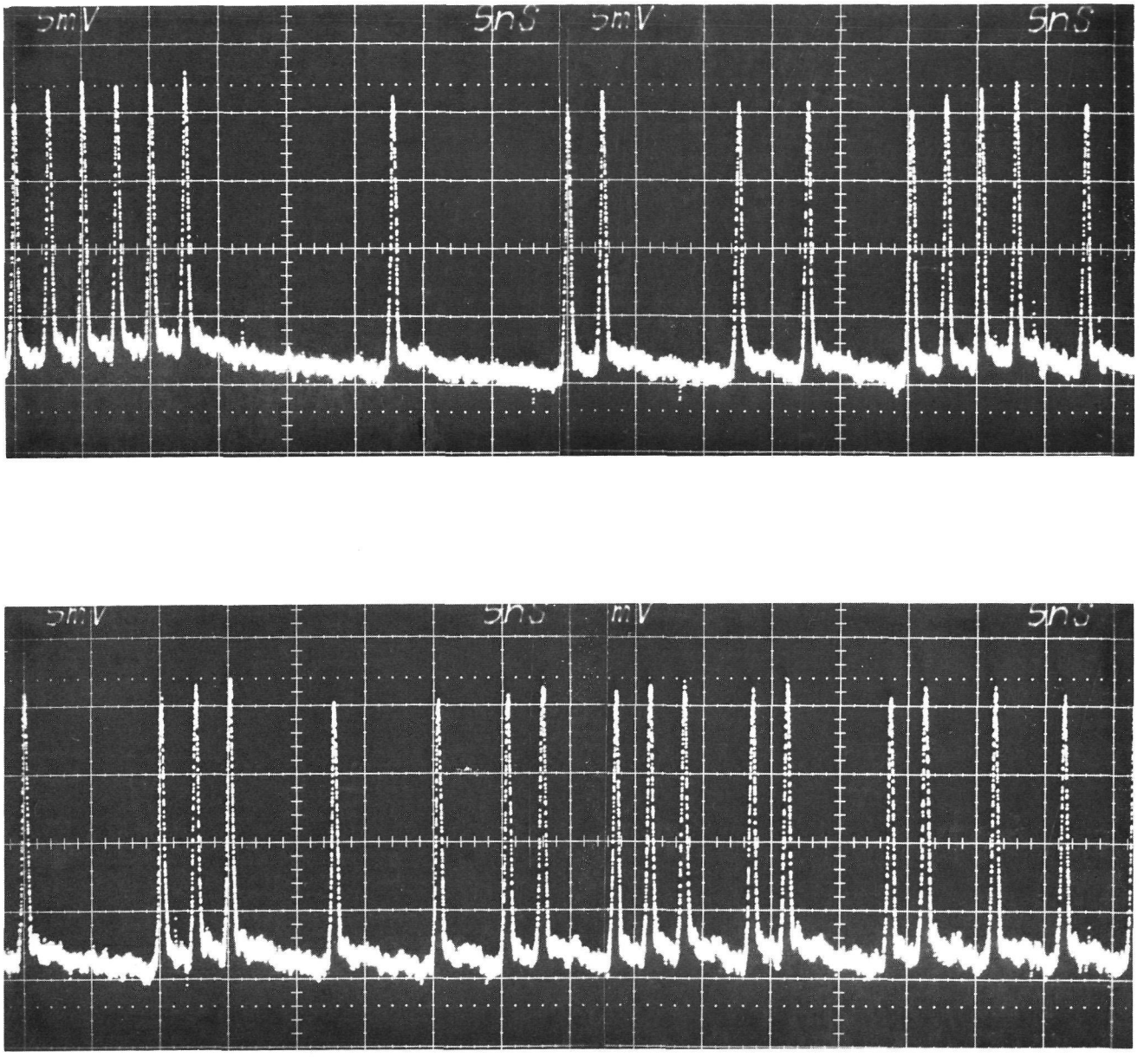

FIGURE 53 EXTINCTION RATIO PHOTOGRAPHS OF A 400 Mbps PGBM OPTICAL SIGNAL USING A 63 BIT PN GENERATOR

The modulator electronics package and power supply were integrated with the modulator assembly and all voltages and electrical timing were adjusted for full automatic compensator operation while using a 63 bit 400 MHz PN generator. The dual driver output waveforms are shown in Figure 54 which correspond to the extinction ratio shown in Figure 53; these waveforms were taken with an instrumentation test-probe installed in the coax cable at the driver outputs. The corresponding waveforms, for the driver Q output, taken at the broadband load "L" and "C" test points are shown in Figure 55; the composite summation of these two waveofrms is shown in Figure 56, which represents the driver output after passing through approximately 1.33 meter of coax cable, through the front crystal matching network, and then through another 1.33 meter of coax to the broadband load. The corresponding waveforms for the $\overline{Q}$ driver output were identical to the above except inverted from those of Figures 55 and 56.

The automatic electronic compensator (AEC) held the compensation bias point to the same value (within ± 1 volt) as the best operating manual set point. The pulse amplifier output waveform is shown in Figure 57 with respect to the Q output of the driver. The negative going pulses were the amplified horizontal polarized pulses detected at the photodiode. The gate driver test point waveform is shown in Figure 58 and is a complement of the gate driver waveform; the Manchester code format is illustrated with the driver Q output. The Manchester code format permitted the gate to function down to frequencies below 10^4 Hz; however, data modulation frequency components within the pass band of the bandpass filter (50 kHz to 175 kHz) could degrade automatic compensate operation.

5.1.6 Fourth Oven Core Crystals and Second Fabricated Oven. The modulator oven core containing the larger aperture crystals (~ 10% larger than the second oven core crystals) was outgassed at 160°C for two days in an ion vacuum system having a vacuum capability of 10^{-8} torr. Using this ion vacuum chamber, it was possible to determine when the components had been thoroughly outgassed by monitoring the

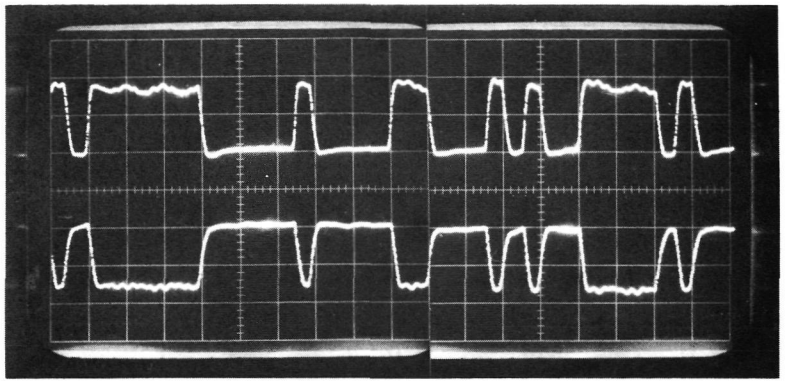

DRIVER OUTPUT
TO CRYSTAL NO. 2

DRIVER OUTPUT
TO CRYSTAL NO. 1

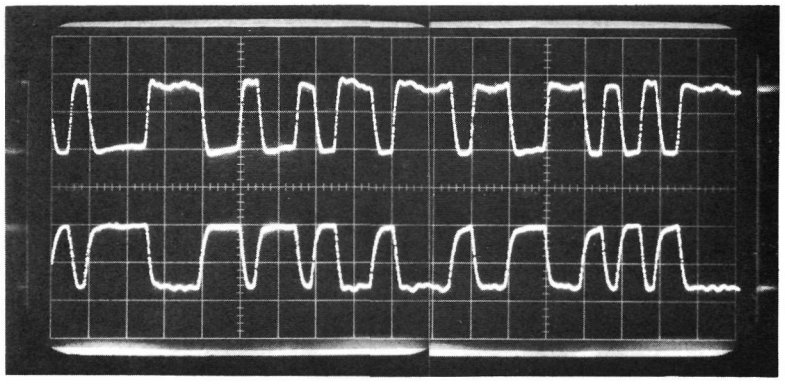

DRIVER OUTPUT
TO CRYSTAL NO. 2

DRIVER OUTPUT
TO CRYSTAL NO. 1

FIGURE 54 400 Mbps MODULATOR DRIVER OUTPUT WAVEFORMS (63 BIT)
VERTICAL 17 V/DIV; HORIZONTAL 5 NS/DIV

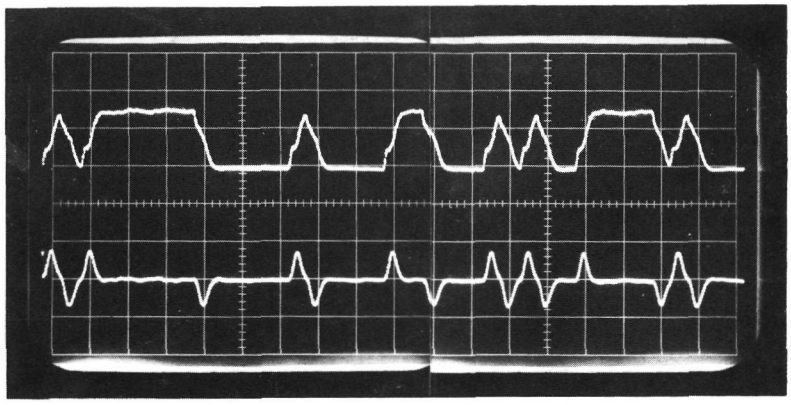

"L"
TEST POINT

"C"
TEST POINT

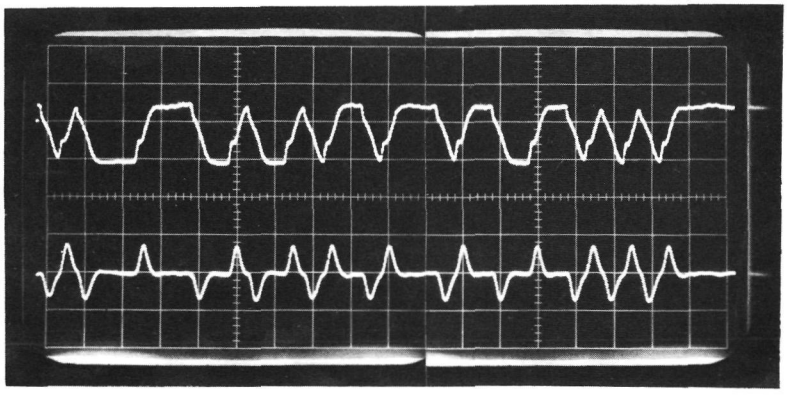

"L"
TEST POINT

"C"
TEST POINT

FIGURE 55 BROADBAND LOAD "L" AND "C" TEST POINTS
63 BIT PN CODE INPUT OPERATING AT 400 Mbps

HORIZONTAL SCALE – 5 NS/DIV
VERTICAL SCALE – 17 V/DIV

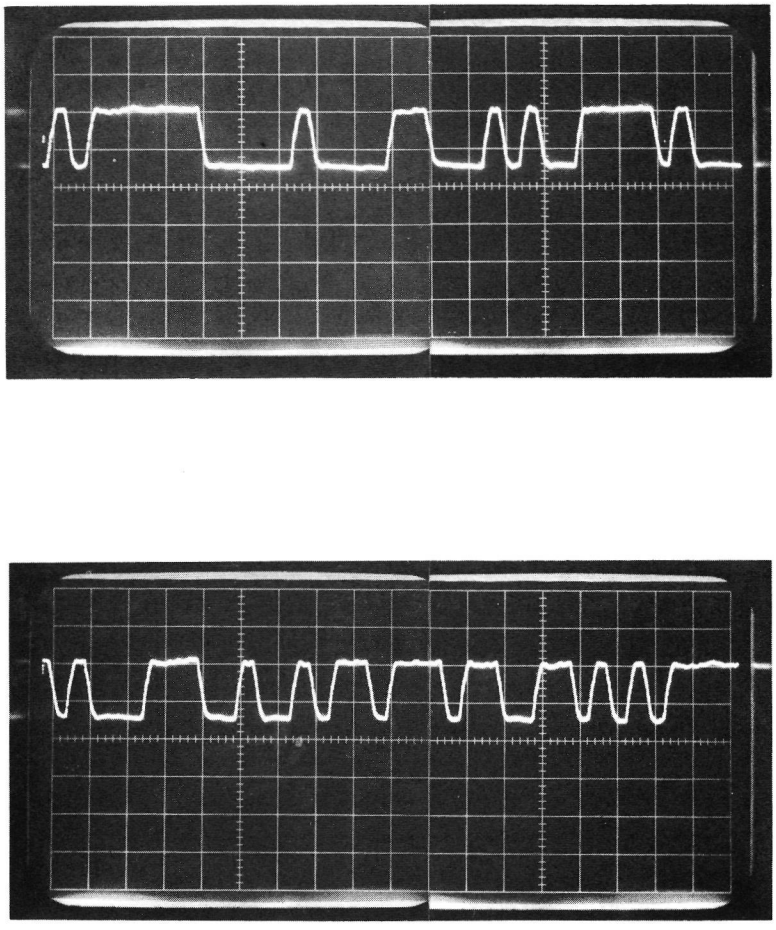

FIGURE 56 DRIVER OUTPUT COMPOSITE SUMMATION OF "L" AND "C" WAVEFORMS SHOWN IN FIGURE 55.

HORIZONTAL SCALE: 5 NS/DIV
VERTICAL SCALE: 17 V/DIV

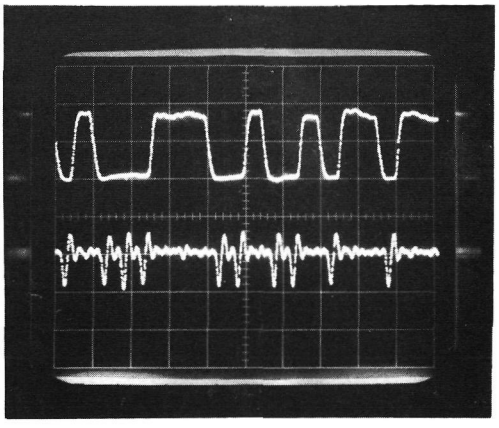

DRIVER
OUTPUT
VERTICAL SCALE: 17 V/DIV

PULSE AMPLIFIER
OUTPUT
VERTICAL SCALE: 50 mV/DIV

FIGURE 57 A SECTION OF THE PHOTODIODE PULSE AMPLIFIER OUTPUT WAVEFORM IS SHOWN WITH RESPECT TO THE Q OUTPUT OF THE DRIVER

HORIZONTAL SCALE: 5 NS/DIV

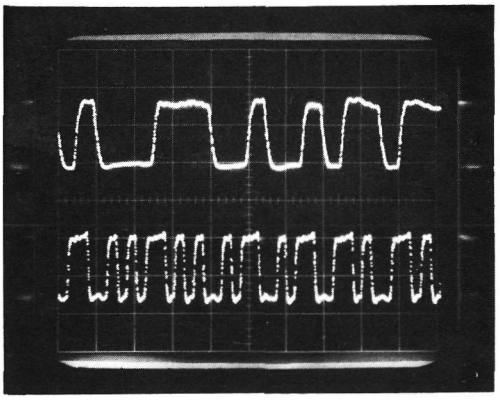

DRIVER OUTPUT
VERTICAL SCALE: 17 V/DIV

MANCHESTER CODE
VERTICAL SCALE: 200 MV/DIV

FIGURE 58 A SECTION OF THE MANCHESTER CODE FORMAT ILLUSTRATED WITH RESPECT TO THE DRIVER Q OUTPUT

HORIZONTAL SCALE: 5 NS/DIV

the vacuum pressure using an ionization gauge. Of course when outgassing occurred, the pressure inside the chamber increased immediately and remained high until the gases had been pumped from the chamber. Therefore, when the vacuum was low and remained low after the oven core had been heated for several hours, the oven core and components were outgassed and were removed from the chamber.

After outgassing, the oven core was mounted in the oven housing. The crystals were then heated to 150°C which is the modulator oven core operating temperature. At 150°C, the crystals were then individually matched to 50 ohms which was the input electronic impedance. Figure 59a and 59b show polar display of the reflection coefficient photographs of the resultant crystal matching network. As seen in the photograph, there were five concentric graticule rings about the center of the screen. The polar display provided a polar plot of the magnitude and phase of the reflection coefficient. If the device under test was a 50 ohm well matched device, the CRT displayed a dot at the center of the screen. If the device was mismatched from the 50 ohm transmission line impedance, then at each frequency the device had a reflection coefficient magnitude and phase that was read off the display. If all energy was reflected, the reflection coefficient was equal to 1.0. Therefore, each point on the CRT trace 1) corresponded to a specific frequency, and 2) represented a value of reflection coefficient magnitude and a specific phase angle. The magnitude of the reflection coefficient of the device under test was read on the concentric circles. In Figure 59a and 59b full scale reflection was 10%, therefore up to a frequency of approximately 700 MHz the percentage reflection was less than 8% for each crystal 50 ohm matching network.

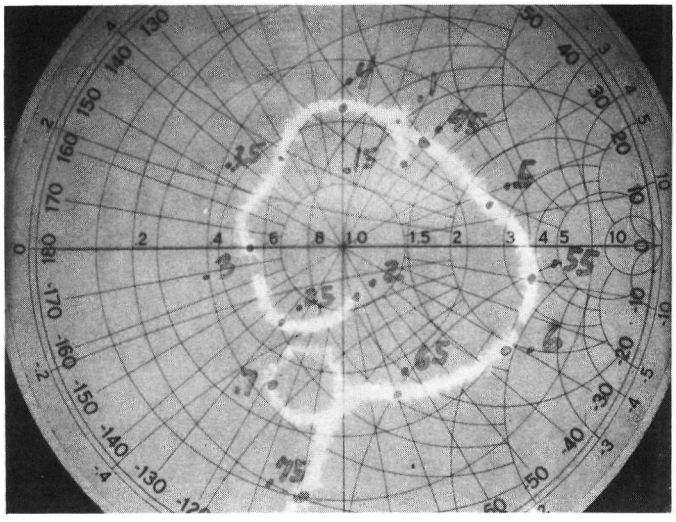

A) STEP MOUNTED CRYSTAL
< 8% FROM 100 TO 750 MHz

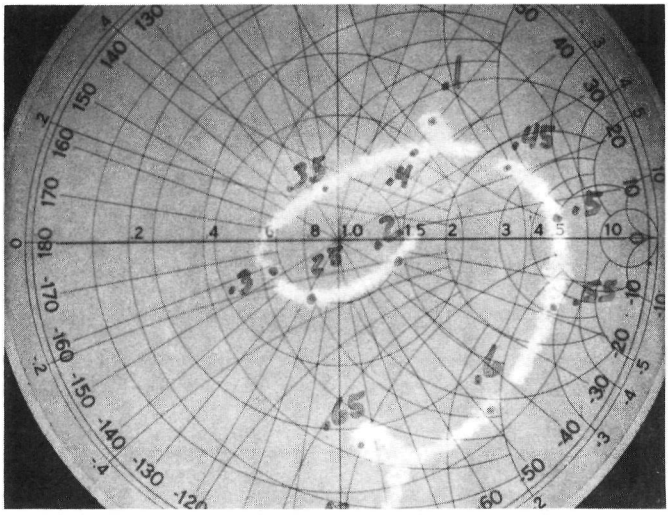

B) FLAT MOUNTED CRYSTAL
< 8% FROM 100 MHz TO 670 MHz

FIGURE 59 POLAR DISPLAY OF REFLECTION COEFFICIENTS OF CRYSTAL MATCHING NETWORK

After the crystals were independently matched to 50 ohms in the oven housing, the modulator package was then assembled. The assembled modulator consisted of two lens translators with lenses (front and back), an optics tail with pellicle, polarization splitter cube, lens to focus signal onto a photodiode, and the polarization beamsplitter cube for converting the PPBM transmitted format to PGBM. After assembly, the modulator was then initially aligned in the 1.06 μm 400 Mpps Nd:YAG laser test bed. The modulator input lens was located where the input beam waist diameter was measured to be 1.05 mm. This lens position was necessary for proper beam waist inside the modulator providing confocal matching of the optical beam parameter of the laser to the modulator. After initial alignment, the modulator optics package was integrated with the electronics package and the crystal oven core was heated to 150°C which was the proper operating temperature of the modulator oven core. When the modulator temperature had stabilized, the modulator input lens position was adjusted for maximum transmitted 1.06 μm light through the modulator optics package. The modulator static optical transmission was 69%. This measured value included the losses from the two 1.06 μm AR coated lenses (input and output lenses), two AR coated 20 mm lithium tantalate crystals and the AR coated pellicle which split off > 1% of the modulator optical beam for the AEC photodiode signal. This tranmission value was close to our goal of 70%, however, when the polarization splitter cube was in the optical beam path, the modulator transmission decreased by 1% to a transmission value of 68%. This was a low loss element and was used when the PGBM format was transmitted.

The modulator static extinction ratio was measured and found to be 69:1. The static extinction ratio exceeded our goal of 50:1. Therefore, initially the static goals were met during this program before beginning the 1000 hour life tests with this acceptable crystal oven core.

After the electronics assembly was integrated with the modulator assembly and all interface parameters optimized, the dynamic performance data was obtained. The modulator was operated in both electronic compensation modes (automatic and manual) and modulator performance was recorded for each mode. The performance was the same for both modes of compensation. The 400 Mbps 63 bit PPBM format dynamic extinction ratio was 22:1 and 17.5:1 worst case for P_1 and P_2 polarizations, respectively. The average extinction ratio for both polarizations was 30:1 or greater. Figure 60 shows the photographs of the entire 63 bit 400 Mbps PPBM modulated optical signal. The range of timing adjustment between the optical pulses and the driver input signal was measured to be $\pm$400 ps. This initial dynamic performance data was good and met most of our goals with considerable timing flexibility.

The dc switching voltage of the crystals was 51 volts; therefore, the effective switching voltage of the pair was 25.5 volts. This lower voltage requirement saved considerable driver power required to operate the 1.06 μm wideband modulator.

The electronics package and power supply were integrated with the modulator assembly. The electronics package power supply, modulator driver and AEC circuits were adjusted for optimum performance with this 1.06 μm wideband modulator. The driver waveforms are shown in Figure 61 using the GFE supplied 63 bit 400 MHz PN generator. These waveforms conrrespond to the extinction ratio shown in Figure 60. These waveforms were taken using an instrumentation test-probe installed in the coax cable at the driver outputs. The driver had rise and fall times of $\leq$ 1000 ps as shown in Figure 62. The timing accuracy appeared to be $\leq \pm$ 320 ps as shown in the Lissajous Pattern plot (I-pattern) in Figure 63. These plots were taken using a sampling scope with two inputs; one the driver output under test and the other the 400 MHz clock with which the driver output timing accruacy was specified. The deviation in the horizontal direction at vertical zero crossing gave the timing accuracy

FIRST
PART
OF PN
CODE

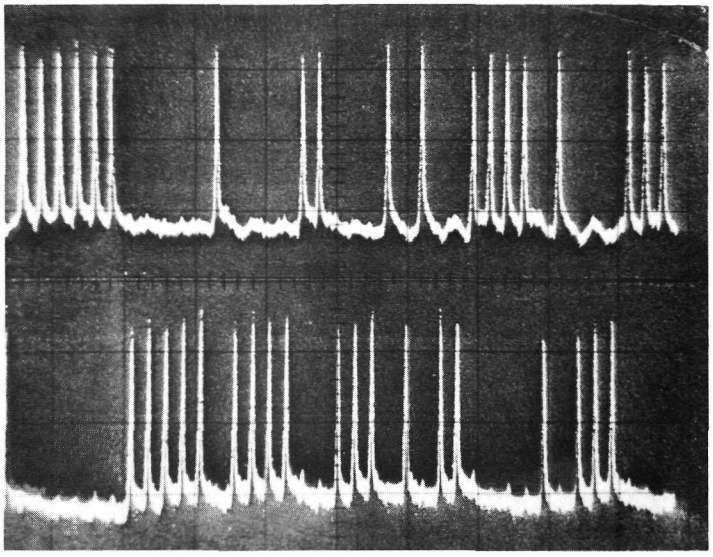

P_1

22:1 worst case

P_2

17.5:1 worst case

SECOND
PART
OF PN
CODE

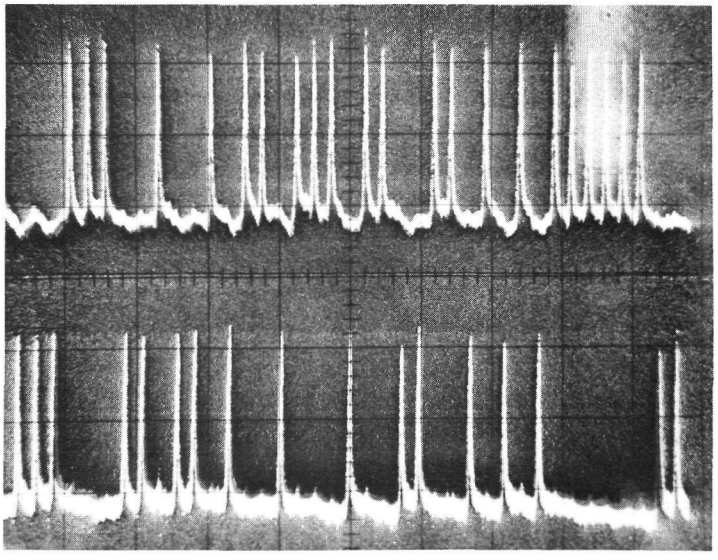

P_1

22:1 worst case

P_2

17.5:1 worst case

Figure 60 63 Bit 400 Mbps PPBM Dynamic Extinction Photographs

Horizontal Scale 10ns/div

Vertical Scale 10mV/div

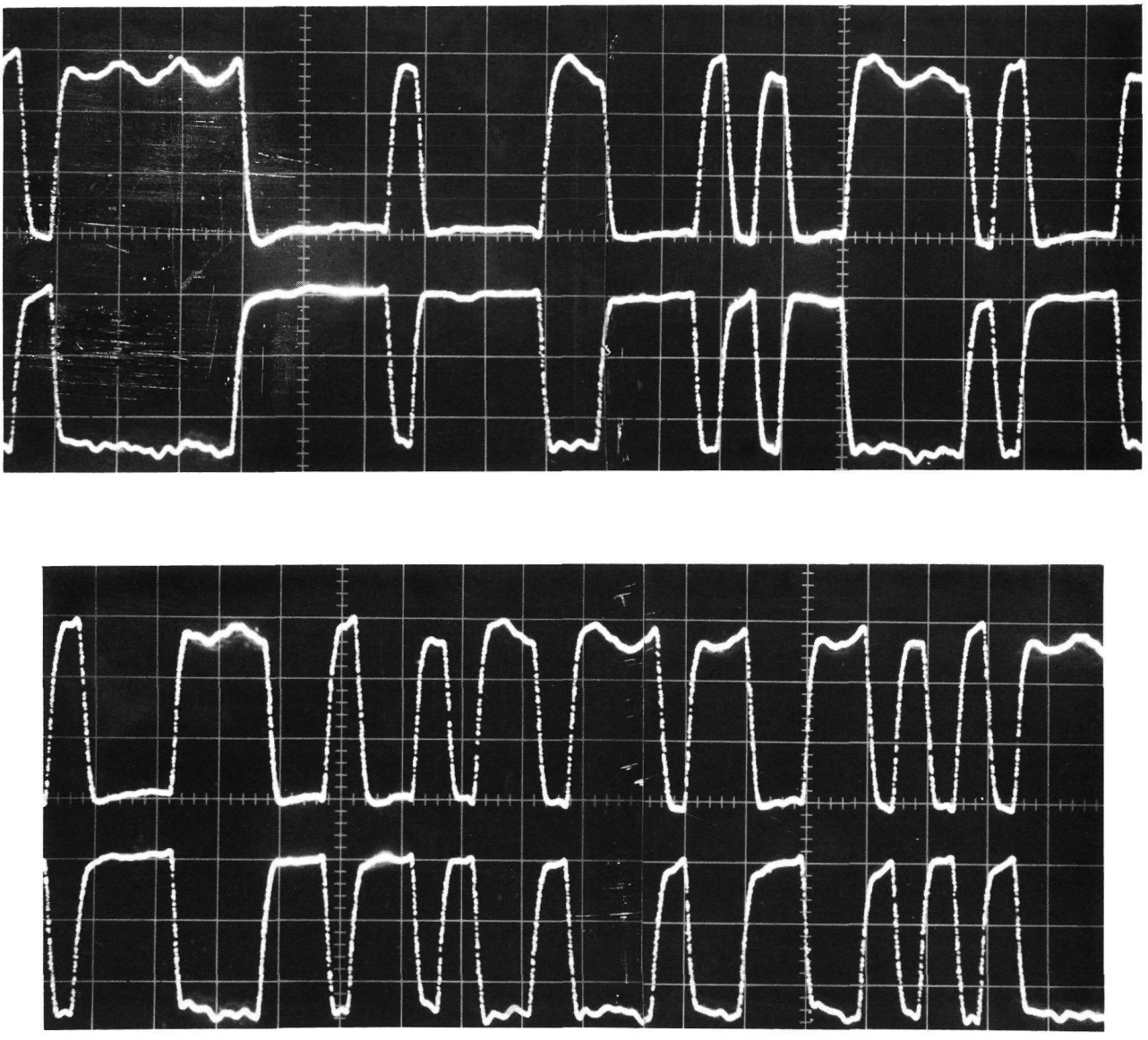

UPPER TRACE: DRIVER OUTPUT NO. 35
LOWER TRACE: DRIVER OUTPUT NO. 36

FIGURE 61 63 BIT 400 Mbps DRIVER OUTPUT WAVEFORMS

HORIZONTAL SCALE: 5 nSEC/DIV
VERTICAL SCALE: 10 VOLT/DIV

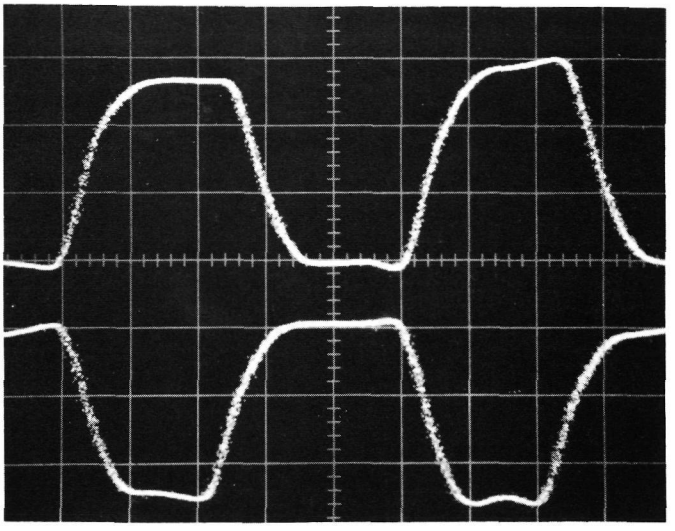

FIGURE 62 MODULATOR DRIVER RISETIME AND FALLTIME

HORIZONTAL SCALE: 1 nSEC/DIV
VERTICAL SCALE: 10 VOLTS/DIV

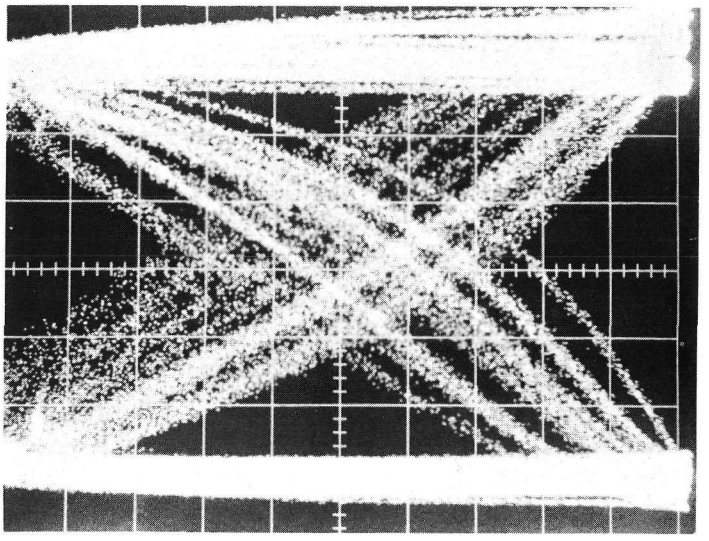

DRIVER NO. 35 OUTPUT

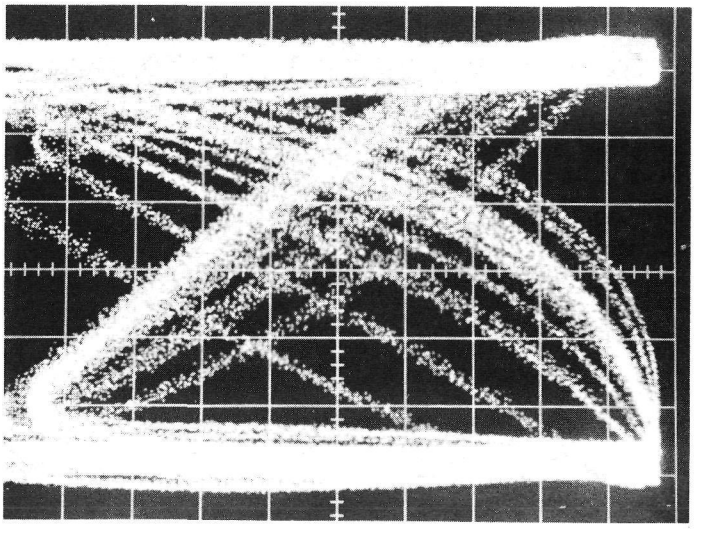

DRIVER NO. 36 OUTPUT

FIGURE 63 LISSAJOUS PATTERN PLOTS (I-PLOTS) OF THE MODULATOR DRIVER OUTPUT TIMING ACCURACY

HORIZONTAL SCALE: 80 PS/DIV

of the driver.

The driver voltage swings were 27 volts for full half wave switching of the modulator crystals. This voltage was close to our goal of 28 volts for full half wave switching of the modulator crystals during this program. However, since the driver voltage swings were lower, the power consumption was also lower. Therefore, the goals of this program were met with a reduced electrical power input level.

5.2 MODULATOR 1000 HOUR LIFE TEST. After completion of the modulator life test, the modulator optical and electrical parameters were examined at appropriate test points with data obtained and recorded by using test probes, photodiodes, oscilloscopes, plotter and cameras. Careful comparison of data before and after the life test indicated that the laser and modulator both optically and electrically had passed the 1000 hour continuous operation life test without any measurable system degradation.

Initially, the modulator had optical transmission of 69%; however, at the end of 1099 hours of continuous operation, the modulator transmission was 71.5%. It was unknown whether the modulator optical transmission improved during this contract period or if this was within the experimental error since the transmission measured consistently between 69% to 72%. However, at the end of the life test, the 1.06 μm wideband modulator transmission exceeded its specification of 70% for this program.

The modulator static extinction ratio initially measured 69:1 and at the conclusion of the life test, the static extinction ratio measured 60:1. During the 1099 hours of continuous laser/modulator operation, the static extinction ratio measured consistenly between 53:1 and 65:1; therefore, no apparent degradation was observed in the static performance of this modulator. After completion of the 1.06 μm wideband laser modulator life test, the measured static extinction ratio exceeded the specified 50:1 for this program.

The dynamic polarization extinction ratios measurement was made using two photodiodes, one photodiode in each of the output orthogonal polarizations with the modulator transmitting the PPBM data format. The photodiode outputs were connected to a dual beam oscilloscope and photographs were taken of the 63 bit PPBM transmitted format as seen in Figure 64. The worst case extinction ratio was then computed for each polarization. The 63 bit PPBM data was also plotted using commercially available photodiodes, an oscilloscope and an X-Y plotter. From this recorded data the worst case extinction ratios for P_1 and P_2 initially measured 22:1 and 20:1 with an average extinction ratio in excess of 30:1 for both polarizations. This data was obtained using the fastest commerical photodiode available from Texas Instruments for detection of 1.06 μm laser wavelength. Since the initial data was acquired, a Rockwell International GaAs avalanche photodiode was received and subsequently used to obtain 1.06 μm modulator dynamic extinction ratio data. This diode was faster than commercially available 1.06 μm photodiodes with greater 1.06 μm sensitivity. Therefore, the signal-to-noise ratio using this photodiode was greater which improved the measured dynamic extinction ratio accuracy.

Figures 65 and 66 show the photographs of the 63 bit PPBM transmitted data. Using this photodiode, oscilloscope, and X-Y plotter the worst case extinction ratios of P_1 and P_2 measured 28:1 and 28:1, respectively, with an average extinction ratio of 36:1 and 42:1 for P_1 and P_2, respectively. The data agreed rather well with the initial data except for P_2 which was the photodiode that had bad reflections in the transmitted code. This was probably due to a bad 50 ohm match for that particular photodiode. This data gathered after 684 hours of continuous operation was exceptionally good and exceeded our dynamic extinction ratio goal for this program.

Figures 67 and 68 show the photographs of the 63 bit PPBM transmitted data using this photodiode, oscilloscope and camera at the conclusion of the 1099 hour modulator life test. The worst case dynamic extinction ratios of P_1 and P_2 measured 30:1 and 31:1, respectively, with an average dynamic extinction ratio of 39:1 and 47:1 for P_1 and P_2, respectively. This data was better than the initial data; however, it was uncertain

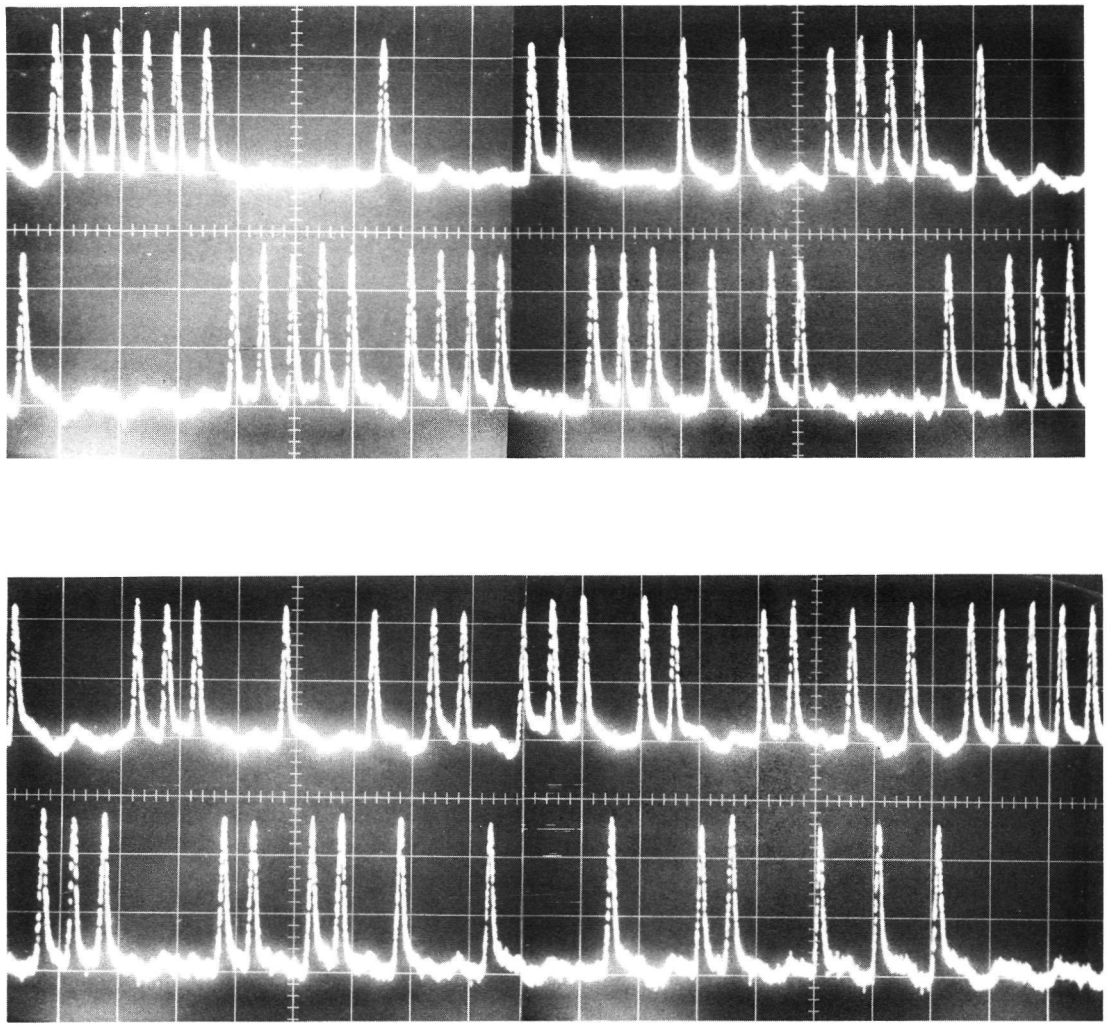

FIGURE 64 63 BIT 400 Mbps PPBM DYNAMIC EXTINCTION RATIO PHOTOGRAPHS AFTER 156 HOURS OF CONTINUOUS OPERATION

HORIZONTAL SCALE 5 NS/DIV
VERTICAL SCALE 10 mV/DIV

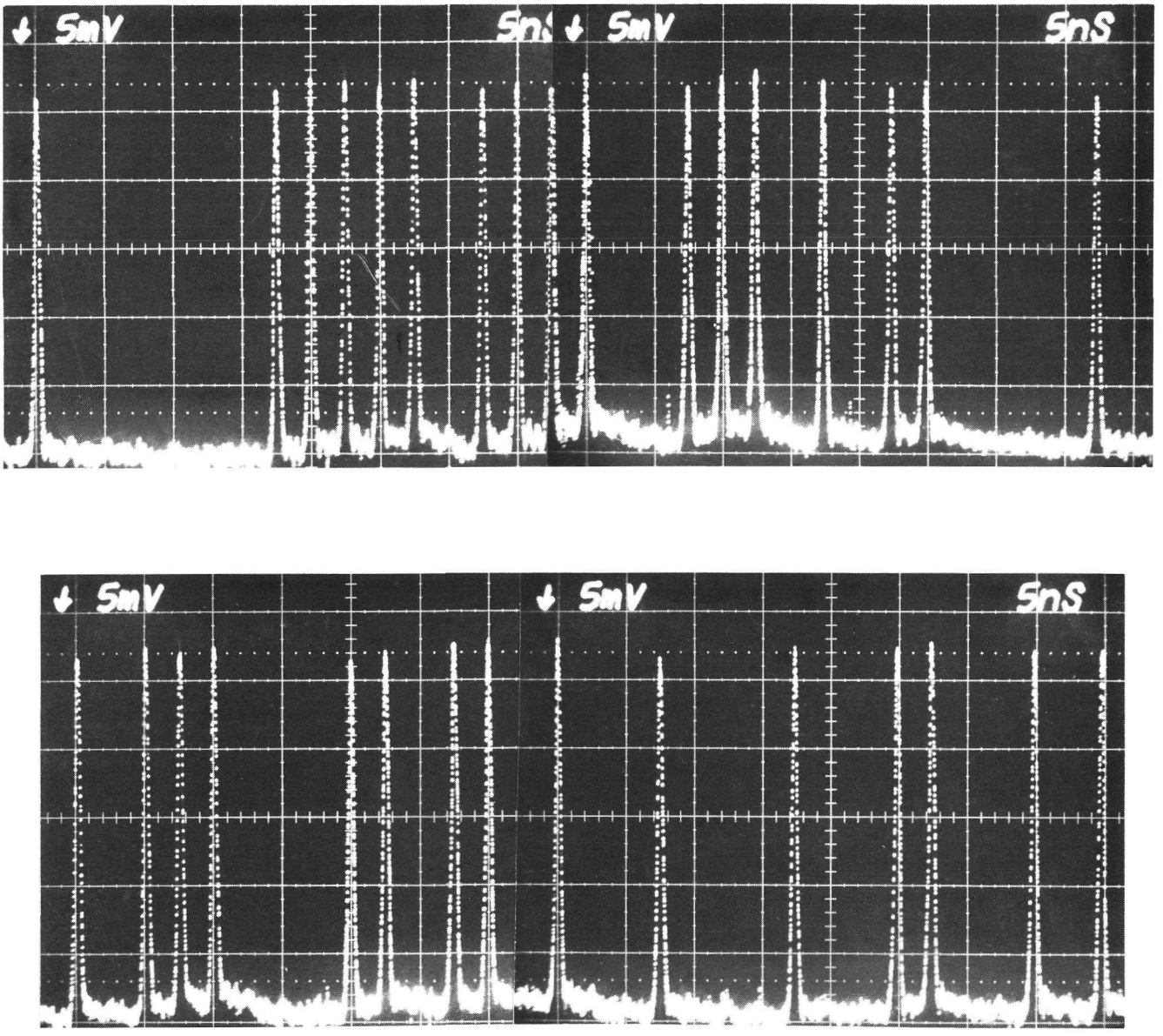

FIGURE 65 63 BIT 400 Mbps PGBM DYNAMIC EXTINCTION RATIO PHOTOGRAPH OF P_2 AFTER 684 HOURS OF CONTINUOUS OPERATION

WORST CASE EXTINCTION RATIO – 28:1

HORIZONTAL SCALE – 5 NS/DIV
VERTICAL SCALE – 5 mV/DIV

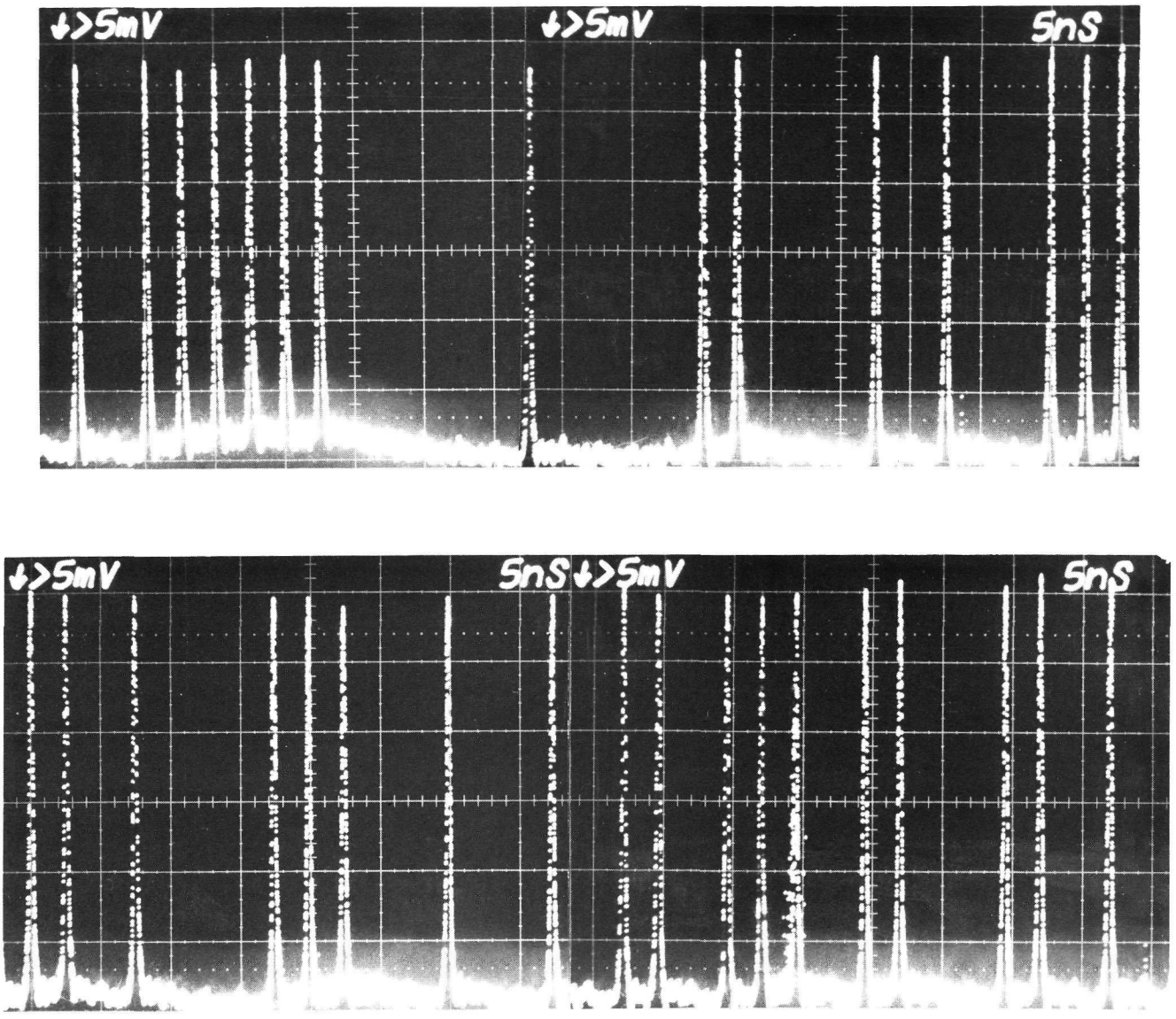

FIGURE 66 63 BIT 400 Mbps PGBM DYNAMIC EXTINCTION RATIO PHOTOGRAPH OF P_1 AFTER 684 HOURS OF CONTINUOUS OPERATION

WORST CASE EXTINCTION RATIO – 28:1
HORIZONTAL SCALE – 5 NS/DIV
VERTICAL SCALE – 5 mV/DIV

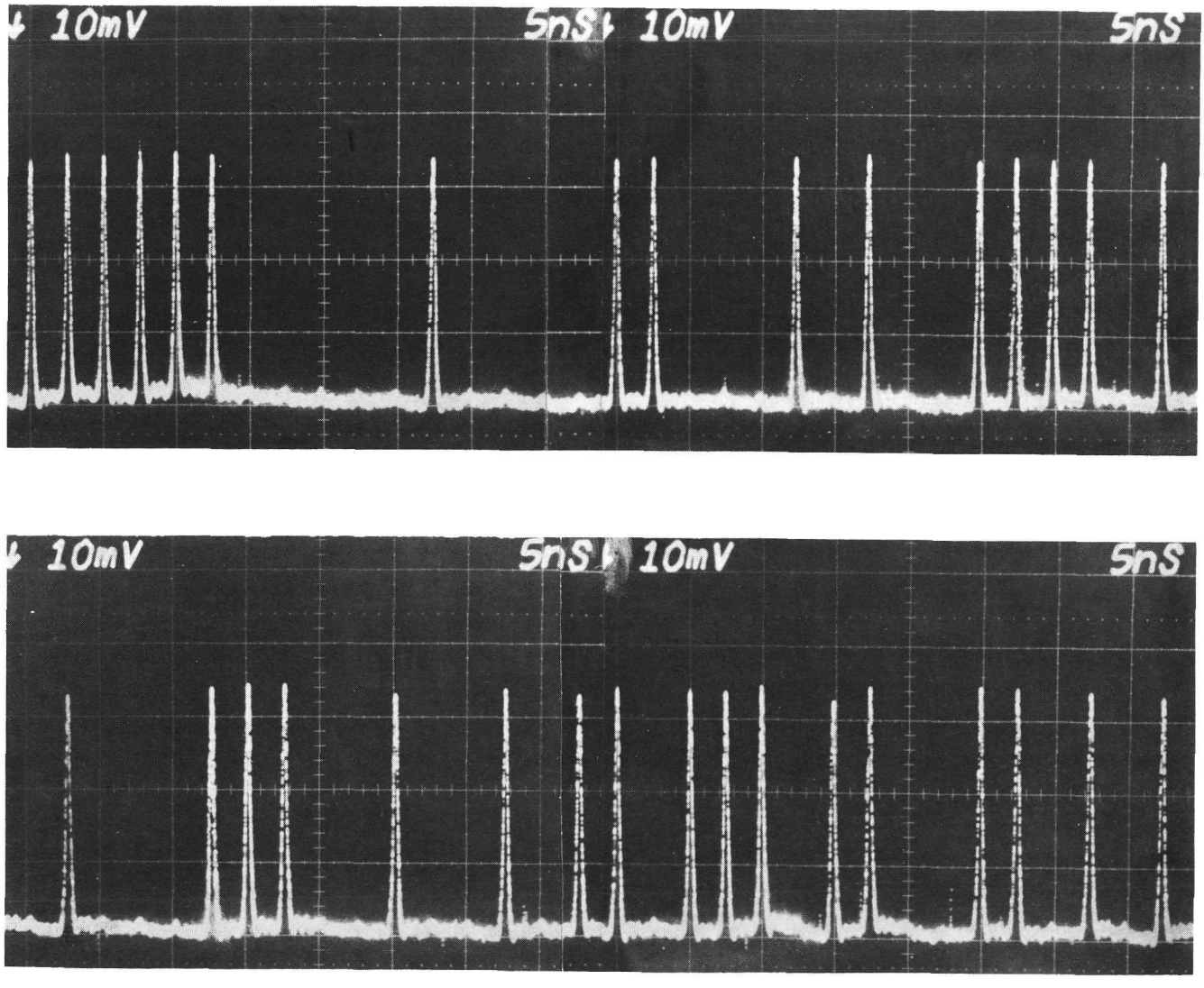

FIGURE 67 63 BIT 400 Mbps PGBM DYNAMIC EXTINCTION RATIO PHOTOGRAPH OF P_1 AFTER 1099 HOURS OF CONTINUOUS OPERATION

WORST CASE EXTINCTION RATIO – 30:1

HORIZONTAL SCALE – 5 NS/DIV

VERTICAL SCALE – 10 mV/DIV

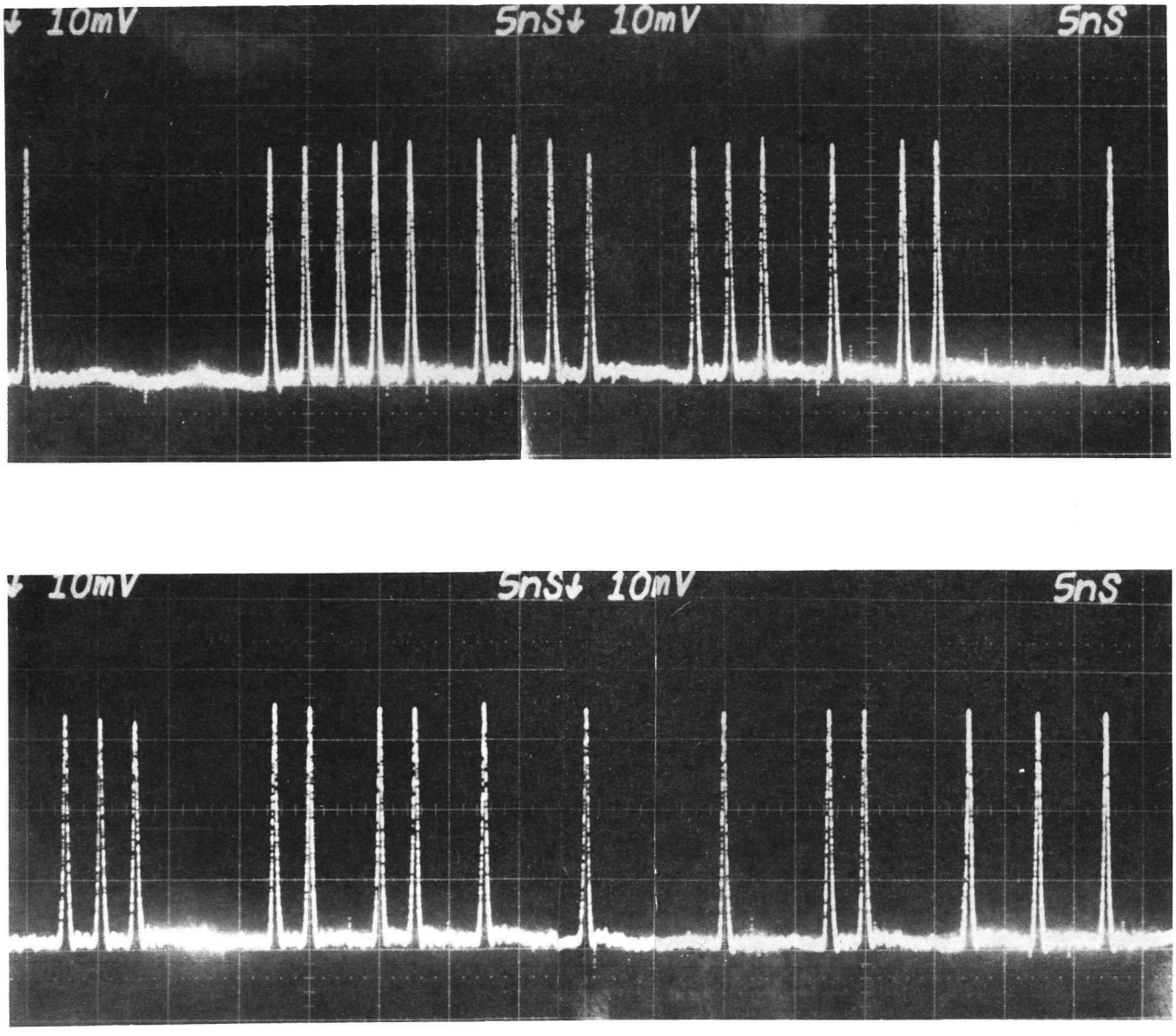

FIGURE 68 63 BIT 400 Mbps PGBM DYNAMIC EXTINCTION RATIO PHOTOGRAPH OF P_2 AFTER 1099 HOURS OF CONTINUOUS OPERATION

WORST CASE EXTINCTION RATIO – 31:1
HORIZONTAL SCALE ~ 5 NS/DIV
VERTICAL SCALE – 10 mV/DIV

whether there was a marked improvement in modulator performance due to crystal strain relief or the analyzing of the data due to the faster photodiode and improved signal-to-noise ratio. It was conceivable that the crystals had become free of mounting strain after 1099 hours of continuous operation. This would result in an improved extinction ratio both statically and dynamically. However, improved static extinction ratio was not observed over the 1099 hour period. Therefore, it was not believed that gradual release of mounting strain resulted in dynamic extinction ratio improvement if indeed the dynamic extinction ratio improved. However, it was known that the Rockwell Internation GaAs avalanche photodiode was faster than the Texas Instruments commerically available Ge photodiode; therefore, our measurement accuracy had improved due to the better detector. In conclusion, it was unknown whether the modulator performance did improve and if it did, what caused the resultant improvement. However, it was certain that no degradation occurred in the modulator performance during this 1099 hour life test. The data obtained at the conclusion of the life test was exceptionally good and exceeded the dynamic extinction ratio goal of 20:1 for this program.

During the life test, the laser was operated continuously without failure; therefore, the tungsten-iodide lamps had 1099 hours of continuous operation. However, only 65 mW of 1.06 μm average optical power was focused into the modulator. Table X lists the performance summary of the 1.06 μm wideband laser modulator 1099 hour life test. As seen from the table, the life test was successful and no apparent degradation was noted in any modulator parameter after 1099 hours of continuous operation.

During the life test, the modulator electronics package performed exceptionally well and no measurable degradation was noted in any electronic component after 1099 hours of continuous operation. The dual driver output waveforms are shown in Figure 69 and correspond to the extinction ratios shown in Figures 67 and 68, respectively. These waveforms were taken with an instrumentation test probe installed in the coax cable at the driver outputs. These waveforms would indicate any failure in driver performance, crystal matching network and power supply. Therefore, the

TABLE X

Performance Log of the 1.06 μm Wideband Modulator Life Test

Hrs	Transmission (Average)	Static Extinction Ratio	Dynamic Extinction Ratio (Worst Case)	
			P_2	P_2
0	69%	69:1	22:1	17.5:1
156	68.5%	65:1	22:1	20:1
348	69%	65:1	25:1	23:1
468	71%	53:1	23:1	25:1
540	69.5%	62:1	25.5:1	22:1
684	71%	55:1	28:1	28:1
779	72%	60:1	30:1	27:1
947	71%	67:1	27:1	30:1
1099	71.5%	60:1	30:1	31:1

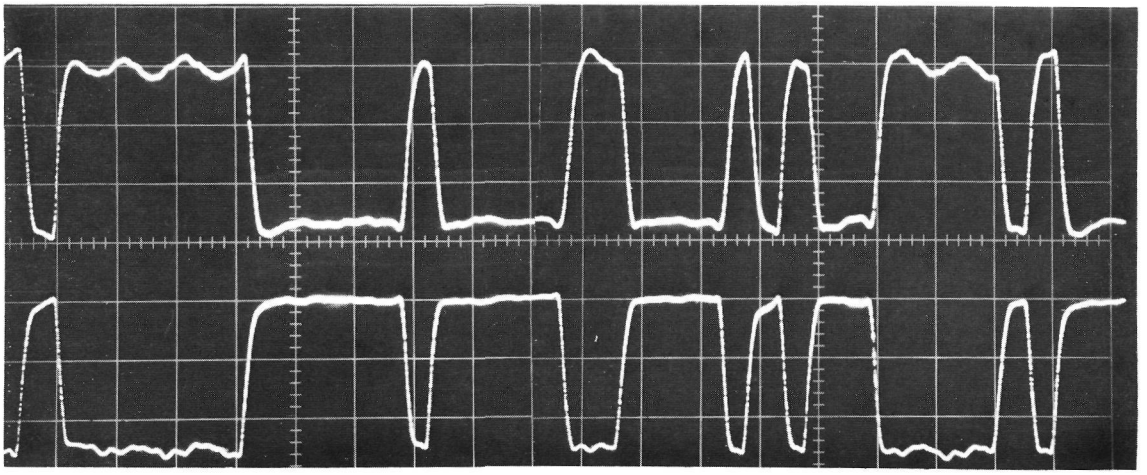

DRIVER
OUTPUT TO
CRYSTAL NO. 2

DRIVER
OUTPUT TO
CRYSTAL NO. 1

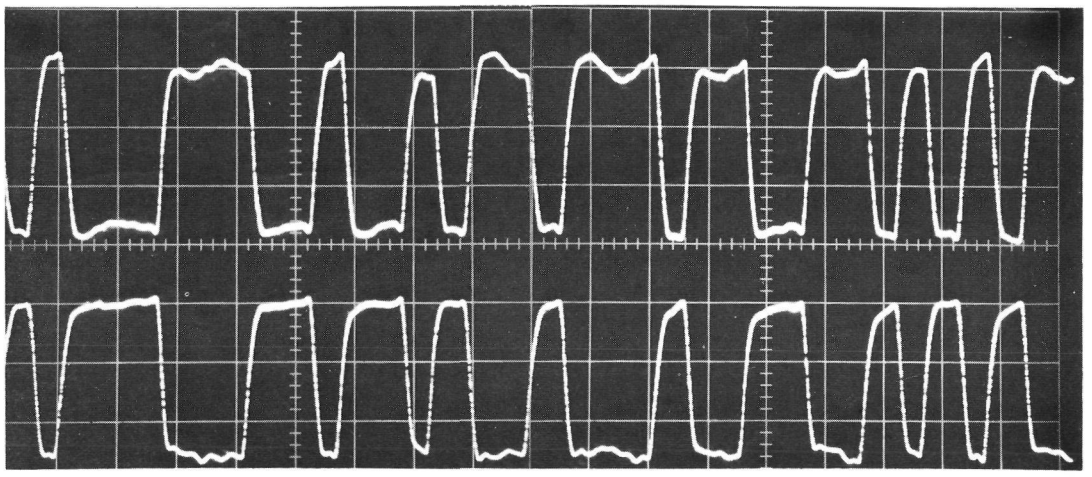

DRIVER
OUTPUT TO
CRYSTAL NO. 2

DRIVER
OUTPUT TO
CRYSTAL NO. 1

FIGURE 69 400 Mbps MODULATOR DRIVER OUTPUT WAVEFORMS (63 BIT)

VERTICAL – 10 V/DIV
HORIZONTAL – 5 nS/DIV

performance during this life test was excellent.

After evaluation of the life test data, the modulator was operated in two different oven core heater standby modes each for five (5) days. Initially, the modulator oven core heater was operated in the medium heat mode (93°C) for overnight (standby) control (16 hours), then the oven was heated and maintained at 150°C for system performance (8 hours). The laser and modulator driver were also shut down overnight (16 hours) while the modulator oven was in the standby mode (93°C). The laser and modulator driver were operated during the workday (8 hours) when the crystal oven core was at 150°C.

The second functional test was one in which the modulator oven core heater was switched to medium heat until the temperature was stable at 93°C (would take approximately 30 minutes) and then the heater was switched to low heat at which the temperature would gradaully decrease to 63°C. The crystal oven core heater remained in the low heat mode overnight (16 hours) in this standby condition. The oven core cooling cycle was just reversed for modulator oven core heating during the workday; the heater control was switched to medium and the crystal oven core temperature would increase to 93°C ($\sim$ 30 minutes) at which time the heater control was switched to operate. In the operational mode it would take approximately 30 minutes for the crystal oven core to stabilize at 150°C.

The purpose of these tests was to determine modulator performance after the crystals were maintained in a lower than operating oven core temperature standby mode for storage or nonimmediate use. This storage mode would limit electrical power consumption when the system would not be transmitting data. However, the system could be operative in less than one hour from this standby mode without system performance degradation. Once the oven core had reached 150°C and was stabilized then data would be transmitted. No degradation was seen in modulator performance in either test after the functional standby mode. The modulator performance parameter of interest in these tests was modulator optical transmission. Modulator transmission ranged from 69% to 70% during the 10-day period

of testing. Static extinction ratio was greater than 50:1 and the worst case dynamic extinction ratio was greater than 25:1 for both polarizations in the PPBM format. Figures 70 and 71 show typical dynamic extinction ratio plots of the P_1 and P_2 polarizations, respectively, during the course of this program using the Rockwell International GaAs avalanche photodiode.

5.3 ELECTRONICS. Complete tests were performed on each module in the electronics assembly. Some of the tests were performed on the bench, however, most of the tests were performed after integration with the modulator assembly. The results of these tests were documented and are given with explanations below under the appropriate module description.

5.3.1 Driver Tests. Using a 63 bit PN code input, the outputs of the dual modulator driver were observed. Figure 69 shows the waveforms for both driver outputs, J35 and J36. These waveforms were taken using an instrumentation test-probe installed in the coax cable at the driver outputs. Although capable of somewhat higher switching voltages the driver was adjusted to switch 27 volts p-p in order to provide full switching to modulator crystals. Driver rise and fall-times were measured to be less than or equal to 1000 ps. Driver timing accuracy was measured by comparing the timing at half switching amplitude to a reference 400 MHz clock signal. The driver outputs were found to have timing errors of $\leq \pm 320$ ps.

5.3.2 Temperature Controller Tests. Tests were also conducted on the temperature controllers at the module level to demonstrate proper operation. The controller, which used pulse width modulation to control the average heater current, was checked for correct frequency, waveform, sensitivity and adjustment range. Typical test results are listed in Table XI.

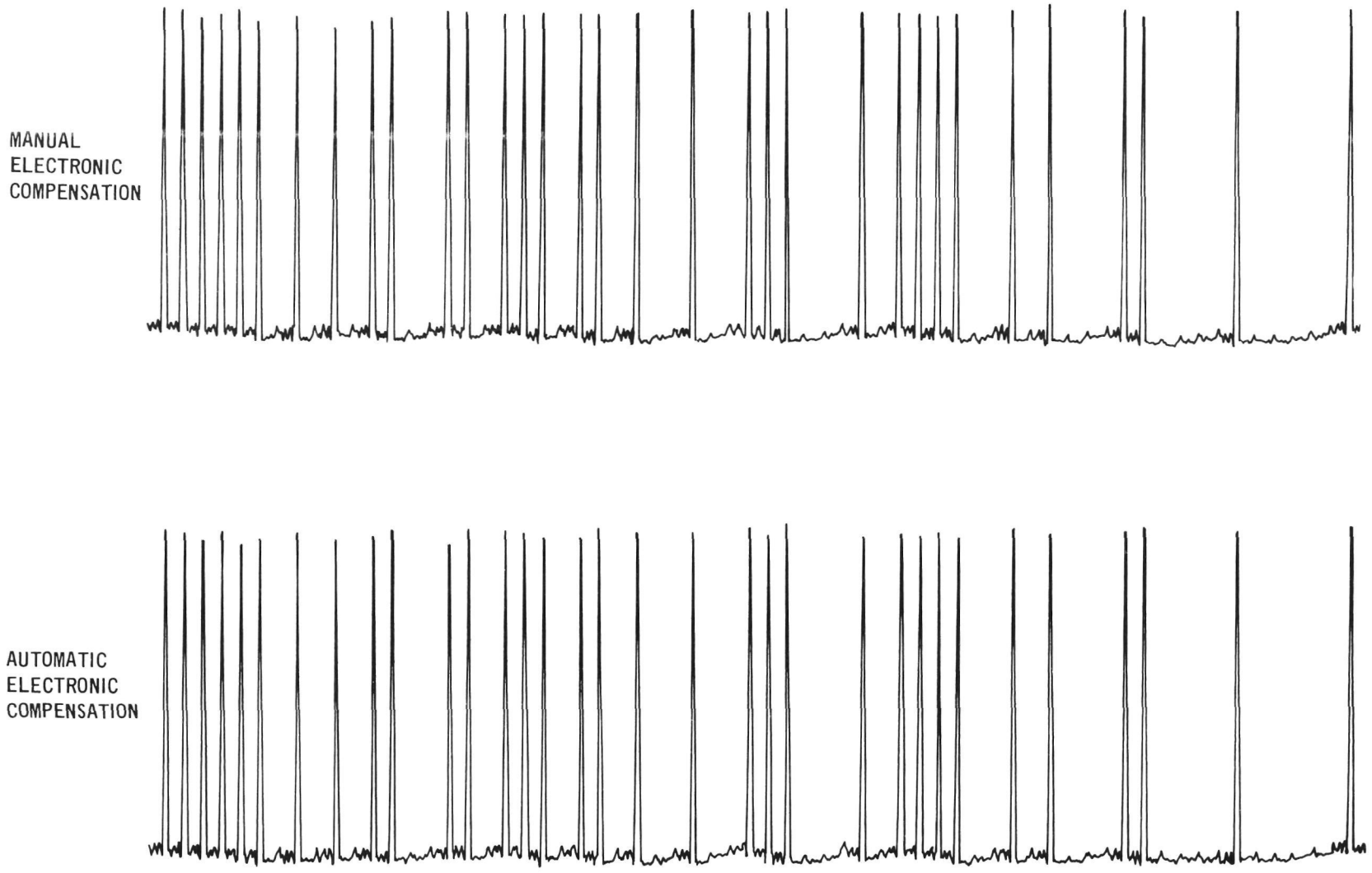

FIGURE 70 DYNAMIC EXTINCTION RATIO PLOT P_1 POLARIZATION

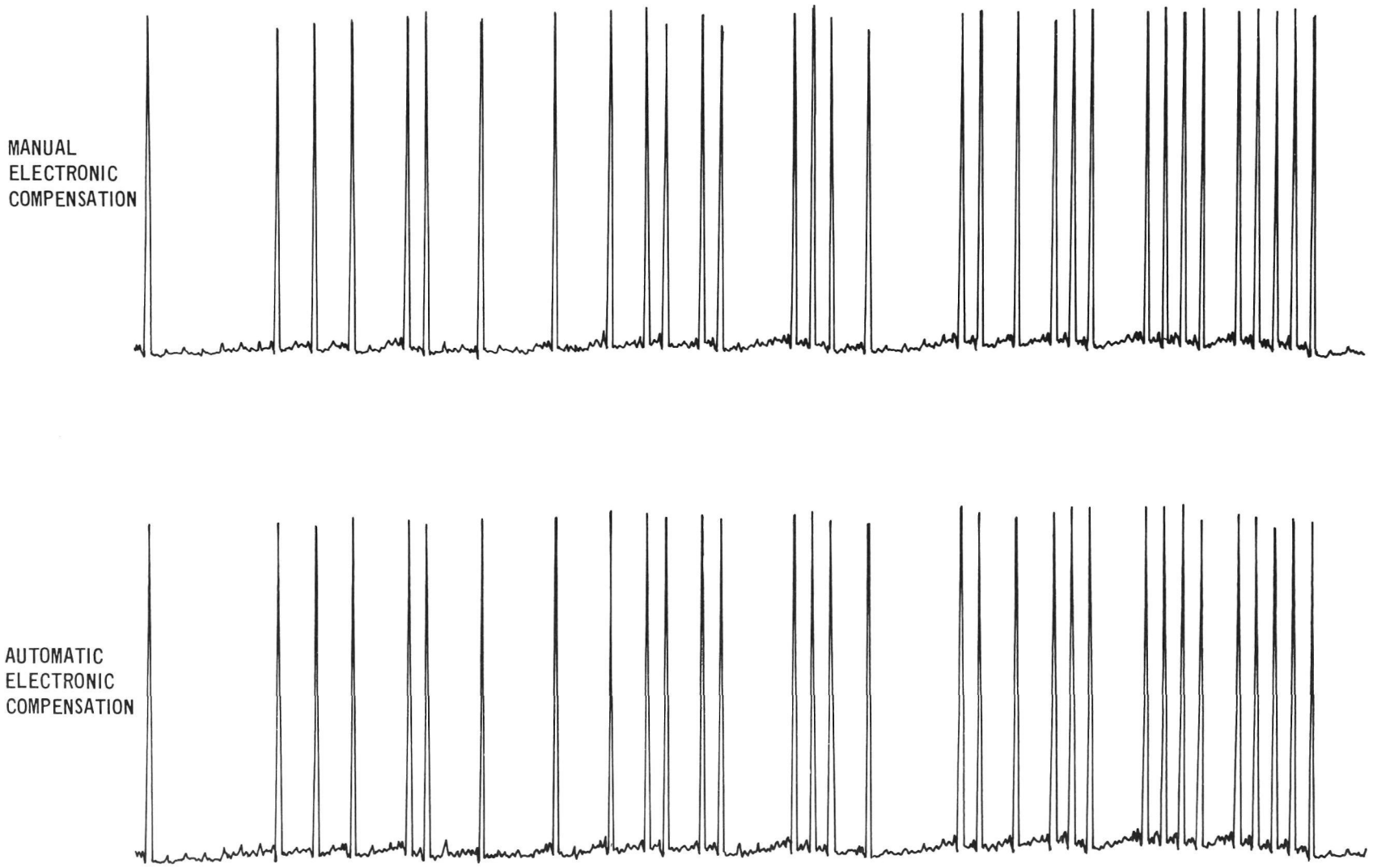

FIGURE 71 DYNAMIC EXTINCTION RATIO PLOT P_2 POLARIZATION

Table XI

Temperature Controller Test Results

Parameter	Value
Frequency	6.0 kHz
Rise Time	7 μs
Fall Time	1 μs
On Level	0.8 volts
Sensitivity	6.9% duty cycle change/ohm input change 0.67 watts/ohm change with 25V heater supply 7.0 watt/°C for a 3%/°C thermistor with a value of 233 Ω at 150°C
Adjustment Range	185-323 ohms for 138°C-152°C

5.3.3 Automatic Electronic Compensator (AEC) Tests - The series of pictures in Figure 72 illustrate typical AEC operation. The pictures on the right show the crystal bias from the AEC (the differential of test points J26 and J30), the AC error signal from the error amplifier (test point J23), and the phase detector reference oscillator signal (test point J28) for several operating conditions. The operating conditions illustrated in Figure 72 were produced by introducing an intentional optical birefringence error on the optical signal by adjusting an external optical compensator placed in front of the modulator.

Note, as the crystal bias voltage changed from the positive end of range to the negative end of range (over 100V p-p), the error amplifier signal change was so small that it could not be detected in the waveforms, however as soon as the bias amplifier reached their end-of-range, the error amplifier signal increased to saturation before the extinction ratio degraded below 10:1. Therefore this indicated that the recovered error signal was sufficient to maintain automatic compensation at any point within the bias amplifier

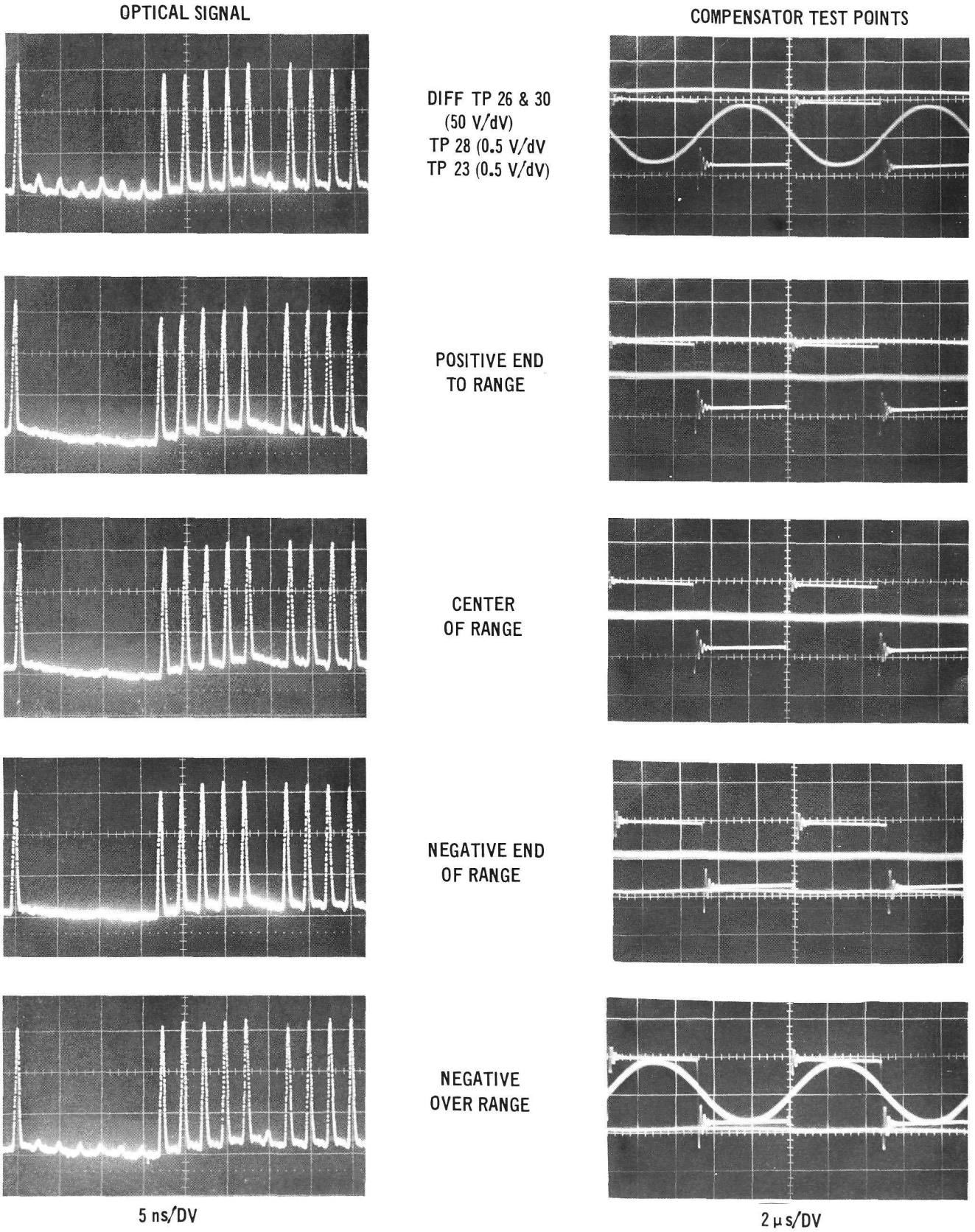

FIGURE 72 AUTOMATIC ELECTRONIC COMPENSATOR OPERATING PHOTOGRAPHS

range without degrading the extinction ratio. These tests were performed for input light level of 50 mw and the compensator was found to perform well.

The gate output test point (TP 18) waveforms are shown in Figure 73 for Manchester code and PN code operation. The modulator driver test point (TP 6) was included for reference. Note that the detected pulses were seen in the PN code operation.

5.3.4 Thermal Differential Compensator Tests - The ideal operating point for automatic electronic compensator was when the average dc field applied to the crystal was zero. Under normal circumstances, however, the applied driver voltage and natural crystal birefringence caused the automatic compensator to operate at a point other than the zero field condition.

A method of compensation was previously devised which utilized the modulator crystals themselves and no additional optical components. This novel method of compensation exploited the temperature dependence of the modulator crystal birefringence in order to produce optical compensation. Normally both modulator crystals were maintained at a uniform temperature inside a boron nitride oven core which was heated by two balanced heater coils located at opposite ends of the core. It was found that by intentionally unbalancing the heaters a precise temperature differential would be created within the oven. This temperature differential caused a change in the birefringence of one crystal with respect to the other and thus produced a net birefringence change which was a function of the differential. By adjusting the temperature differential, up to three fringes (half waves) of optical compensation would be obtained, which was greater than the $\pm$ one fringe required. Termed "thermal differential compensation" (TDC) the modulator unit was designed to utilize this scheme (described in Section 2.6.4.3) for obtaining a zero field condition as the nominal

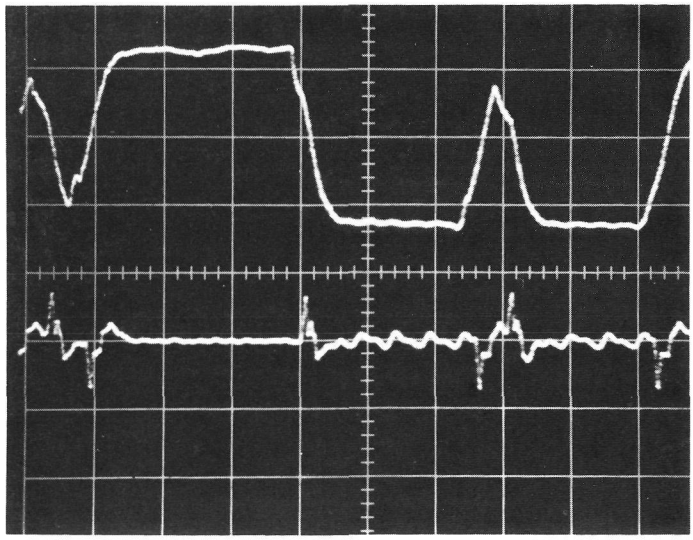

MODULATOR DRIVER
TP 6 (10 v/dV)

GATE OUTPUT
TP 18 (100 mV/dV)

PN CODE OPERATION

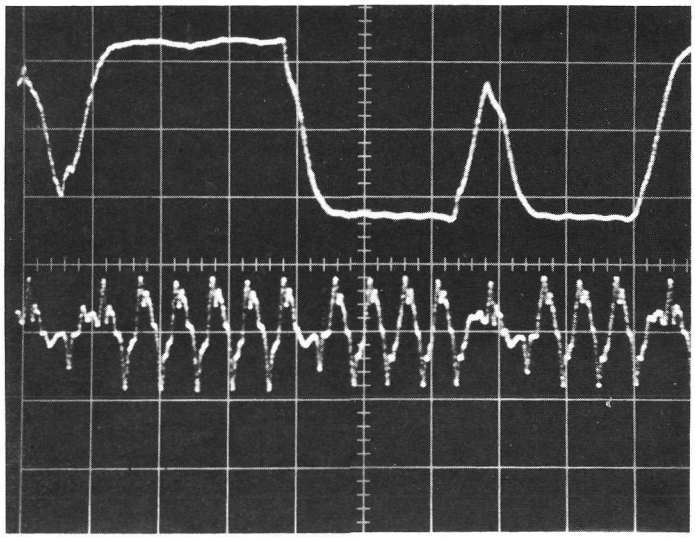

MODULATOR DRIVER
TP 6 (10 V/dV)

GATE OUTPUT
TP 18 (100 mV/dV)

MANCHESTER CODE OPERATION

FIGURE 73 AEC GATE OUTPUT TEST POINT

operating point of the automatic electronic compensator. This technique can be electronically automated if warranted.

5.3.5 Modulator Power Supply Tests - The regulated supplies were each checked for adjustment range, short circuit current limit, ac ripple, and crowbar settings. The adjustment range tests were made with no load. The ac ripple was taken with 50% of the current limit load. All tests were taken using the lab bench ac power at 110 V 60 Hz. Table XII contains typical recorded data, and Figure 39 gives a block diagram of the power supply.

A measurement of the voltage and current was made for each power supply voltage under typical modulator operating conditions. The current from a given regulator to a particular modulator assembly was also measured. From this information the power provided by any regulator and the power consumed by an assembly was calculated as shown in Table XIII.

Table XII

Modulator Power Supply Test Data

Regulator	Adjustment Range		Short Circuit	50% Load	Crowbar Setting
	Low	High	Current	AC Ripple	
Volts	Volts	Volts	mA	mV	Volts
+2.0	-	-	600	<2	N/A
+5.0	<0.1	8.7	600	<2	7.0
-3.2	-	-	800	<2	N/A
-5.2	<0.1	7.5	2350	<2	7.5
+15.0	<0.1	21.9	550	<2	17
-15.0	<0.1	21.9	500	<2	17
+6.0	<0.1	70.0	65	<5	6.5
+7.3	5.8	10.5	830	<5	11.5
+6.5	4.0	9.0	660	<5	10
+6.5	4.3	9.0	660	<5	10
+30	27	36.0	770	<5	41
+25	<0.1	39.9	770	<5	26.5
-200	<0.1	280.	36	<2	N/A

Table XIII

Voltage and Power Breakdown for a

400 Mbps Modulator Unit

Sub Unit	Power Supply (Nominal Voltage Designation)													
	+2.0	+5.0	-3.2	-5.2	+15	-15	+60.0	+7.3	+6.5	+6.5	+3.0	+2.5	-200	(Watts)
Driver	505			4300				1378	445	500	1760			8.888
Load											13005			13.005
Temp. Cont.					270	211						1269		1.750
Heater										7320				7.32
AEC	223	155	311	273	838	61	34						18	1.913
Total Power	728	155	311	4573	1108	272	34	1378	445	7820	14765	1269	18	32.876

NOTE: All power values in milliwatts except for total power listed in the last column.

6. CONCLUSIONS AND RECOMMENDATIONS

The 1.06 micrometer wideband laser modulator, designed for a 400 Mbps modulator, was built and tested during this program. The modulator package consisted of a modulator assembly, electronics package, and a laboratory power supply package necessary for modulation data rate ranging from 10^4 to 4×10^8 bits per second. The modulator was designed to operate in a single pass optical configuration which transmits either pulse gated binary modulation (PGBM) or pulse polarization binary modulation (PPBM) as a modulation format. The modulator consisted of an optics assembly, wideband modulator driver, automatic electronic compensator, manual electronic compensator, manual thermal differential compensator, load box, and temperature controller.

Tests were performed on the 1.06 μm 400 Mbps modulator in order to establish performance characteristics and verify design goals. These tests included the measurement of static extinction ratio, dynamic extinction ratio, and optical transmission. The static extinction ratio was found to be 60:1. The worst case dynamic extinction ratios were 30:1 for P_1 and 31:1 for P_2. The average dynamic extinction ratios were found to be 39:1 for P_1 and 47:1 for P_2. Optical transmission was measured to be 71.5%. The beam output characteristics of the modulator were found to be the same as the input characteristics, thereby indicating no additional degradation due to the modulator. Additional tests were performed to verify modulator operation in the automatic compensator mode to be as good as in the manual compensation mode.

A 1099 hour life test was performed on this modulator without any component degradation. The modulator maintained optical transmission which ranged from 68.5 to 72%. The static extinction ratio ranged from 53:1 to 69:1. The worst case dynamic extinction ratio ranged from 22:1 to 30:1 for P_1 and from 17.5:1 to 31:1 for P_2. The life test was successful and no apparent degradation was noted in any modulator parameter during or after the 1099 hours of continuous operation.

Comparing the measured modulator parameters with the expected values for these parameters it was found that the modulator met or exceeded goals in every area listed in Table XIV. The modulator performance obtained indicated the improvement which single pass operation can achieve over the previously employed double pass operation. Therefore, the test results demonstrate the superiority of single pass operation over the double pass operation both in the simplicity of optical alignment and the improvement in modulator performance. The individually matched crystals and dual output driver manifested itself in the improved dynamic performance. The thermal differential compensator, which was employed in this 1.06 μm modulator system, was found to perform well in conjunction with the manual electronic and automatic electronic compensators. By employing the thermal differential compensator, the average voltage across the modulator crystals was kept at zero.

As shown in Table XV the optical transmission was lower than the possible transmission value for such a modulator. The reason for the lower transmission was because of the optical safety factor of the modulator crystals. With only a safety factor of < 1.75, the 81% transmission for the crystal pair cannot be achieved due to scattering. If the crystal cross sections were increased 15%, the modulator transmission should increase 5 to 7%; however, this increase in modulator transmission would result in an increased modulator power consumption increase of < 15%. The power consumption would increase from 32.8 watts to 38 watts. This increased power consumption would be due to increased modulator crystal switching voltage which would increase from 27 volts to 31 volts. Therefore, the modulator optical transmission would increase at the expense of increasing electrical power consumption.

TABLE XIV

1.06 Micrometer Wideband Laser Modulator Performance

Parameter	Goal	Measured Value
Static Extinction Ratio	50:1	60:1
Dynamic Extinction Ratio (worst case)	20:1	30:1 P_1 31:1 P_2
Optical Transmission	70%	71.5%
Total Power Consumption	$\leq$ 45 watts	32.8 watts
Weight (Modulator Subassembly)	$\leq$ 2.0 Kg	1.25 Kg
Volume (Modulator Subassembly)	$\leq 2 \times 10^3$ cm^3	600 cm^3

TABLE XV

Expected and Achieved Optical
Transmission for Modulator Optical Components

Component	Expected Transmission	Achieved Transmission
Crystals (2 crystals - Single Pass	81%	76%
Lenses (2)	98%	98.2%
Pellicle Beamsplitter	99%	97.6%
Polarization Beamsplitter (Use for PGBM Data Transmission)	98%	98%
TOTAL TRANSMISSION FOR PGBM	77%	71.0%
TOTAL TRANSMISSION FOR PPBM	78.6%	71.5%

APPENDIX I

OPERATING INSTRUCTIONS

The operating instructions given in this section were designed to give the user the information necessary for both initial modulator setup and normal operation. Although the instructions may seem complicated or detailed, once a stable system configuration has been achieved only the few steps indicated are required for day-to-day operation.

A. MODULATOR TURN-ON PROCEDURE. Once the modulator has been positioned in its operational location, but before initial optical alignment and electrical interfacing, the steps listed below should be followed:

a. All power supply switches should be in the OFF position and the laser should be OFF or else the optical input to the modulator blocked.

b. Connect power cable from power supply package to electronics package and all semirigid cables from electronics package to modulator optics package.

c. Turn the "Heater Control" switch to the LOW position.

d. Turn the "Main Power" switch to the ON position.

e. Allow 30 minutes for the modulator oven to reach the low heat temperature (63°C).

f. Turn the "Heater Control" switch to the MEDIUM position.

g. Connect the output of the data source to be used to a 50 ohm input scope. Verify that the data is present with the correct code and correct logic swings (upper levels: -0.85V; lower levels: -1.85V).

h. Connect the data source to the modulator driver input, J33, (do not turn data source power off while making this connection). Be sure to use a trombone between data source and driver input for timing adjustment. Verify that the "Driver Power" switch is OFF.

i Turn the "Electronics" switch to the ON position. Verify that code is present at test point 22 (use 50 ohm impedance scope). A small signal should be present (0.48V p-p).

j. Turn the modulator "Driver Power" switch to OUTPUT only. This should be done while monitoring L_1 and L_2 on a sampling scope; there should

be a dc level shift of approximately 30 volts.

k. Turn the modulator "Driver Power" switch to OPERATE and the "Output Stage" switch to OPERATE. The dc signal should change to a modulation signal.

l. Connect the output of the clock signal (400 MHz sine wave) to a 50 ohm input scope. Verify that the p-p level is correct for the Manchester code input level (1.1V $\pm$ 0.3V p-p).

m. Connect this clock signal output to the electronics package for the Manchester Code Input, J19. Be sure and use a trombone between the clock signal and J19 for timing adjustment.

n. The modulator can be operated with either manual or automatic compensation. If manual compensation is to be used, position the "Compensation" switch to "MAN". If automatic compensation is to be used, turn the "Photodiode Bias" switch to the ON position and turn the "Compensator" switch to AUTO.

o. When the modulator heater control switch has been in the MEDIUM position for at least 30 minutes, turn the heater control switch to OPERATE.

p. Allow 15 minutes for the modulator oven temperature to regulate and stabilize.

NOTES

a. Do not connect any input to the modulator driver which can cause the output stage to remain on for more than four milliseconds. If the driver output is on for periods longer than this the crowbar protection circuit will respond, necessitating a reset of this circuit before normal modulator operation can be resumed. For the same reason data codes with greater than 70% logic "1" duty cycles for any four millisecond period should not be used.

b. The low heat and medium heat modes have been incorporated as a precaution to prevent unnecessary thermal shocks to the modulator crystals, and should be used under all conditions.

c. For optimum modulator operation allow a 30-minute warmup for drivers after turn-on.

B. MODULATOR TURN-OFF PROCEDURE. This procedure assumes that the modulator has been fully integrated and optically interfaced at both input and output for proper operation.

Emergency Turn-off of Entire Modulator:

Turn "Main Power" switch to OFF position.

Emergency Turn-off of All Modulator Electronics Except Heaters:

Turn "Electronics" switch to OFF position.

Normal Turn-off:

For a complete turn-off of the modulator follow all the steps listed below.

For day-to-day operation (i.e., when modulation format is not being changed between turn-off and turn-on) only Steps a, b and c should be used.

a. Turn the "Electronics" switch to the OFF position.
b. Turn the laser off or block the modulator optical input.
c. Turn the heater control switch to the MEDIUM position.
d. Turn the "Diode Bias" switch to the OFF position.
e. Turn the "Driver Power" switch to the OFF position.
f. Allow 30 minutes for the modulator oven to cool to medium heat.
g. Turn the heater control switch for the modulator to the LOW position.
h. Allow 30 minutes for the modulator oven to cool to low heat.
i. Turn the "Main Power" switch to the OFF position.

C. INITIAL ALIGNMENT. Initial modulator alignment consists of three procedures: optical alignment, electrical input interfacing and timing, and compensator adjustments on the modulator units. Once made, these procedures should not have to be repeated unless the system configuration is changed.

C-1 Optical Alignment Procedure. The steps of the alignment procedure follow in order. Figure 74 shows the adjustment locations on the modulator baseplate, modulator mount, optics tail, and modulator lens holders.

a. Verify that the optical input parameters have been met before proceeding to align the modulator. The optical input interface specifications are given in Section 4 of this report.
b. Turn on the modulators following the turn-on procedure given in Section A.
c. Loosen the locking screw on the modulator Huber camera mount (see Figure 72).
d. Loosen the modulator lens locking screws and remove the front and rear lenses from the units.
e. Turn the modulator driver electronics off, and turn the photodiode bias off.
f. Place the compensator selector switch in the "MAN" position.
g. Slide the polarization beamsplitter in the optics tail out of the beam path.
h. Translate and rotate the modulators using the y, θ_x and θ_y adjustments (see Figure 74) until light is transmitted through the modulators. The x translation is made by sliding the modulator assembly in the beam path.
i. If all four crystal edges are not equally sharp, translate and rotate the modulators until all edges are equally sharp and until maximum light is transmitted through the crystals.
j. Place the front lens in the front lens holder and position the lens so that light passes through the crystals.
k. Adjust the front lens along the beam axis to produce focused spot on the white paper viewing screen.
l. Place an optical power meter at the output of the modulator and optimized optical transmission of the modulator.
m. Slide the polarization beamsplitter into the beam path.
n. Rotate the manual compensator adjust control knob to produce minimum transmitted light through the modulator as observed on the viewing screen or power meter.

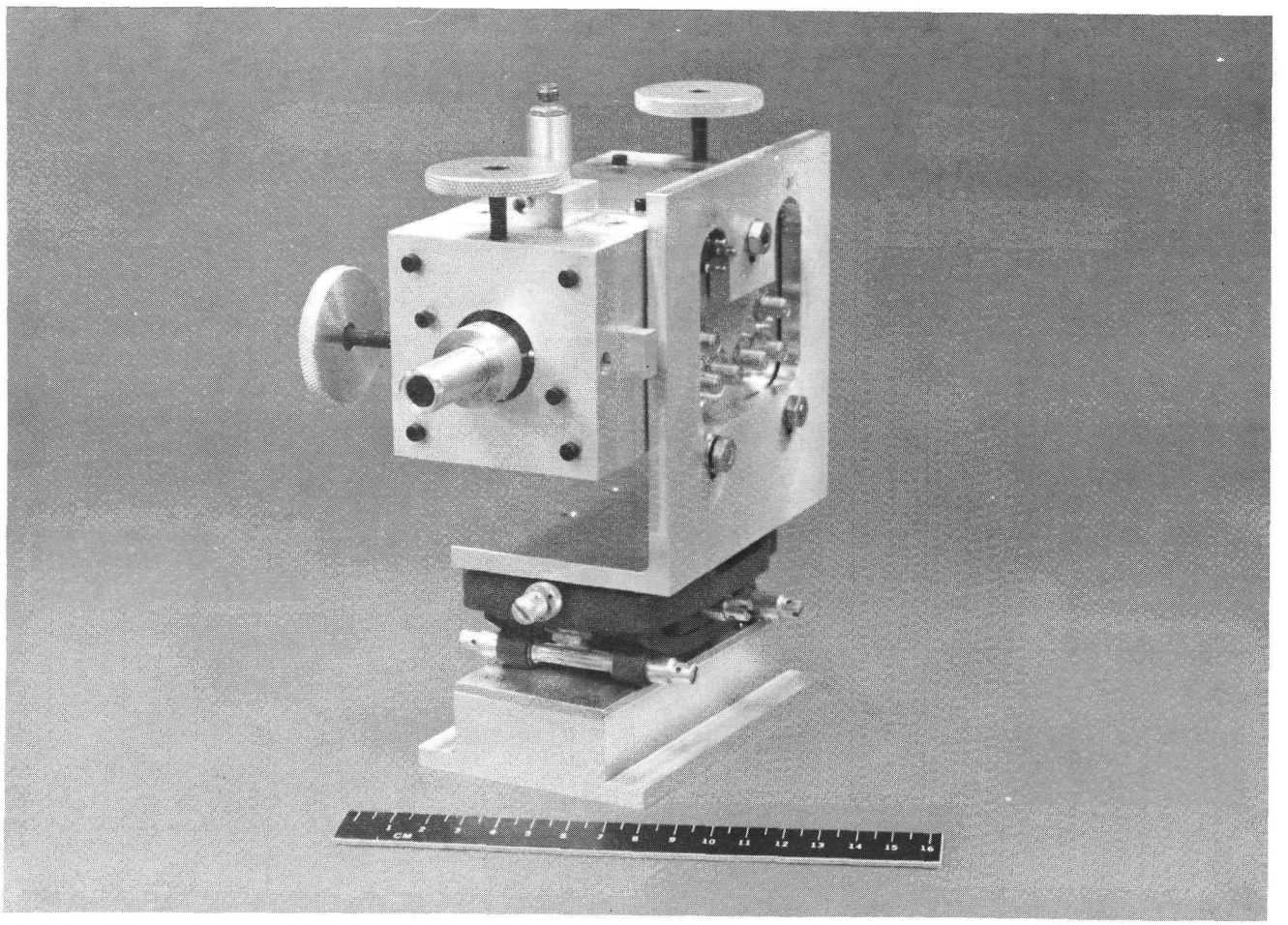

FIGURE 74 ADJUSTMENTS LOCATIONS ON MODULATOR ASSEMBLY

o. Make slight adjustments of the front lens holder positions in order to optimize the static extinction ratio.

p. Tighten all of the locking screws on the modulator mount and front lens holder, one at a time, while observing the transmitted light on the viewing screen. Care should be taken not to degrade the alignment while tightening these screws.

q. Insert the output lens of the modulator and adjust the depth in order to collimate the output beam.

r. Remove the white paper viewing screen.

s. Tighten the output lens holder locking screws on the modulator.

t. If no other work is to be done with the modulator at this time turn the modulator off using the turn-off procedure given in Section B.

C-2 Electrical Input and Timing Procedure.

a. If the modulator is not turned on as the result of previous activities, turn the modulator on following the turn-on procedure given in Section A.

b. Set up the electronics to produce the 63 bit code sequence.

c. Connect the PN code output to the driver input. As a part of this connection a variable length delay line should be installed between the output of the PN code electronics and the modulator driver.

d. Connect the driver test points (L_1 and L_2) to an oscilloscope to verify that the code is being properly reproduced by the driver. (A Tektronic model 561A with a 3T2 random sampling sweep and a 3S2 sampling unit using S-4 sampling heads or some equivalent equipment is recommended.)

e. Install two silicon avalanche photodiodes (Texas Instruments TIXL56 or equivalent) at the modulator output in order to observe the modulated optical signal. The diode output should be observed on an oscilloscope equivalent to that described in step (d) above. An external polarization beamsplitter must be used for this setup, with the polarization beamsplitter in the optics tail out of the beam path.

f. Adjust the variable delay line connected between the PN code electronics and the modulator while observing the modulated output with the photodiodes and oscilloscope. The line should be adjusted so that all bits in the code are either maximum amplitude "1's" or minimum amplitude "0's". No half amplitude bits should be observed when the timing set by the delay line is correct.

g. Set the compensator selector switch to the "MAN" position.

h. Simultaneously observe the modulator optical output (with the polarization prism in the beam path in the optics tail) and driver test point 22. A high level on the test point should correspond to an optical one on the modulator output. The manual compensator can be adjusted if necessary to satisfy this condition. (The modulated output must contain the "1" and "0" data format corresponding to the "1" and "0" data format on the driver input signal. This code configuration is required for proper system operation.

i. Connect the gate drive test point (TP22) to the oscilloscope along with the driver test point L1. Adjust the 400 MHz clock signal line length (Ref. A-m) until the proper Manchester Code is present, see Figure 36.

   NOTE: This adjustment must be made after the adjustment in C-2-f above and must be repeated whenever the adjustment of C-2-f is repeated.

j. If no further work is to be done at this time, turn the modulator off using the turn-off procedure given in Section B.

C-3 Automatic Electronic Compensator Diode Adjustment Procedure. After initial modulator alignment it is usually advisable to slightly readjust the position of the diode associated with the automatic electronic compensator (AEC) in order to optimize AEC performance. The compensator diode adjustment and locking screws are shown in Figure 74.

a. Remove the coax cable between J16 and J17 on the modulator electronics package and connect J16 to a sampling oscilloscope.

b. If the modulator is not already on, turn it on following the turn-on procedure given in Section A.

c. Turn the "Photodiode Bias" switch to on and observe the optical pulses on the oscilloscope.

d. Adjust the manual compensator for best extinction ratio.

e. Loosen the diode adjust locking screws (Figure 74).

f. Adjust the diode alignment screws for peak pulse amplitude on the oscilloscope.

g. Tighten the diode adjust locking screws.

h. Using the manual compensator adjust the modulator bias back-and-forth about the best extinction ratio point and observe that the best extinction ratio point on TP16 occurs at the same bias point as the output monitor diode.

i. If the extinction ratios does not peak at the same point loosen the lens mount locking screw and rotate the lens mount until both peak occurs at the same point.

   NOTE: Do not move the lens mount in or out of the modulator optics tail assembly.

j. Tighten the lens mount lokcing screw and repeat steps "d" through "g".

k. Reinstall the coax between J16 and J17.

l. Switch the compensator mode selector switch on the modulator unit from MAN to AUTO and observe that the optical output extinction ratio does not change.

   NOTE: Because circuit power is off, some of the compensator circuits in the manual mode and under certain conditions, switching to the AUTO mode will cause the compensator to drive to end of range before all circuits become stable after turn-on. If this should happen, simply block the laser beam from going into the modulator for 10 to 15 seconds; the compensator will stabilize and then compensate correctly when the beam is reapplied.

m. If no further work is to be done at this time, turn the modulator off, following the turn-off procedure given in Section B.

C-4 Thermal Differential Compensator Adjustment Procedure. As described earlier, the thermal differential compensator (TDC) should be adjusted so that the voltage applied by the electrical compensator (either manual or automatic) to the modulator crystals for normal operation is equal to the average voltage applied to the crystals by the modulator driver. For this modulator unit that average voltage is approximately 18 volts. Because the range of the electronic compensator is -12 to +55V the desired 18V setting is near middle range. The procedure for obtaining the correct TDC operating is given below.

a. If the modulator is not already on, turn it on following the turn-on procedure given in Section A.

b. With the modulator unit in the manual electronic compensator (MEC) mode and with the PN code applied to the modulator drivers observe the modulated optical output.

c. Adjust the MEC to obtain a good extinction ratio with the correct output polarity.

d. Rotate the MEC adjust control to each end of its range. If the polarity of the optical outpout is nearly inverted from the correct polarity at both ends of the range no adjustment of the TDC is necessary. The bias voltage at TP26 should be approximately 18 volts when operating with a good extinction and the proper data wave form.

e. If this is not the case, make a slight adjustment of the TDC control screw (< 1/8 revolution; see Figure 48) and allow approximately three minutes settling time.

f. Repeat steps (d) and (e) until the condition set forth in (d) has been satisfied.

g. If no further work is to be done at this time, turn the modulator off using the turn-off procedure given in Section B.

D. OPERATING MODES. Although the operating modes for the communications system include the option of PGBM and PPBM operation with 63 bit, no change in the modulator is required for these options other than sliding the polarization splitter cube into and out of the beam path. The major modes of operation for the modulator are manual or automatic optical compensation. Since both operating modes make use of the thermal differential

compensator the difference between these modes lies in the use of either the manual or automatic electronic compensator for obtaining maximum extinction ratio of the optcial output.

D-1 Manual Electronic Compensation. Once the thermal differential compensator has been adjusted as described in Section C-4 to operate in the manual optical compensation mode simply throw the compensation selector switch to the MAN position and adjust the compensator control to obtain a maximum extinction ratio of the modulated optical output. However, for complete system operation it may be desirable to adjust the bias control while observing system error rate performance.

D-2 Automatic Electronic Compensation. Once the thermal differential compensator has been adjusted and the automatic electronic compensator diode aligned as described in Sections C-3 and C-4 to operate in the automatic optical compensation mode simply throw the compensation selector switch to AUTO and the "Photodiode Bias" switch to ON. The automatic electronic compensator will then automatically set and maintain a maximum extinction ratio.

E. MODULATOR MAINTENANCE. The modulator designed and fabricated during this program should provide reliable operation without the need for adjustments or maintenance. However, should maintenance be required the procedures outlined in the following sections should be followed.

E-1 Cleaning and Maintaining Optical Components. In order to obtain maximum modulator performance, especially optical transmission, all optical surfaces encountered by the beam must be clean. Because all optical surfaces are antireflection coated to lower optical losses, smoke or vapors as well as airborne particulate matter which accumulates on the surfaces will lower optical transmission. It is, therefore, best to operate the modulator in an environment free of the above pollutants. The modulator is a self-contained unit with no optical surfaces exposed except the input and output lenses.

If the optical surfaces do become contaminated, as evidenced either by observable scatter at the surface where a beam strikes or by a decrease in optical transmission, cleaning can be accomplished. The coatings on the surfaces are of the "hard" type and therefore cleaning should not degrade the coatings. A cleaning procedure is given below.

a. Remove dust and particulate matter from the surface by blowing clean, dry compressed air on the surface. The optical component can be cleaned while still in its mount for this procedure.
b. Hold the component using plastic gloves or finger shields to avoid finger oil contamination.
c. Apply one or two drops of high purity ethanol or methanol to the surface to be cleaned.
d. Wipe the surface dry with lint-free lens tissue using gentle motions. Use the same portion of the tissue for only one wipe.
e. If streaks are observed, repeat steps (b), (c), and (d) until the surface is clean.
f. Replace the component in its holder, and realign if necessary following the optical alignment procedure given in Section 4.3.1.
g. Under no circumstances should cleaning the modulator crystals be attempted.

E-2 Electrical Maintenance. If at any time the modulator unit or some portion of a modulator unit should fail to function properly, a check should first be made to verify that the proper voltages are being supplied by the power supply to the modulator. This procedure is given below.

a. With the power supply power switch turned off, check the fuses at the rear of the modulator power supply unit.
b. If the fuses are all intact, check power supply voltages.
c. With the power supply connected to the modulator unit, turn the modulator on following the turn-on procedure given in Section A.

d. Using the voltage test points shown in Figure 49 check the power supply output voltages with a voltmeter. The nominal voltages are marked on the power supply packages; readings may be slightly different because of adjustments for optimum operation and line lose.
e. If the correct voltages are all present at the test points, turn the modulator off following the turn-off procedure given in Section B.

Problems associated with the modulator can usually be attributed to one of the unit modules simply by observing the system. Because of the inner circuit complexity of most of the modulator modules, it is not recommended that repair of a module be attempted in the field. The defective module should be removed and returned to the factory for repair. Removal procedures are given below, and Figure 75 gives a wiring diagram of the modulator chassis which should aid in module replacement.

General Removal Procedure (for all modules):

a. Check to be sure that the modulator is turned off. If not, turn the unit off following the procedure of Section B.
b. Mark each cable and wire before disconnecting or unsoldering to correspond with its pin or connector number.

Modulator Assembly

a. Remove the seven semirigid coaxial cables with SMC connectors from the modulator assembly. (See Figure 76.)
b. Unsolder each of the wires attached to the side of the modulator assembly.
c. Remove the three bolts which attach the modulator assembly to the chassis, and lift off the modulator assembly itself.
d. After reinstalling the modulator, remove the oven access cover and insert a thermocouple or other temperature monitor in one of the holes in the oven core. Replace the oven cover.
e. Follow turn-on procedure in Section A.
f. With the power supply heat selector switch in the "OPERATE" position, adjust the temperature controller temperature adjust control (Figure 48) until the oven temperature is set at 150 $\pm$ 1°C.

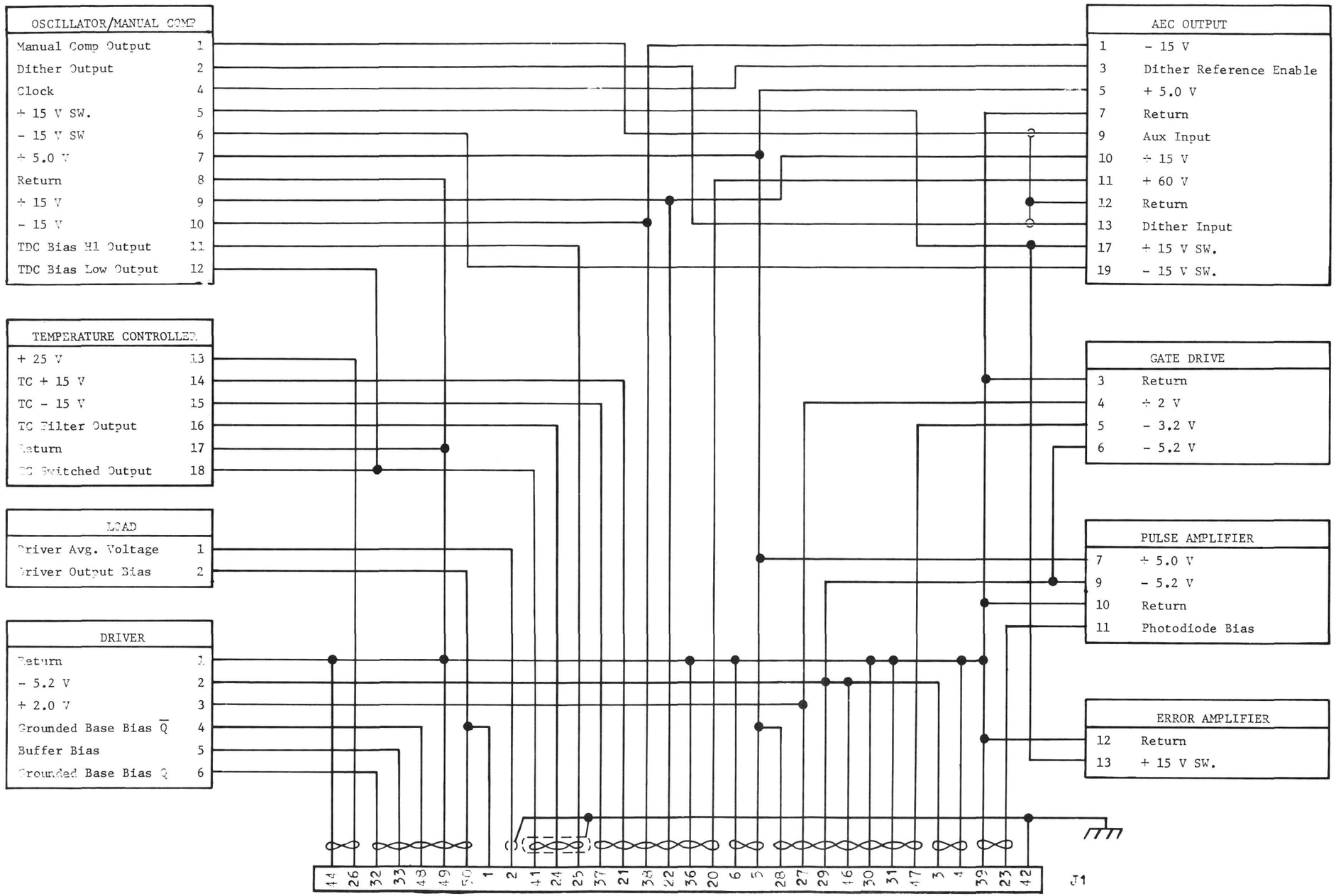

FIGURE 75 MODULATOR ELECTRONICS PACKAGE WIRING DIAGRAM

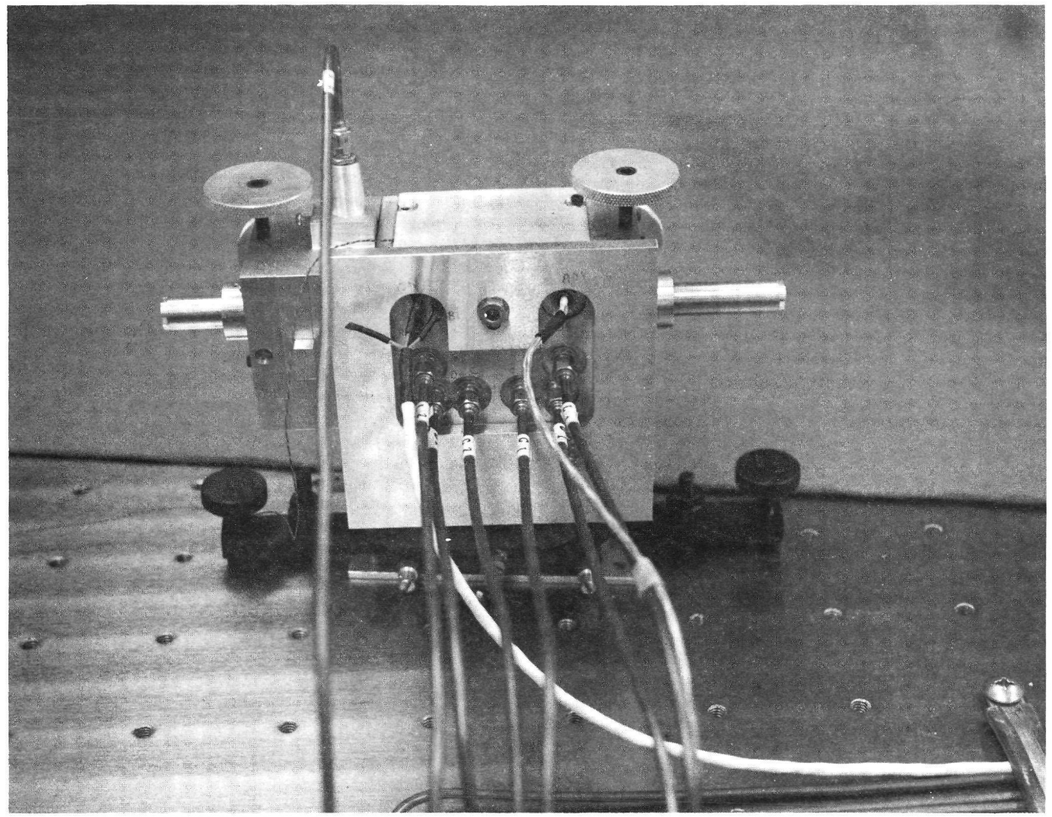

FIGURE 76 ELECTRICAL CONNECTIONS TO MODULATOR ASSEMBLY

g. Remove the oven cover and thermocouple, and then replace the cover again.

Electronic Package Modules

a. Remove the semirigid coaxial cables attached to the ends of the modulator driver.
b. Remove the two chassis covers.
c. To remove the driver module, remove two screws from the bottom side.
d. To remove the load module, remove two screws from the bottom side and two from within the chassis wiring area.
e. To remove either of the amplifier, temperature controller/oscillator/manual controller, or the AEC output module remove two screws from within the chassis wiring area and one from the front of each module. Two screws through the bottom of the front support bracket may also be loosened.
f. Each of the modules have enought wire length to slide the module from the package and then unsolder the wires from the terminals.
g. After reinstalling the removed module, follow turn-on procedure in Section A with special note to any different voltage requirements for a repaired driver module and to readjusting a repaired temperature controller (Section d through g of the modulator assembly above) or a repaired thermal differential compensator, Section C-4.